THE TRIBOLOGICAL AND WEAR PROPERTIES OF CARBON-GRAPHITE COMPOSITES

by

J H MORRIS

A thesis submitted to the Faculty of Engineering, University of Cape Town, in fulfillment of the Degree of Master of Applied Science.

September 1994

Department of Materials Engineering

ACKNOWLEDGEMENTS

I would like to thank all the people who have assisted me during the course of this work and contributed to its final completion. In particular I would like to mention the following people:-

Professor A. Ball, my supervisor, for his advice, patience and encouragement during the research project.

Professor C. Allen and Dr. J. A. Williams for their helpful suggestions and assistance.

Messrs. N. Dreze, G. Newins, R. Hendricks for their technical assistance.

I am grateful to Messrs. B. Greeves and J. Petersen for their photographic work.

The financial support of the Foundation for Research and Development is gratefully acknowledged.

Finally, thanks are due to the staff and students of the Department of Materials Engineering whose support and encouragement made my time in Cape Town a very enjoyable experience.

ABSTRACT

A range of carbon-graphites with differing properties has been evaluated for wear resistance. These include carbons with a high degree of graphitic order (natural and synthetic graphite), those with little or no such order (pitch bonded cokes, glassy carbons) and impregnated grades. Testing has been carried out using abrasive wear, dry sliding wear, particle erosion, slurry erosion, cavitation erosion and the corresponding wear rates have been related to the bulk properties of the different materials. In all tests; hardness, elastic modulus, porosity and the presence of fillers were found to influence the wear rates of the various grades. Maximum wear rates were consistently observed with the softer, more porous unfilled carbons.

In abrasive environments, the wear behaviour of each carbon-graphite is dominated by their ability to resist indentation by hard particles and in the case of an antimony impregnated grade, the ability to undergo plastic deformation. Abrasion against fine grit particles leads to a reduced load per abrasive particle and a corresponding reduction in wear loss.

A surface transfer film of crushed and compacted debris is formed on the counterface during dry sliding wear. The more graphitic carbon films are formed more rapidly, are thicker but appear to be less mechanically coherent. Delamination of sheets of material from the specimen surface is the dominant wear mechanism in all the carbon grades once a steady state wear regime has been established.

Impregnation can improve a carbons resistance to both air borne and water borne particle erosion. It can also reduce wear caused by cavitation erosion by decreasing porosity and creating fewer large areas for cavitation attack

The mechanisms responsible for the various performances have been studied by scanning electron and optical microscopy and microstructural requirements for improved performances are discussed.

TABLE OF CONTENTS

CHAPTER 1

INTRODUCTION

The self lubricating properties and ability to transfer an electrical current to a moving conductor led to the first applications of carbon as a material for electrical brushes in the early part of this century. The first application as a purely mechanical component was as seal rings in steam turbines. The expansion of the jet aircraft, petroleum and chemical industries led to an increase in demand for mechanical seals and carbon became the accepted choice.

Solid carbon-graphite ("carbon") materials are now widely used in a variety of tribological applications of which the most important are electrical brushes, seals and bearings. High thermal conductivity, low chemical reactivity and self lubricating properties account for the low wear rates of carbons against metal counterfaces. Carbon is a favoured material for such applications since it can operate satisfactorily either running dry against a counterface, or in the presence of many liquids. Generally these materials can withstand very high temperatures (melting point $\approx$ 4500°C) and are non welding; however some of the metal filled grades can adhere to the counterface causing seizure at very high running speeds [28].

Carbon-graphite components experience a variety of erosive environments in their many sliding applications: Erosion of the carbon components by solid particle impact can occur where components are exposed to gas borne particles or erosive slurries; cavitation erosion often effects components in liquid environments such as pumps and impellers; and in some situations bearing partners cannot be initially smooth and may cause abrasive wear. During the life of a carbon component damage caused by individual asperity or particle interactions builds up and at each stage of its life the worn surface is the result of many superimposed wear events.

Variations in the wear performances are discussed in this report and an attempt is made to reconcile the wear rates of the various grades with their observed wear modes, microstructure and bulk mechanical behaviour.

CHAPTER 2

LITERATURE SURVEY

The more fundamental aspects of the wear of carbon-graphite (carbon) are reviewed in this chapter. The primary application of these materials is as an annular component in mechanical seals, consequently previous studies have concentrated on their sliding wear behaviour. Erosion can also be a limiting factor in the life of a carbon-graphite component. Thus the erosive wear mechanisms of various materials have also been detailed so that comparisons with carbon can be made.

2.1 The Structure and Properties of Graphite

Graphite is a highly anisotropic material and shows large directional variation in many of its mechanical, thermal and electrical properties. The most common crystal structure of graphite consists of parallel layers of hexagonal carbon rings stacked successively on top of each other in the sequence ABABAB. The carbon atoms within the planes are strongly covalently bonded with an atomic spacing of 1.417 Å, whilst the interatomic spacing between basal planes is much larger at 3.354 Å; the bonding between the layers arises largely from weaker Van der Waals forces. A small proportion of naturally occurring graphite, and about 10-30% of synthetic graphite have the basal planes arranged in the sequence ABCABCA; this is known as rhombohedral graphite. A third form, turbostratic graphite, can exist in which the layers remain but the stacking sequence of the planes is random [1].

The atomic structure of graphitic carbon is very different from that of other materials and gives rise to a remarkable range of property values[2-5]. Graphite has good electrical and thermal conductivity, moderate strength and good thermal shock resistance [6,7]. Its refractory character and stability make it valuable for many high temperature applications where both metals and polymers are relatively unstable. Graphite's major disadvantage in this field of

application is its lack of oxidation resistance at high temperatures; carbons composed largely of synthetic or natural graphite can ignite if heated in air above 700°C[8, 62].

2.2 Manufacture of Carbon-graphite

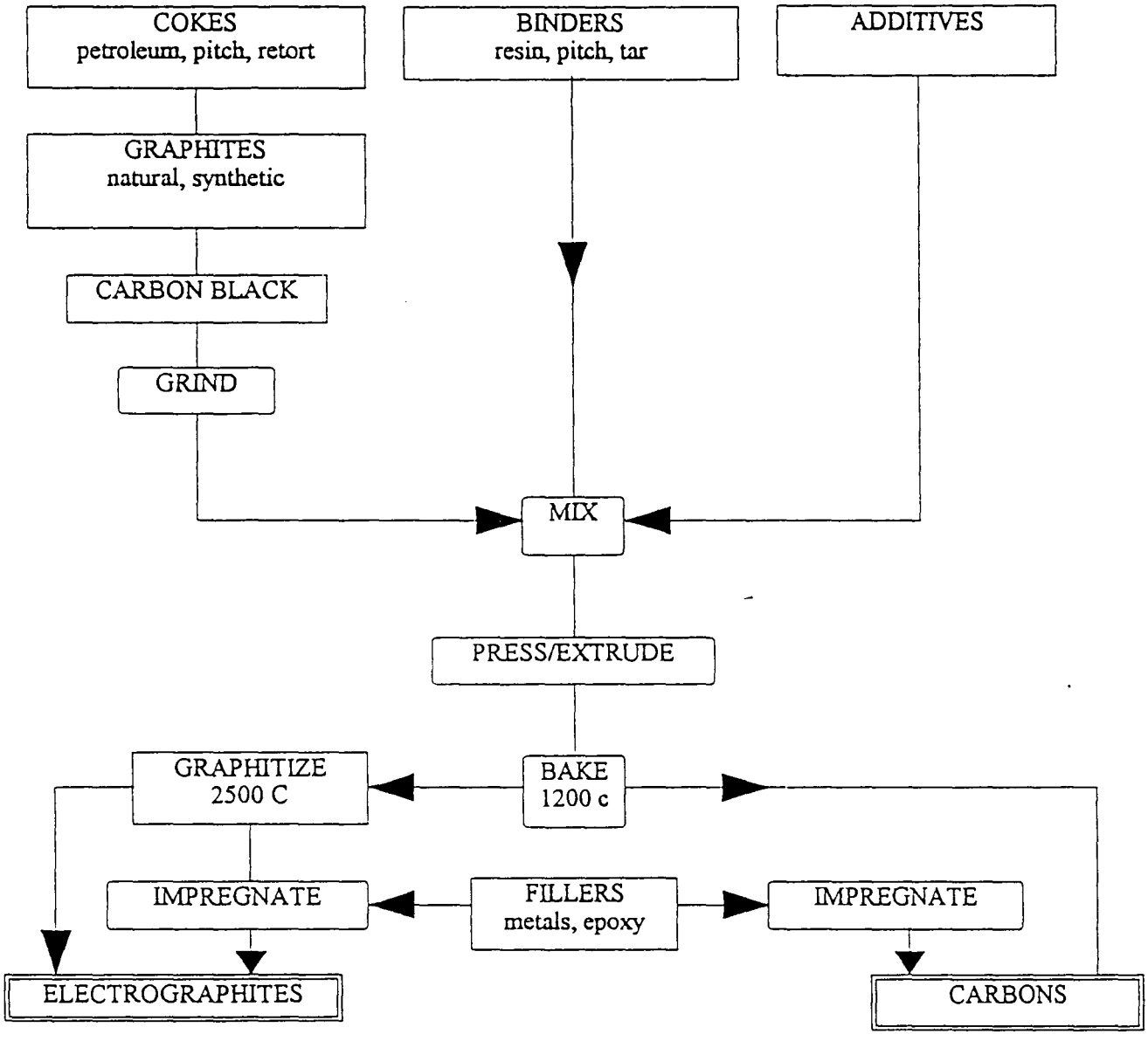

Fig 2.1: Schematic diagram showing the basic manufacture process for carbons and electrographites. (From Williams, J. A. [10])

Many grades of carbon-graphite are commercially available; the basic manufacturing route for all is summarised in fig. 2.1. Various dry carbon-rich compounds are ground to a powder and then mixed with a viscous binder. This mixture is then pressed or extruded into a "green" block and baked at above 1000°C in order to carbonise the binder and any organic impurities; the material is now generically known as a "carbon". Subsequently the component may be impregnated with resins, metals or inorganic salts for particular applications. The term "electrographites" is commonly used to describe the more highly graphitic carbons. These have been further heat treated at temperatures above 2000°C, at which structural reordering towards the graphitic form occurs [9].

It has been shown [11] that the characteristics of the raw materials can influence the properties of graphitic carbon. It is possible for a carbon with a high proportion of graphite among its starting materials to have a higher graphitic content than an electrographite formed with materials which are not readily graphitised. However this is unusual and heat treatment is generally regarded as a powerful means of reducing impurities.

2.3 Structure and Properties of Properties of Carbon-graphite

The microstructure and mechanical properties of manufactured carbons and graphites depend on the characteristics of the raw materials and the temperature of its processing. Elastic modulus [12,7] has been shown to be low or quite high depending on the constituents. The graphitisation treatment can produce a two to five times increase in thermal and electrical conductivity and a twofold decrease in elastic moduli.

Carbon-graphites contain a proportion of their carbon in the form of large (tens of microns in diameter) graphitic regions as well as quantities of nongraphitic carbon [5]. Dislocations, vacancies, interstitials and stacking faults are present in even the most graphitic regions. Significant porosity is apparent arising from both incomplete densification at the pressing stage of processing and from the loss of volatile factions during baking, it can be controlled so that a range of porosities from 20% to less than 0.01% can be obtained [13,14].

Some representative properties of the engineering grades of carbon include [15,16]:

- *Elastic moduli* . Carbon-graphite is a low modulus material (range 7 - 35 GPa), typically 10-15 times lower than steel. It is also brittle and requires care in handling including minimisation of impact loads when used in design of machine elements.

- *Tensile strengths* are much lower than compressive strengths, by as much as a factor of 10, and the strength properties tend to decrease with increasing graphitic content. Typical values vary from 10 - 15 MPa in plain carbons and from 20 - 70 MPa in impregnated grades.

- *Thermal expansion* coefficients are 25 % to 50% that of steel [17]. Typically $3 - 5 \times 10^{-6}\ K^{-1}$

- The *thermal conductivity* of the most highly graphitic grades (35 $Wm^{-1}K^{-1}$) is comparable to aluminium. The material is dimensionally stable at elevated temperatures and is not susceptible to thermal shock.

- The *Self lubricating* properties of carbon materials allow them to operate either running dry against a counterface or in the presence of liquids. A friction coefficient of 0.2 can be reduced to 0.05 in the presence of many liquids including water, acids and alkalis.

2.4 Applications

Carbon-graphites are widely used in industry for mechanical seals. Face seals in low duty pumps in such applications as cars and washing machines, rings in turbine seals and vanes in rotary gas pumps use carbon-graphite as a basic material. The low elastic modulus exhibited by the carbons helps provide conformity to the opposing surface and minimizes the seal gap over the contact region. They also display self lubricating characteristics and can therefore prolong counterface life. Carbons are inert and their general lack of reactivity makes them particularly suitable for use in hostile environments, especially

when the service conditions are severe in terms of the likelihood of dry running. In addition, by impregnation with metals or resins, the component can be made hard enough to cope with abrasive slurries.

The fluid sealing and self lubricating properties of carbons are ideal for contact / non-contact types of gland rings and their ability to perform well under high pressure is useful for mechanisms operating at great depths such as submarine propeller shafts. Other applications include glands on water turbines in hydroelectric installations and they can also be found in the variable displacement fuel pumps of jet engines. Carbon-graphite materials have been utilised in aircraft brakes since the second world war, after initial problems when components wore out after only a few hours it was reported, by Savage [63], that in the absence of water vapour, graphite has no lubricating properties, additions such as lead iodide, silver iodide, calcium carbonate, cadmium bromide and others [62] have been found to effectively reduce wear where adsorbable gases are present.

Despite displaying inferior mechanical properties to those of plain and impregnated carbons, electrographitic materials have found a universal role as brush materials in rotating electrical machinery. Their high electrical conductivity, low wear, low contact resistance and low friction make them particularly suitable for such applications.

2.5 Abrasion

Abrasive wear is likely to occur whenever a hard asperity or a trapped particle is dragged across a softer surface. It is conventionally divided into two categories; *two body* abrasive wear, that is due to fixed asperities, and *three body* wear which occurs when the abrasive particles are free to roll or move between the solid surfaces[18]. Such damaging hard particles may be external contaminants, products of corrosion or the debris from previous wear events. During the life of a carbon component damage caused by individual asperity or particle interactions builds up and, at each stage of its life the worn surface is the result of many superimposed wear events.

Abrasive Wear of Multiphase Materials

The abrasion resistance of materials containing inclusions or hard second phases is in general dependent on the test conditions employed, the nature and properties of the abrasive, as well as the microstructure and mechanical properties of the heterogeneous material being abraded [19]. Krushschov [20] reported that the wear resistance of various heterogeneous materials was equal to the sum of products of the volumetric percentage proportion of the constituents, multiplied by their relative wear resistance. This "additive" correlation is found to be limiting in assessing the abrasive wear of brittle and porous materials such as manufactured carbons and electrographite.

Abrasive Wear of Carbon-Graphite

Carbon-graphites generally exhibit poor abrasive wear resistance in abrasive environments when compared to other structural materials. Lancaster [1], Porgess & Wilman [22] and Gordelier & Skinner[23] all showed that the abrasive wear rate of carbons are significantly higher than those of soft metals and polymers when sliding in the same conditions.

A significant property of a manufactured carbon in relation to its wear is its relatively low elastic modulus. By surface profilometry of grooves made in single pass experiments with conical indentors Lancaster[21] showed that the grooves exhibited considerable elastic recovery for cones with base angles less than 20°. These are an order of magnitude larger than those typical of metals, 0.5°-2°. The experiments showed that elastic deformation contributed insignificantly to wear, the wear debris originated mainly from those parts of the surface layers in which the elastic limit in tension had been exceeded. Thus, abrasive wear is only likely to occur for carbons sliding against very rough counterfaces or in the presence of sharp, hard abrasive particles.

The wear rate of carbon-graphite running against continuously fresh abrasive paper was shown by Porgess and Wilman[22] to be particle size dependent. They found that the wear rate increased dramatically with increasing abrasive particle size. However, above a critical grit diameter the wear rate was found to

level off as shown in fig. 2.2. This was attributed to a decrease in the number of abrasive grits in contact with the wear surface. Despite there being a higher load per grit there were fewer grits per unit area and consequently, above a threshold value, large areas of the wear surface were untouched by the abrasive paper. Against a continuously fresh metal counterface, Lancaster also found the wear to be high and very dependent on the surface roughness of the metal [21]. As an absence of pile-up along the groove edges was observed, the carbons were found to exhibit negligible plasticity. He concluded that the relationship between rate and surface roughness could be explained in terms of the proportion of elastic to permanent deformation produced in the materials and that the rates of wear of different carbon-graphites are least for those materials with high hardness and low elastic modulus.

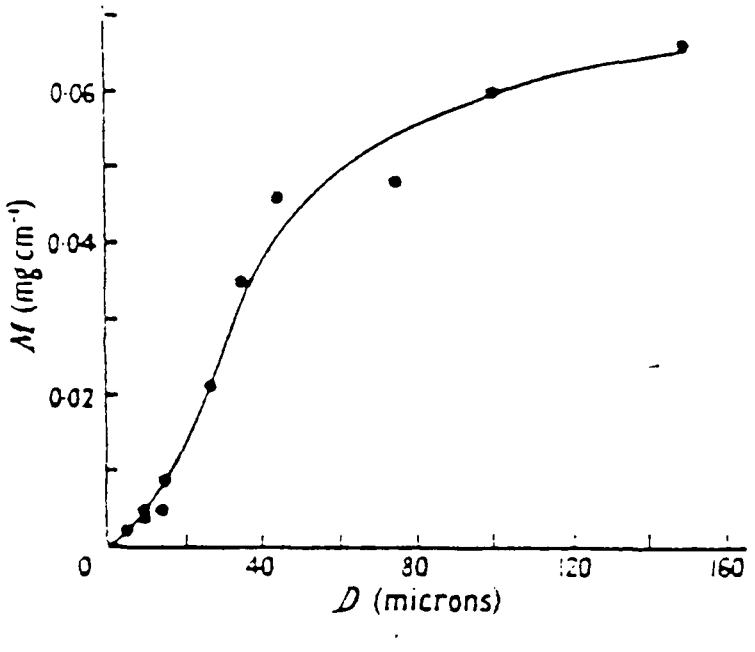

Fig. 2.2: Variation of wear per unit distance M of graphite on emery papers, with mean particle diameter D (from Porgess, P. V. K. and Wilman, H., "Surface re-orientation, friction and wear in the uni-directional abrasion of graphite", Proc. Physical Society, (1960), 76, 513-525)

The influence of grit diameter on wear during sliding abrasion has also been observed by Larsen-Badse[24]. He showed that for copper samples running against abrasive papers, the wear rate decreased above a critical grit size. It was concluded that some of the abrasive grits were in contact with the metal only elastically and consequently these did not contribute to the cutting of the

metal. The effect was very pronounced for fine grits and virtually disappeared for grit diameters above the critical value.

Inverse proportionality between the rate of wear and hardness has been observed with metals (Khrushschov [25]), polymers (Böhm, Betz & Ball [26]) and other brittle materials (Moore and King [27]) sliding against abrasive paper or cloth. Lancaster [1] found a similar relationship between wear rate and indentation hardness for different carbon graphites, shown in fig. 2.3. The lack of ductility in carbons is cited as the main reason why the wear rates in carbon graphites are significantly higher than those of polymers and metals sliding in the same conditions. Plain carbons suffer extensive fragmentation , whilst the polymers and metals undergo plastic flow.

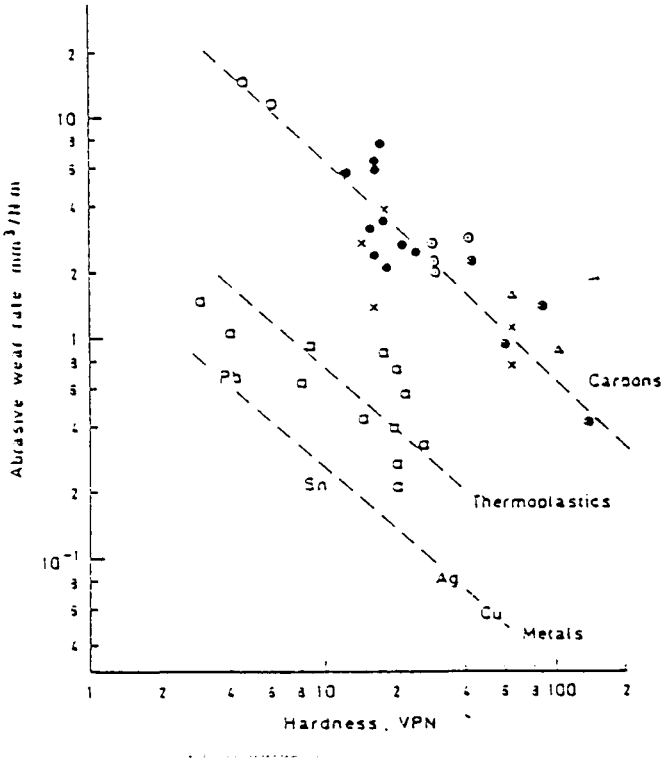

Fig. 2.3: The comparative wear rates of carbons, polymers and soft metals (data from Lancaster, J. K., Treatise on Materials Science and Technology, Academic Press, (1979),13, 153). O, natural graphites; x, impregnated carbon graphites; ●, electrographites; ⊗, low/nongraphitic carbons; ⊙, carbon graphites; Δ, carbon-carbonfibre composites

The main conclusions that can be drawn from the previous work in this field is that the abrasive wear rates for different carbons will be least for those materials with low elastic modulus and high hardness. The ability of a grade to deform plastically can also lead to superior wear rates.

2.6 Dry Sliding Wear of Carbon

Solid carbon-graphite materials are widely used in a variety of tribological applications of which the most important are electrical brushes, seals and bearings. High thermal conductivity, low chemical reactivity and self lubricating properties account for the low wear rates observed against metal counterfaces. Carbon is a favoured material for such applications since it can operate satisfactorily either running dry against a counterface, or in the presence of many liquids. Generally these materials can withstand very high temperatures and are non welding; however some of the metal filled grades can adhere to the counterface causing seizure at very high running speeds [28].

Previous research has shown that carbons wear by abrasion against hard rough surfaces since the counterface is usually harder and its asperities will abrade the carbon surface [21,22]. Against very smooth counterfaces however, the number of contact points is sufficiently large to ensure that the load is carried elastically throughout. When lubricating effectively, a transfer film develops on the counter surface and carbon vs. carbon results. Under these conditions wear rate is minimal.

Transfer Layer Formation

Transfer films have been shown to occur most readily from more highly graphitic carbon and in general lead to a smoother counterface. Before such film formation the wear rate of the carbon is very dependent on the roughness of the counterface. Lancaster [21] and Porgess and Wilman [22] have shown that the abrasive wear rate of carbons is particle size dependent and is inversely proportional to their indentation hardness when slid against rough surfaces (as detailed in ch 2.5).

Graphitic materials often develop a preferred orientation in which the basal planes of the crystallites become aligned at a small angle to the general plane of the surface. Conversely, non-graphitic carbons do not exhibit a preferred orientation and instead it has been observed that they often acquire a surface layer of compacted wear debris[29]. Lancaster [30] has also suggested that the extreme anisotropy of the graphite lattice could lead to single grains showing very high hardness. He postulated that some of these grains could become embedded within the counterface and act as nucleation sites for the transfer layer.

Sliding Wear Processes

The physical mechanisms of wear most relevant to the dry sliding wear of carbons may be classified under the general headings of abrasive wear, adhesion and delamination by a fatigue process.

During the initial stages of contact sliding the dominant wear process is that of abrasive wear. The wear rate of the carbon is high and the debris produced if unable to escape the contact zone, may be compacted into one or both of the sliding surfaces modifying their subsequent behaviour. Gordelier & Skinner [23] suggested that the presence of a transfer layer does not indicate the end of abrasive wear, a degree of which will continue until transferred carbon-graphite regions are well established. In addition manufactured carbons inevitably contain hard inclusions, oxides and carbides; these may be released during the sliding process and introduce an element of three body abrasion [1].

The significance of adhesion as a factor in the wear process is uncertain; hypotheses have been formulated based on the processes that occur in metals [31,32]. It has been suggested that adhesion acts with sub-surface fatigue processes, eventually the weak adhesion force being sufficient to detach a wear fragment from the carbon-graphite surface. The simplest theory of transfer states that it should occur if the shear strength of the adhesive bond between the two asperities is greater than that of the transferring material. Thus one might expect the "softer" carbon material to transfer to the "harder" counterface.

After a transfer layer has been well established, wear enters an equilibrium phase in which the load supporting layers are worn and replenished. In this steady state low wear rate regime the dominant wear process is one of delamination by a fatigue process[33]. The surface layer on the carbon formed as a result of sliding is gradually lost, as each lamella breaks away the carbon beneath it is exposed with a relatively unchanged form. This area becomes rapidly modified and the local wear rate is high until sufficient debris has been produced to consolidate into a coherent surface layer once again. This layer is subsequently lost in a process analogous to fatigue.

Friction

The friction and wear of carbon-graphite in the early stages of formation of the transferred layer and the manner of its formation have been studied by a number of research groups. Longley et al [34], Lancaster [35] and Booser & Wilcock [28] showed that carbons with a wide range of graphitic content displayed very similar values of coefficients of friction when running against metal surfaces of similar roughness.

During the initial stages of contact the wear rate of carbon is comparatively high and the debris produced if unable to escape from the contact zone, may be compacted either into a.) a transferred film on the counterface or b.) a debris layer on the worn surface, thus modifying their subsequent behaviour. For this reason the original structure of the carbon graphite may only be important in so far as it controls the production of the surface film. The degradation of carbons into finely divided wear debris is more readily achieved by weaker graphitic material than by stronger nongraphitic carbons. Thus, consolidated debris films can only be formed during sliding against hard counterfaces, whereas films from graphitic carbons form on both hard and soft counterfaces [29].

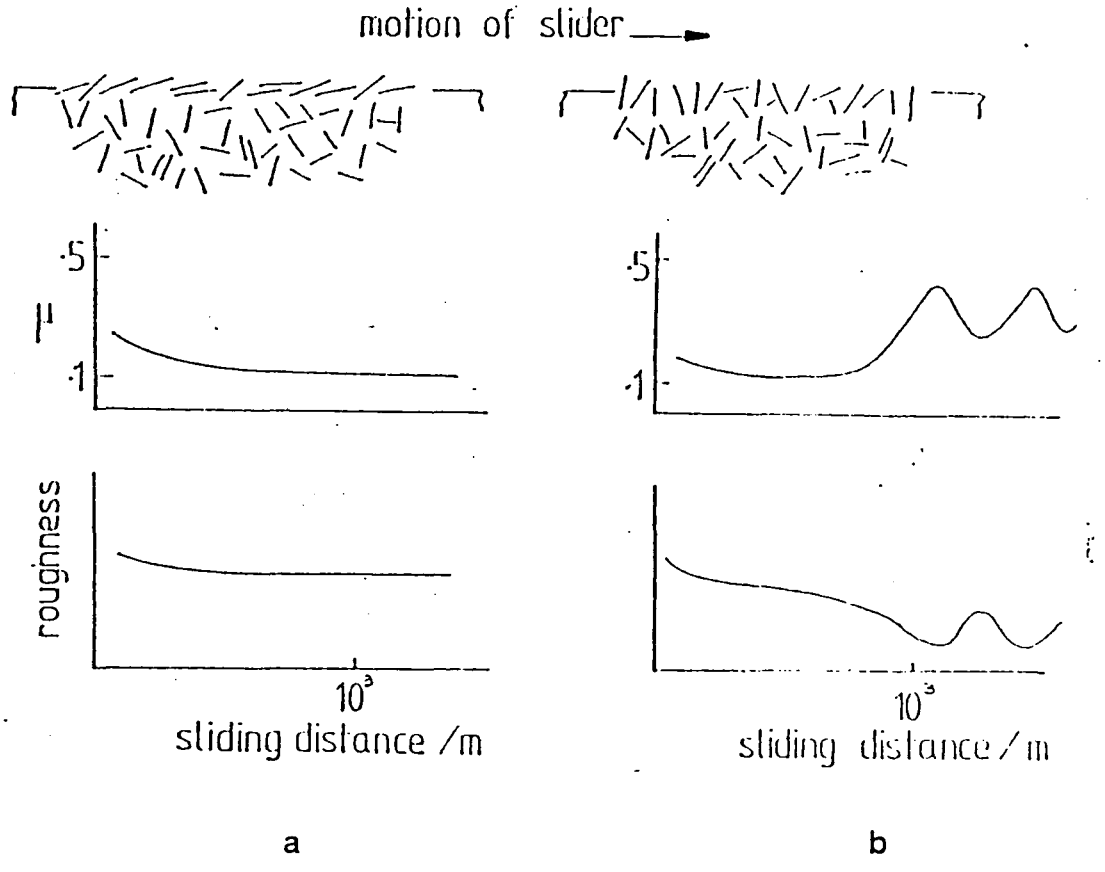

Fig. 2.4: Frictional behaviour of a) electrographite and b) low graphitic carbon. The build -up of friction force in b) is associated with the formation of a particularly smooth surface film leading to an increase in the true area of contact. Disruption, and exposure of the rougher underlying carbon, reduces friction until the film becomes established once more and the process repeats cyclically. (From Williams, J. A. [10])

The difference in frictional behaviour of carbons with a high degree of graphiticity and nongraphitic carbons appears to be quite distinct when running against a steel counterface. The former has wear debris consisting of a relatively large proportion of lamella carbon which forms a surface layer with the crystallites oriented with their basal planes tilted at about 10° to the wear surface as indicated in fig. 2.4a. The coefficient of friction (μ) settles at about 0.1 and the surface roughness of the carbon also stabilises. Conversely, the crystallites in low or nongraphitic carbon appear to be oriented differently with a considerable proportion having their basal planes normal to the surface

(fig. 2.4b). Consequently the wear debris is extremely fine and if this debris is unable to escape, it may build up at the interface to form a hard flat layer. The true area of contact between the slider and the counterface grows significantly and the friction factor can rise by a factor of 4 or more. This situation appears to be only quasistable; the compacted layer eventually blisters away from the surface exposing the relatively rough, unmodified surface of the carbon below: μ falls because of the decrease in the true contact area. As the compacted debris layer reforms μ increases correspondingly and the cyclic process starts again[29].

The Effect of Counterface Roughness

Carbon-graphite seals are normally employed in combination with a smooth bearing partner. However, in some situations the bearing partner cannot be maintained in a smooth condition; external contaminants or products of corrosion may cause considerable roughening. Thus the wear of carbon against a variety of surface roughnesses is of practical interest.

Hollander and Lancaster [36] investigated the relationship between counterface roughness (Ra) and the mean wear rates of a soft metal and an electrographite. The wear rate of the soft metal was found to increase relatively slowly with counterface roughness Ra. Conversely, for the electrographite the increase in wear with counterface roughness was much more rapid as shown in fig. 2.5. On even the roughest surface the elastic criterion for the electrographite was not exceeded; it was therefore suggested that localised surface fatigue contributed a major role in the wear of carbons.

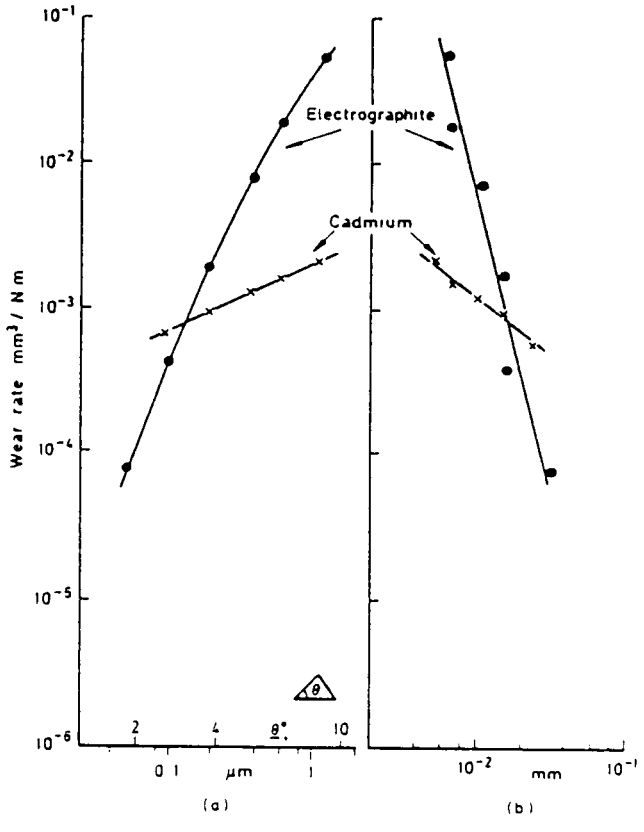

Fig. 2.5: Variation in wear rate for an electrographitic carbon and cadmium as a function of a.) metal counterface roughness Ra; b.) average radius of counterface asperities.(from Hollander, A. E. and Lancaster, J. K., Wear, (1973), 25, 155)

2.7 Solid Particle Erosion

The erosion of materials by solid particle impact is of importance in many technological applications, where components are exposed to gas or liquid borne erosive particles. The severity of erosion is dependent on several factors which include the size, shape, velocity and frequency of impact of the erosive particles as well as the mechanical properties of both the target and erodent materials. For the purpose of this survey the modes of erosion and target variables will be the principal consideration.

A detailed study of solid particle erosion of carbon-graphite appears to have not been made; this is probably due to the fact that their main application is as a sliding material. However, carbon-graphite seals are used in pumps and impellers and could be subjected to erosion from both air and liquid borne particles thus this thesis considers these wear types. Studies have been made into the erosive behaviour of various brittle materials[38,39], polymers [26] and alloys [37] and for the purpose of this survey comparisons will be made with these.

2.7a Air-Borne Particle Erosion

Modes of Erosion

Erosion may be divided into two categories: ductile erosion, involving the removal of material by plastic deformation and brittle erosion involving the removal of material by fracture processes. Carbon-graphites normally fracture in a brittle fashion [1,11,21], although ductile erosion may occur in the impregnated grades. The following mechanisms have been identified for material removal under gas/air borne particle erosion.

Ductile Erosion

The erosion of soft, tough materials such as polymers is predominantly ductile. Material loss can occur in two ways; cutting wear due to impact at low angles (shown in fig. 2.6) and extrusion and fragmentation due to normal impact. In practice the ductile erosion of materials is a combination of these two processes.

Cutting Wear

Finnie [40] discovered that ductile erosion reaches a maximum at a particular angle of impact due to cutting wear. He proposed that the mode by which the erodent particles remove material from a ductile target surface, involves the displacement of material from a damage crater produced by the impact event. An impacting particle pushes material forward, leaving a groove in its wake and a lip at the end of the groove when it leaves the impact site (fig. 2.6). He

assumed that the particles remained intact after impact and that they left the target surface when their perpendicular velocity was zero. Finnie's theory correlates well for low angle/glancing erosion but estimates zero erosion for normal impact.

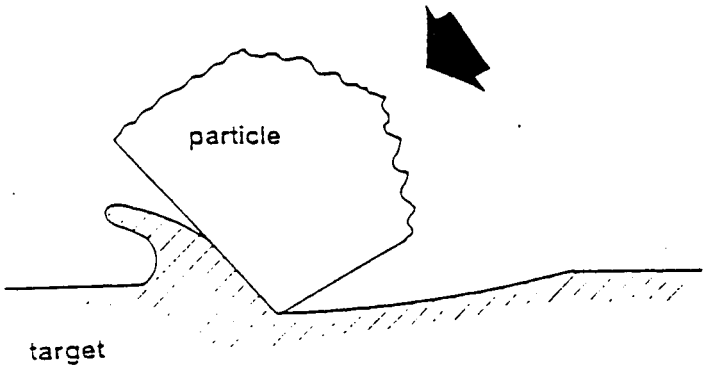

Fig. 2.6: Material loss through cutting wear [40]

Extrusion and Fragmentation

For larger values of impact angle ($\alpha \approx 90°$), the mechanism of erosion ceases to be one of cutting and could be described as one of repeated impact wear. When the erodent particle strikes the surface of a ductile specimen, material extrudes to the edge of the damage zone to form "shear lips" that are vulnerable to subsequent impacts. Tilly [41] proposed a two stage mechanism, as shown in fig. 2.7, involving a primary stage of extrusion and a secondary stage due to particle fragmentation. He suggested that if the impacting particle is brittle and fragments during impact, secondary erosion can occur when the fragmented pieces scour the surface.

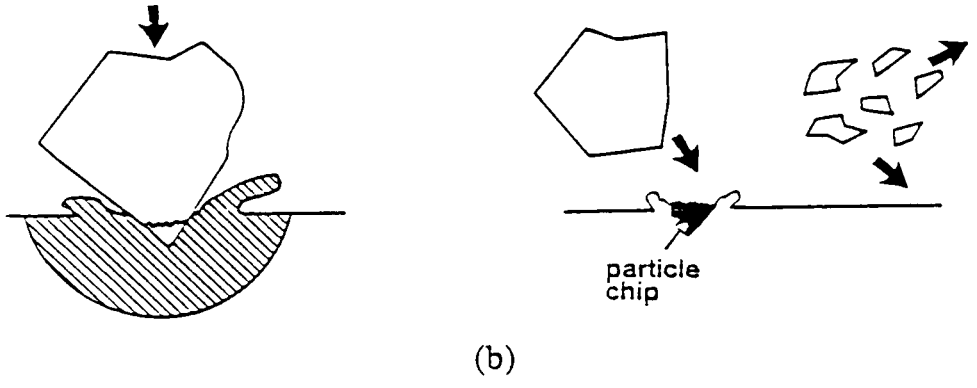

Fig. 2.7: Two stage mechanism of ductile erosion involving a) extrusion and the formation of "shear lips" and b) secondary erosion by particle fragmentation [41]

Brittle Erosion

Material loss in the solid particle erosion of brittle materials occurs through the formation and interaction of a network of subsurface cracks. In order for material removal to occur, the subsurface stresses must reach a critical value to initiate microcracking and the microcracks must propagate in order to release chips of material. Hence for a brittle material to have good erosion resistance it must have a high resistance to crack initiation and a high fracture toughness.

The modes of deformation and fracture depend on the particle velocity, impact angle, shape and mechanical properties relative to those of the target material. Blunt particles travelling at low velocities set up Hertzian stress fields in the target which initiates cone cracking. Sharp particles travelling at high velocities produce inelastic deformation zones and initiate median and lateral cracking.

Spallation and chipping are the most effective forms of material removal in brittle materials and thus it is of importance to understand the impact conditions that effect initiation and propagation of lateral cracks. Lawn and Swain [42] described the loading sequence for a sharp indentor on a brittle material which leads to crack growth and chipping. The mechanism of crack formation during sharp

particle impact is shown in fig. 2.8: Conical cracks are initiated on the target surface at the site of impact (a)-(c). Lateral cracks, which initiate from the conical cracks, form in order to relieve the strain caused by the impact (d)-(e). These lateral cracks run almost parallel to the target surface (e) and material is lost in the form of a chip when the crack intersects with the surface (f).

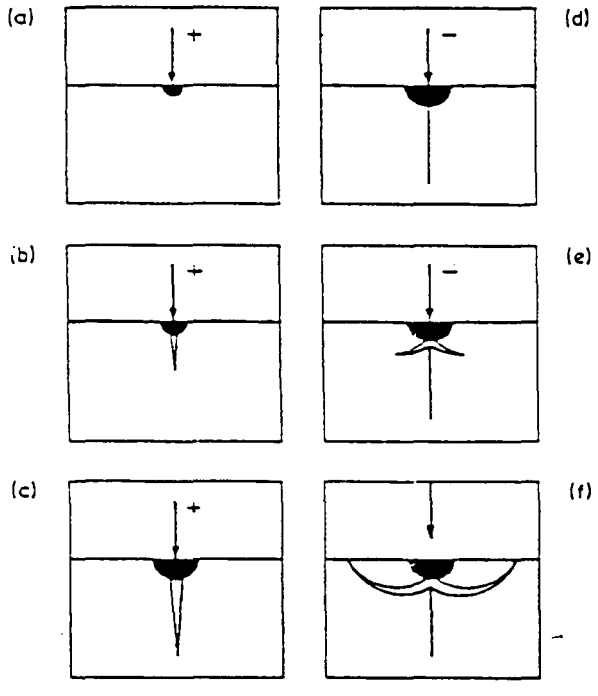

Fig. 2.8: Schematic diagram of crack growth during sharp particle impact [42]

The initiation of lateral cracks in brittle materials is almost inevitable, the most important factor in determining the erosion rate is the resistance to irreversible deformation and propagation of lateral cracks.

Target Variables

Hardness

Brittle materials have been shown to display an inverse relationship between target hardness and erosion rates [43]. A high hardness will reduce the amount of irreversible deformation at the impact site and therefore the driving force for

lateral crack formation will be lower. Additionally, particle blunting will occur more readily on striking a hard material. In general the minimising of lateral spalling through energy absorption will improve a materials erosive resistance.

Microstructure

Vaughan [38] observed that the erosive damage in brittle materials is often of a similar size to the grain size and that consequently the microstructure of a material will effect the erosion rate. Wiederhorn et al [44] described how porosity affected the erosion rates of materials by inhibiting crack propagation by blunting crack tips. Equally lateral cracks which form on impact can either be contained within the grain or pass through many grains. In the case of the latter crack propagation will be inhibited by the grain boundaries, this effectively reduces the size of the damage zone and reduces erosion rates.

2.7b Slurry Erosion

Slurry erosion concerns the removal of material by impingement of solid erodent particles suspended in carrier fluid. The wear models described in air-borne particle erosion equally apply to erosion due to particles in a liquid carrier. However, additional factors associated with liquid borne solid particle erosion are the deceleration of the particle near the target surface due to the viscosity of the liquid, the debris cleaning effect of the carrier fluid and corrosion processes [46].

Effect of Carrier Fluid

A study was made by Zu [45,47] to compare the differences between the aqueous slurry erosion and the airborne solid particle erosion of aluminium under the same experimental conditions (impact angle 40°, particle velocity:- 4.5 ms^{-1}, mean SiO_2 erodent particle diameter:- 700 μm). He found that a heterogeneous surface composite layer, due to embedment of fine silica erodent particle fragments only formed during airborne solid particle erosion. Zu concluded that as the slurry erosion surface was free from embedment a fluid cleaning effect must be operative. The fluid washes debris of detached target material away

before they can be reattached onto the target surface by subsequent impacting particles. Water also washes broken fragments of erodent particles away preventing adhesion and embedment [45,47].

The wear rates Zu observed were significantly higher for water borne erosion than air borne erosion. The surface composite layer that formed under the airborne erosion conditions resulted in a surface layer that was harder than that formed during slurry erosion. This difference in hardness was partly accounted for by the higher erosion resistance shown by the aluminium specimens subjected to airborne erosion. Significant embedment was observed leading to an enhanced measured performance. Steady state mass loss is reached only when the rate of embedment and adhesion is surpassed by material removal caused by airborne impacting particles.

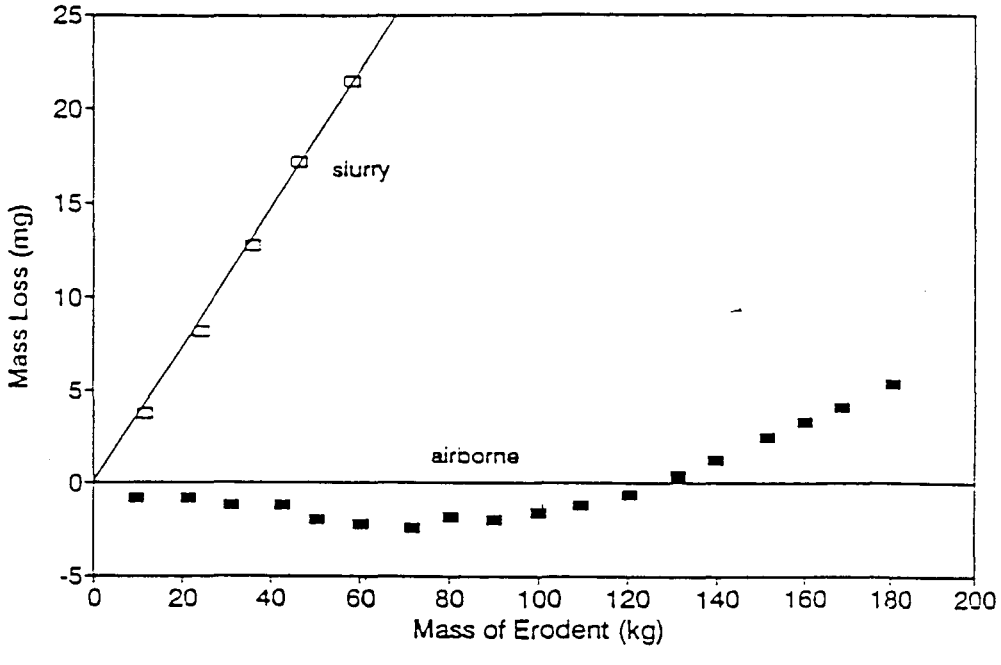

Fig. 2.9: Erosive wear of an aluminium alloy as a function of erodent used. Slurry and airborne particle velocities:- 4.5 ms^{-1}; mean SiO_2 erodent particle diameter:- 700 μm; Impact angle:- 40°. (From Zu [47]).

2.8 Vibratory Cavitation Erosion

Another common form of erosive wear is cavitation erosion, which often affects engineering components used in liquid environments eg. pumps, impellers, pistons, bearings, valves and ship propeller shafts. Cavitation is often defined as the formation, growth and collapse of vapour bubbles due to local pressure fluctuations. It is a liquid phenomenon and does not occur under normal circumstances in either solid or gas. In its primary application as one of the annular components in mechanical seals, carbon-graphite components wear to a "saddle shaped" profile characteristic of successfully running seals (this is associated with the development of a very thin hydrodynamic film which separates the two loaded surfaces). It has been suggested that cavitation erosion occurs in the region of the lubricated contact within which the pressure gradient is negative.

All materials are susceptible in varying degrees to cavitation erosion damage which involves the removal of material from solid flow boundaries. The inception of cavities and the subsequent intensity of cavitation is little influenced by the particular construction materials of the system. However the resultant erosion damage to the material is a function of the composition, microstructure and mechanical characteristics of the material [49].

The growth and collapse of bubbles generates stress pulses which have the characteristics of a shock wave, the magnitude of which determines the level of elastic and plastic deformation in the surface regions of the material being eroded. A bubble collapsing close to a specimen surface suffers from geometrical constraints and becomes involuted, forming a jet of liquid which impacts the solid [50]. Vyas and Preece [51] suggested that this only played a minor role in erosion, as the major part of erosion by cavitation in vibratory systems results from the integrated effect of a whole cloud of bubbles. This is because a cloud of collapsing bubbles will create combined wave damages at greater distances.

A number of previous investigations have attempted to develop a means of predicting material performance under cavitation erosion [26,49,52,53]. The most convenient criteria for such predictions are macroscopic mechanical properties.

Heathcock, Protheroe and Ball [54] studied the behaviour of a range of materials in vibratory cavitation conditions and established that improved performances were attained by materials with one or more of the following properties: a high elastic resilience, a high resistance to the accumulation of fatigue damage under repeated shock loading conditions, a tough microstructure which is resistant to the propagation of microcracks. The influence of fillers on the erosive behaviour of various of multiphase materials [49,53] is also considered of importance to this research: Wilson and Ball [53] found that an aluminium alloy reinforced with 20 vol.% silicon carbide particulates displayed an erosion resistance which was slightly above that of its unreinforced state; the presence of high modulus silicon carbide reinforcement was said to improve the elastic resilience of the alloy. Wang and Hutchings [52] suggested that filler materials may also provide regions of elastic modulus mismatch and plastic strain mismatch in a matrix and can act as nuclei for rupture, giving higher wear rates.

The erosion is not necessarily controlled by the bulk properties of a material and is largely affected by the microstructure [50]. The degree and depth of deformation and the mode or rate of subsequent material removal is essentially determined by the ability of the material to absorb and dissipate cavitation energy. In general Preece [50] found that a fine grain size combined with a ductile mode of erosion was beneficial to erosion resistance. Heathcock [54], after studying a wide range of materials reiterated this and added that a cavitation erosion resistant material should contain no second phase particles or erosion initiating sites in surfaces exposed to cavitation.

CHAPTER 3

MATERIALS AND EXPERIMENTAL METHODS

3.1 Materials Characterisation

The grades of commercial carbon tested are shown in Table 3.1.1. Those designated CY2, CY10 and CY9 are baked carbons, EY9 is an electrographite (being the graphitised form of CY9). Grades CY2C, CY10C are CY grades impregnated with epoxy and MY10K is a CY grade impregnated with antimony. The fillers occupy approximately 15% of the impregnated grades volume. All samples tested were supplied by Morganite Special Carbons Limited (UK).

Grade	Generic name	Hardness (scleroscope)	Thermal conductivity*	Dynamic Elastic modulus*	Application
			$W\ m^{-1}\ K^{-1}$	GPa	
CY2	plain carbon	60	0.03	18	Bearings and sealing rings
CY9	plain carbon	55	0.25	17	Bearings and sealing rings
CY10	plain carbon	67	0.03	18	Bearings, piston & sealing rings and vanes
EY9	electrographite	50	0.20	10	Bearings, gland and sealing rings, electrical brushes
CY2C	epoxy impregnated carbon	80	0.03	24	Bearings, gland and sealing rings
CY10C	epoxy impregnated carbon	83	0.03	23	Bearings, steam joints, rings and vanes
MY10K	antimony impregnated carbon	80	0.03	34	Sealing rings

*Table 3.1.1: Properties of carbon-graphites investigated. * Manufacturers data*

From the data shown in Table 3.1.1 it can be seen that the impregnated grades exhibit higher elastic moduli and hardnesses than the plain carbons. The electrographitic carbon EY9 displays inferior elastic modulus but has a high

conductivity and hence is used predominantly in electrical applications. The plain carbon CY9 also has a high thermal conductivity in comparison to the other unfilled grades suggesting a more highly graphitic structure.

Scanning Electron Microscopy

In order to account for differences in the wear rates, scanning electron microscopy (SEM) was utilised to determine the mode of material removal and the benefits of impregnation or graphitisation.

Specimens were prepared by abrading on successive silicon carbide papers, polished on a 3 μm diamond wheel and ultrasonically cleaned. The polished grades were then mounted on aluminium stubs and, because of the high conductivity of carbon-graphite sputtercoating was found to be unnecessary . A moderately low accelerating voltage of 15 kV was used to prevent surface damage. A back scattered electron/secondary electron mix (BSE/SE) was used to improve topographic contrast and prevent flaring from sharp edges.

Scanning electron and light microscopy revealed considerable porosity in some of the samples. This is probably due to the loss of volatile factions during the bake or incomplete densification during the pressing stage. This porosity is particularly apparent in the unfilled electrographitic and plain carbon grades (figs. 3.1.1, 3.1.2, 3.1.3 & 3.1.5). Porosity is not however as apparent in the CY grades which have been impregnated with epoxy (fig. 3.1.4, 3.1.6) and molten antimony (fig. 3.1.7).

Fig. 3.1.1 (left): SEM micrograph of the highly graphitic electrographite EY9. Smearing of the surface, as a result of the polishing process conceals considerable porosity

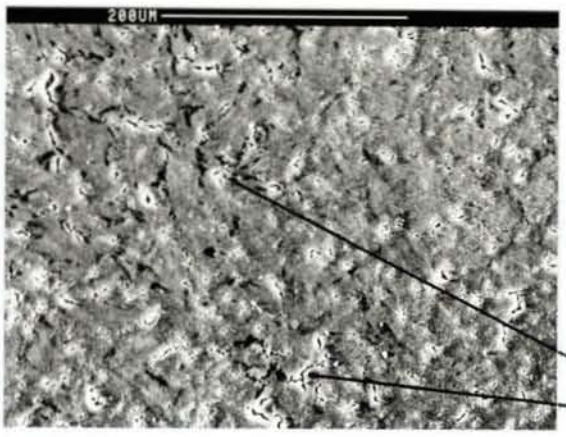

Fig. 3.1.2: SEM micrograph showing the polished surface of CY9 plain carbon

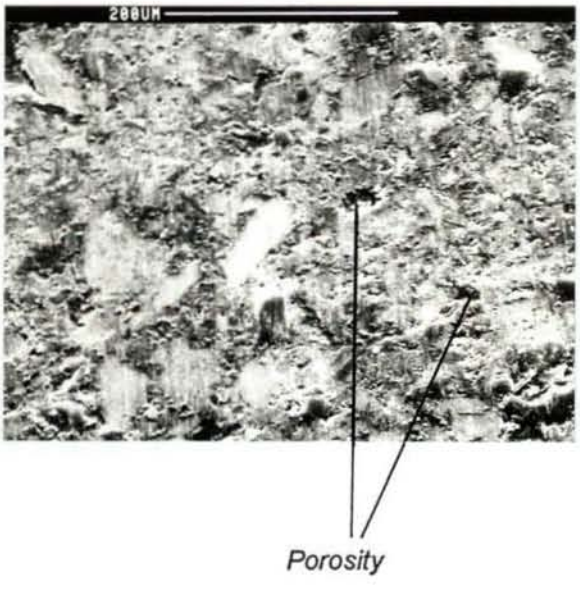

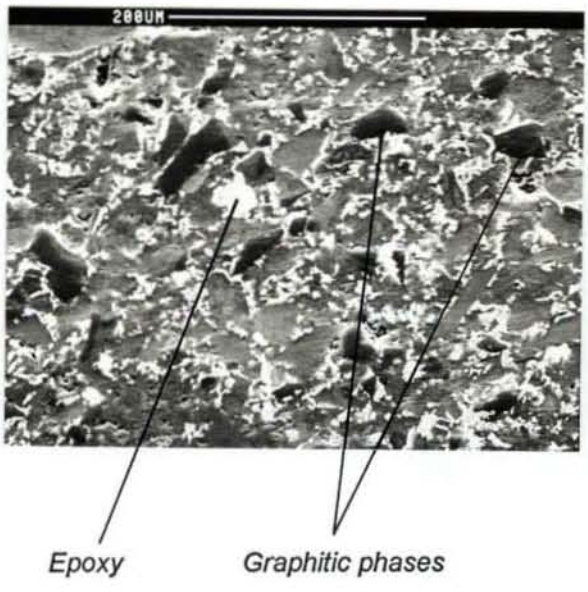

Fig. 3.1.3 (left): SEM micrograph showing the polished surface of CY2 plain carbon

Fig. 3.1.4 (right): SEM micrograph showing the polished surface of a CY2C grade. The effect of epoxy impregnation on overall porosity can be seen by comparing fig. 3.1.3 and fig. 3.1.4. The impregnant is shown as the light regions on the surface

Fig. 3.1.5 (left): SEM micrograph of the polished surface of the plain carbon CY10

Fig. 3.1.6 (right): SEM micrograph showing the polished surface of a CY10C grade. The effect of epoxy impregnation on overall porosity can be seen by comparing fig. 3.1.5 and fig. 3.1.6.

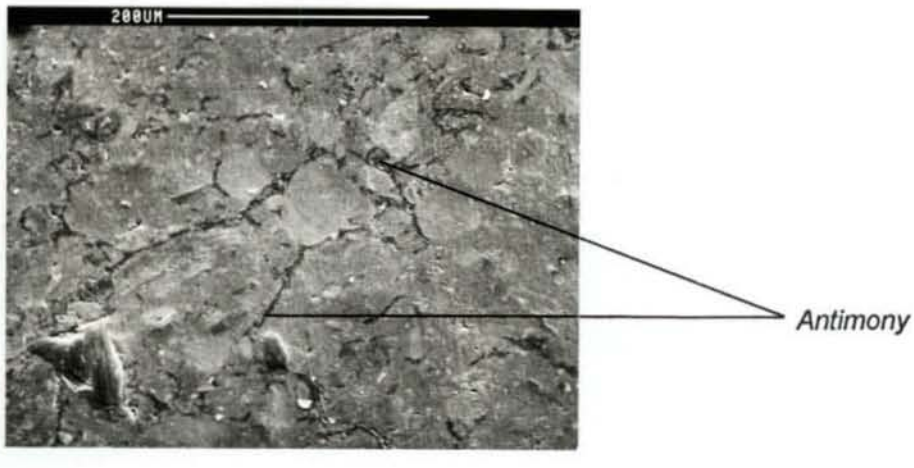

Fig. 3.1.7: SEM micrograph of the polished surface of antimony impregnated grade (MY10K)

Mercury Intrusion Porosimetry

To measure the extent of the porosity revealed by the scanning electron microscope, mercury intrusion was performed by MINTEK (Council for Mineral Technology), using a Quantasorb Porosimeter [56]. Samples were degassed *in vacuo* at room temperature (± 21°C), then immersed in mercury at a low pressure. The mercury is then pressurised and a series of pressures (0-60 000 psi) and corresponding volumes of intruded mercury determined. From the pressure, the surface tension of mercury, and an assumed wetting angle, the pore diameter can be calculated. A circular pore opening was assumed. Values of true density were measured by Helium pycnometry and are shown in Table 3.1.1a

Total pore volume (**A**) is calculated via equation (i)

$$A = (vol.\ solid + pores) - (Vol.\ solid) \qquad .....(i)$$

Where:
- TPV = Total pore volume in cm^3g^{-1}
- (Vol. solid + pores) is measured when the cell is filled before the intrusion by the porosimeter
- (Vol. solid) is calculated from 1/density

Macropore volume (**B**) applies to pores in the size range 1μm - 300 nm radius.

Mesopore volume (**C**) applies to pores in the size range 1.7 - 300 nm radius. Quantities **B** and **C** are calculated by the porosimeter software, micropore volume (**D**) is calculated via equation (ii),

$$D = A - (B + C) \qquad .....(ii)$$

Percentage porosity (**E**) is calculated via equation (iii)

$$\%\ Porosity = \frac{TPV}{(Vol.\ solid + pores)} \times 100 \qquad ....(iii)$$

Surface area is calculated from the intruded volume data, assuming that the pores are cylinders, closed at one end.

Grade	True Density	A Total Pore Volume	B Macropore Volume	C Mesopore Volume	D Micropore Volume
	$g\ cm^{-3}$	$cm^3g^{-1}x\ 10^{-3}$	$cm^3g^{-1}x\ 10^{-3}$	$cm^3g^{-1}x\ 10^{-3}$	$cm^3g^{-1}x\ 10^{-3}$
CY2	1.9514	67.7	54.9	3.24	9.55
CY9	1.9912	87.7	82.5	4.57	0.63
CY10	1.9388	110.3	99.4	6.97	3.93
EY9	2.0565	95.3	81.4	10.30	3.6
CY2C	1.8479	6.9	16.4	11.50	-
CY10C	1.8462	22.4	24.1	5.99	-
MY10K	2.4952	16.5	6.8	10.20	-

a.)

Grade	% Porosity	Specific Surface Area	Mean Pore Radius	Median Pore Radius
	E	m^2g^{-1}	nm	nm
CY2	11.67	3.70	212.90	268.21
CY9	14.87	3.44	215.83	247.19
CY10	17.62	4.93	537.55	804.02
EY9	16.39	5.06	127.52	163.45
CY2C	1.26	7.97	37.28	66.04
CY10C	3.97	4.99	59.25	86.62
MY10K	3.95	6.73	23.59	5.21

b.)

Table 3.1.2 a) and b): Pore volume and surface area characteristics of carbon-graphite samples, determined by mercury-intrusion porosimetry

From the data given in table 3.1.2 a) and b) it is apparent that the plain carbons and electrographite have greater porosities than the epoxy and antimony-impregnated carbon. The unfilled grades have extremely large pores well into the macropore range (1 μm - 300 nm), whilst the pores in the impregnated carbons are evenly spread over both the macropore and mesopore (1.7 - 300 nm) ranges.

Only CY2 and CY10 have any contribution to the total pore volume from micropores, this contribution is however, small. The difference in the mean and median pore radius of Table 3.1.2 b) show that the pore size distribution does not fall within a narrow range; rather a spread of pore sizes across the entire pore size range.

Hardness Testing

The difference in size and hardness of the various grains composing carbons-graphite made the use of more conventional Vickers and Rockwell tests unsuitable. For this reason hardness values were measured using a Shore model C Scleroscope [57]. A diamond tipped "hammer" was dropped from a fixed height down a calibrated glass tube onto the surface of the carbon specimen under test. The rebound height was visually observed and is the average of ten readings. The height of rebound of the hammer is a measure of the hardness of the material. It should be noted that the scleroscope does not provide a true measure of the permanent deformation of these materials, it is however a readily measurable quantity that differs significantly in the various carbon grades. There is no correlation between Scleroscope and Rockwell or Vickers hardness.

WEAR TESTS

The range of material was subjected to various forms of wear and erosion and further characterised using the following techniques:

- Abrasive wear

- Dry sliding wear
- Dry particle erosion
- Slurry erosion
- Cavitation erosion

3.2 Abrasion Testing

Dry abrasive wear tests were performed on each grade using a modified Rockwell belt sanding machine shown in fig. 3.2.1. Specimens, of length 10 mm and cross sectional area 10 mm x 10mm, were loaded against a continuous bonded abrasive belt which is running horizontally at a constant velocity. The specimen is made to traverse normal to the direction of the belt movement so that it always abrades against unworn particles. The total abrasion distance traversed by each of the grades was 3 metres. Wear was measured by weight loss taking an average of two runs per material and the conditions employed for testing are shown in Table 3.2.1. Wear rates are expressed as volume lost per unit load per unit of abrasion distance, calculated from mass loss and density measurements.

Applied load	10 N
Nominal Contact Pressure	0.1 MPa
Abrasive Type	Al_2O_3 (Alumina)
Abrasive Belt Speed	0.26 ms^{-1}
Abrasive Grit Diameters	23μm (400 paper), 85μm (180 paper), 266μm (80 paper)

Table 3.2.1: Conditions employed for abrasion testing of the carbon-graphite grades against three different grades of bonded abrasive belt.

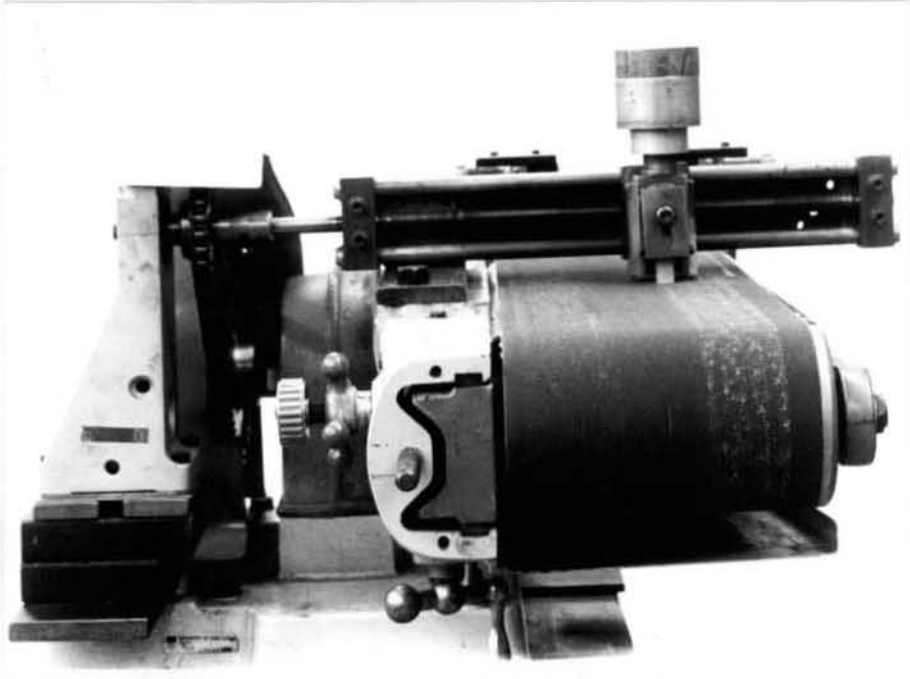

Fig. 3.2.1 The test rig used for each abrasive wear experiment. The specimen is made to traverse normal to the direction of the belt movement ensuring that it always abrades against unworn particles. The specimen is clamped in a holder which allows movement only in the vertical direction. Weights are placed above the specimen, providing a constant normal load.

Additional specimens were prepared for optical and scanning microscopy by abrading on successive silicon carbide papers and finally polishing on a 3 μm diamond wheel. These specimens were then abraded against 180 paper (85 μm grit size) and the surface morphology monitored by direct observation in the SEM.

3.3 Dry Sliding Wear

The apparatus used in the experimental investigation to be described is illustrated in fig. 3.3.1. It has been shown by Lancaster [1] that the sliding wear of carbon graphites does not follow a linear relationship with load and that excessive wear can occur at high contact pressures and sliding velocities. It was therefore necessary to run preliminary tests in order to establish a suitable

value, (i.e. product of nominal face pressure and sliding velocity), to ensure that realistic wear rates were achieved.

Testing was carried out on a pin and disc rig using a 0.25 cm^2 square carbon graphite (EY9) test piece pressed against a rotating 0.14m diameter stainless steel disc of surface roughness 0.3 μm. The speed of rotation of the disc was set at 275 rev/min corresponding to a surface speed of 2.01 ms^{-1}; excessive heating of the counterface was avoided by the use of a water cooling system which kept the underside of the disc at a constant temperature. The applied load was varied in order to provide PV values ranging from 0.1 to 0.4 MPa ms^{-1}, and the mass loss measured after each kilometre. A PV value of 0.2 MPa ms^{-1} was found to be suitable to run the tests under dry conditions. Excessive wear of the carbon pins was seen to occur at greater values of PV.

Fig. 3.3.1: The pin on disc test apparatus, (a) stationary pin slider within holder, (b) revolving 431 stainless steel counterface, (c) rev. counter, (d) rev speed control, (e) hanging weight, (f) transducer, (g) chart recorder.

In order to ensure full facial contact between the slider and the counterface all specimens were "run-in" against an abrasive counterface (1200 grit), cleaned

ultrasonically in alcohol and air dried prior to testing. Care was taken at all times to preserve the integrity of any compacted debris layer on the specimen surface.

Once suitable parameters for load and velocity were found, dry sliding wear rate tests were run over the range of carbon graphite grades. The speed of rotation was set at 275 rev min^{-1} (2.01 ms^{-1}), and the load applied was 1.0 kg. Friction and mass loss measurements were taken over the course of each test. Counterface roughnesses of 0.1μm, 0.3μ, 0.8μm and 1.5μm (Ra) were used to establish a relationship between dry sliding wear rate and surface roughness.

The frictional force generated at the sliding interface is transmitted via a brass bolt which presses against a pressure monitoring transducer. This signal is then transmitted through to a chart recorder which converts the signal to a voltage. The transducer calibration was performed by Marcus [64] and is represented by the following equation.

$$F = \frac{V \times 110}{2.8} - 0.07$$

Where:
- F = frictional force generated at the interface
- V = voltage

Wear rates were calculated from cumulative mass loss measurements averaged over the sliding distance in the steady state wear regime. Scanning electron microscopy was employed to establish wear modes and to monitor the development of transfer films.

3.4 Dry Particle Erosion

A conventional gas stream erosion rig was used to effect dry particle erosion on the various carbon grades. A schematic diagram of the test rig is shown in fig. 3.4.1. Compressed air is fed into the inlet tube via a compressed air regulator (A). Erodent particles (120 μm, SiC) are fed through a vibratory hopper (B) into the air stream via a venturi valve (C). The particles accelerate in

the air stream along a 3 m (10 mm diameter) stainless steel tube where they reach an exit velocity of 40 ms^{-1}. The 1 cm^2 target was orientated at 45° with respect to the air stream (D). The air leaves the erosion chamber (E) and spent particles are collected (F).

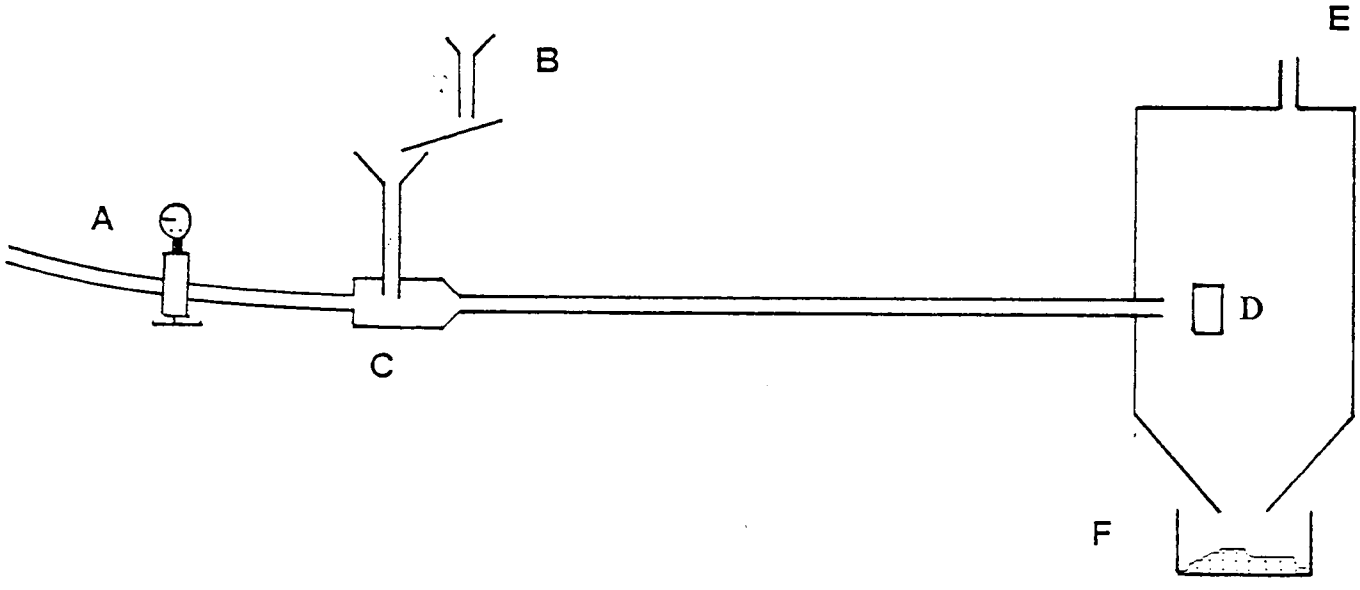

Fig. 3.4.1: Schematic showing the air-blast type erosion rig used for solid particle erosion testing of each material

All tests were conducted using the same airstream pressure, corresponding to an average particle velocity of 40 ms^{-1}. The particle velocity was determined using the double rotating disk method of Ruff and Ives [58] and is further explained in appendix (i).

The target specimens were ground to a 1200 grit finish on successive silicon carbide papers, cleaned ultrasonically in alcohol and air-dried prior to testing. Mass losses of the specimens were measured after receiving each 20 g dose of erodent and erosion rates were calculated from the steady state regions on plots of cumulative volume loss as a function of total erodent mass.

Energy dispersive spectroscopy (EDS) was used to identify and to distinguish between target and erodent debris in the impact sites.

Single Impact Testing

In order to study the morphology of single impacts on target surfaces, specimens were polished to a 1 μm finish using diamond paste and were subjected to erosion with <0.3 g of erodent. The lightly eroded surfaces were then examined in the SEM.

3.5 Slurry Erosion

A schematic view of the equipment used to produce slurry erosion is shown in fig. 3.5.1. The driving fluid is circulated from a holding tank and fed to the ejector by centrifugal pump. A low pressure region created inside the ejector causes a mixture of carrier fluid and erodent particles to be drawn up through a vertical tube, this is further mixed with the driving fluid and the resulting slurry is accelerated through the exit nozzle to strike the specimen surface. After impact the erodent particles settle in a slurry-tank while the carrier fluid flows through a filter back into the holding tank.

Impact velocity	6.5 ms^{-1}
Erodent type	500 μm silica sand
Erodent concentration	12 % by mass
Impact angle	90°
Carrier fluid	Distilled water

Table 3.5.1: Conditions employed for slurry erosion testing of the various carbon-graphite grades.

Test procedure

Each individual test was conducted with fresh erodent, to ensure that any degradation and particle blunting of the silica sand is insignificant. Test specimens were ground to a 1200 grit finish using successive silica papers and cleaned prior to testing. Worn targets were air-dried and weighed at regular intervals in order to obtain mass losses. The results are expressed as cumulative volume loss, calculated from the mass loss and density measurements.

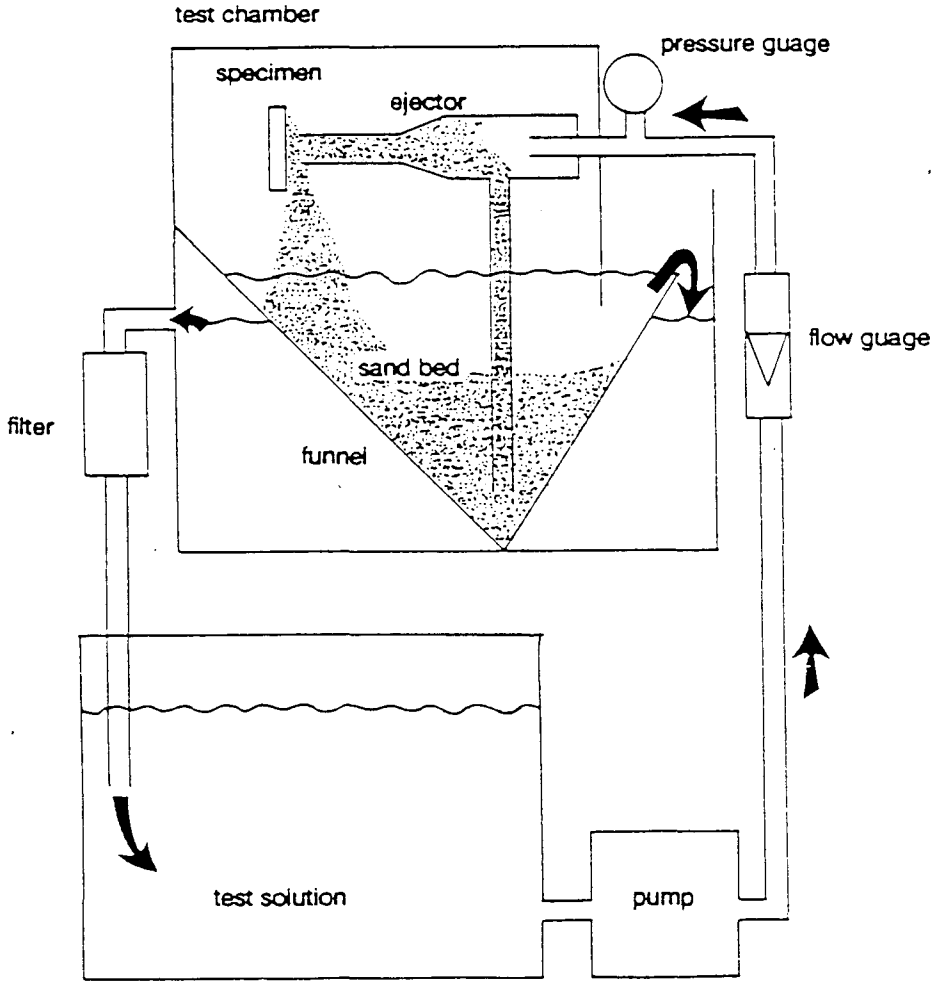

Fig. 3.5.1: The slurry erosion test apparatus (from Bester [46])

3.6 Cavitation Erosion

A schematic diagram showing the vibratory cavitation erosion test employed to induce cavitation erosion wear in the test samples is shown in fig. 3.6.1. The apparatus consists of an piezoelectric transducer vibrating at a frequency of approximately 20 kHz. The oscillations produced are amplified by a horn by a factor of approximately 3.5. Specimens are clamped beneath the drill tip and immersed in a bath containing distilled water. Optimum cavitation erosion with this test configuration has been shown by Heathcock [54] to occur for wear surfaces situated 0.35 mm from the drill tip, for this reason the separating distance was set at this value and reset after each weighing.

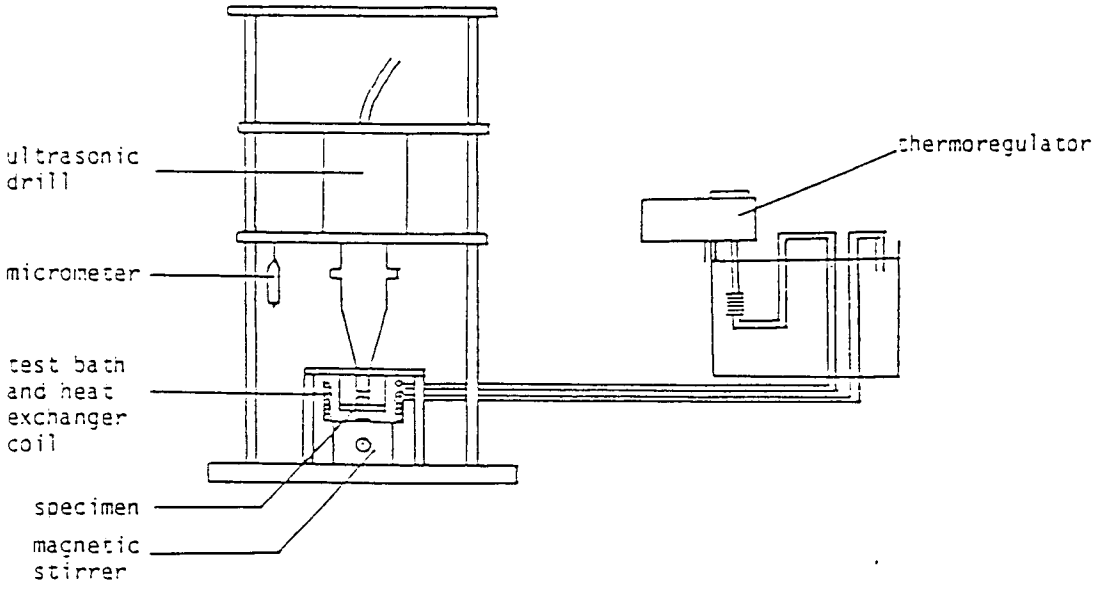

Fig. 3.6.1: Schematic showing the vibratory cavitation erosion rig configuration. The apparatus consisted of an ultrasonic drill (18.5 - 20 kHz) below which the specimens to be eroded are clamped and submerged in a bath of distilled water. (After Heathcock [61])

Distilled water was used as the cavitating liquid and was kept at a temperature of 25°C by a thermostat/cooling coil arrangement. Target surfaces were prepared

to a 600 grit finish using SiC papers and each specimen was eroded and weighed at regular intervals until specimen failure, additional tests were performed using finely polished target surfaces in order to see the effect of surface finish on erosion rates. Cavitation erosion rates were determined from the steady state regions of cumulative volume loss and erosion time plots.

Topographical changes of the worn specimen surfaces were monitored using scanning electron microscopy. Subsurface damage was studied by the use of taper sections of eroded surfaces.

CHAPTER 4

RESULTS

4.1 Abrasive Wear

The abrasive loss results, after an abrasion length of 3.66 m are summarised in fig 4.1.1. Wear rates are given as volume loss per unit load per unit of abrasion distance and have the units :-

$$mm^3/Nm$$

The electrographite and the more highly graphitic plain carbons exhibited significantly higher abrasive wear rates than the impregnated grades. A similar trend in wear rates was noted for all grades of abrasives. From a grit size of 23 μm to 85 μm all materials displayed significant increases in wear rates; however the change in wear rate from 85 μm to 266 μm was less pronounced.

Research into the abrasive wear behaviour of various polymers, using a similar test configuration and conditions, was performed by Böhm, Betz and Ball [26]. Abrasive wear rates varied from 0.14 mm^3/Nm to 0.5 mm^3/Nm in the different polymeric materials. In comparison, the carbon-graphite materials exhibited poor wear behaviour with abrasive wear rates varying from 0.2 mm^3/Nm in the antimony impregnated material to 2.7 mm^3/Nm for the electrographitic grade.

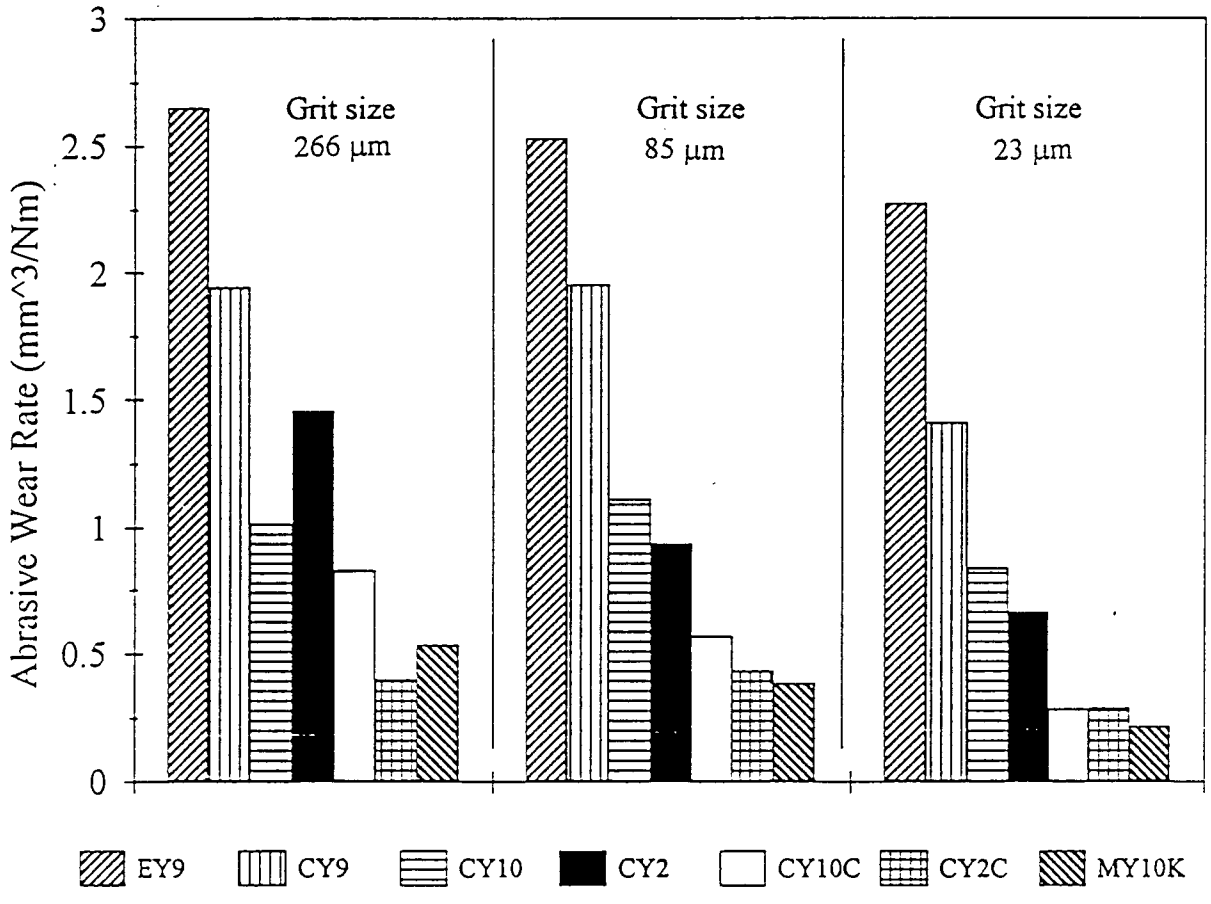

Fig. 4.1.1: Abrasive wear rates for each carbon grade (grit sizes 266µm, 85 µm, 23 µm)

Surface Damage of the Abraded Materials

Scanning electron microscope observation of the worn surface of the various carbon grades produced qualitative information on the nature of the surface damage.

The low hardness, low toughness plain carbons and the electrographite suffered extensive fragmentation at the groove edges and showed negligible build up of material as seen in figs. 4.1.2 and 4.1.3. Conversely, the antimony impregnated grade shown in fig. 4.1.4 and to a much lesser extent the epoxy filled carbons exhibited evidence of ploughing and there was appreciable material pile up

along the trough edges. Fewer microcracks were seen with the tougher filled carbons, although there is evidence of ductility the mode of material loss is predominantly brittle.

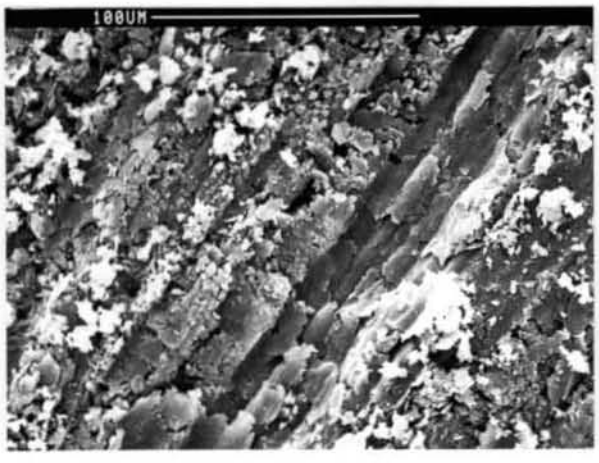

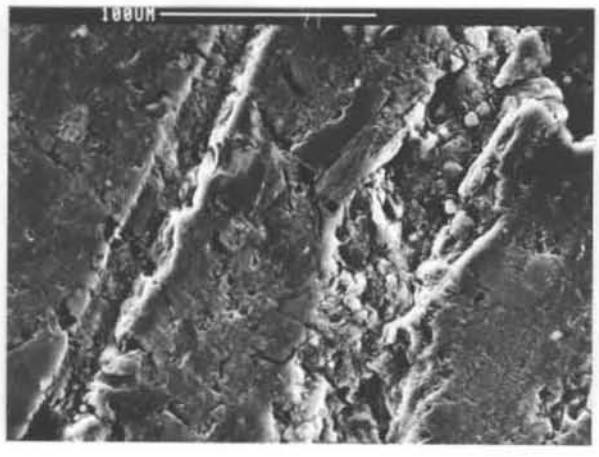

Fig. 4.1.2 (left): The abraded surface of electrographite EY9 (grit size 85 μm)
Fig. 4.1.3 (right): The abraded surface of plain carbon CY10C (grit size 85 μm)

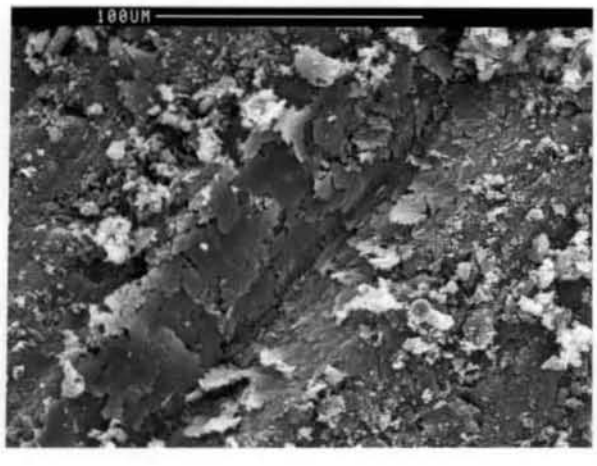

Sliding Direction of carbon

Fig. 4.1.4: The abraded surface of antimony impregnated carbon MY10K (grit size 85 μm)

The Relationship Between Abrasive Wear and Mechanical Properties

a) The Effect of Hardness on Abrasive Wear

The results shown in figs. 4.1.5 and 4.1.6 indicate that there is a general trend of increased abrasive wear with reduced scleroscope hardness. The harder

epoxy and antimony impregnated carbons exhibited greater resistance to indentation from the abrasive particles and consequently displayed a superior wear rate to that of the plain carbons and electrographite.

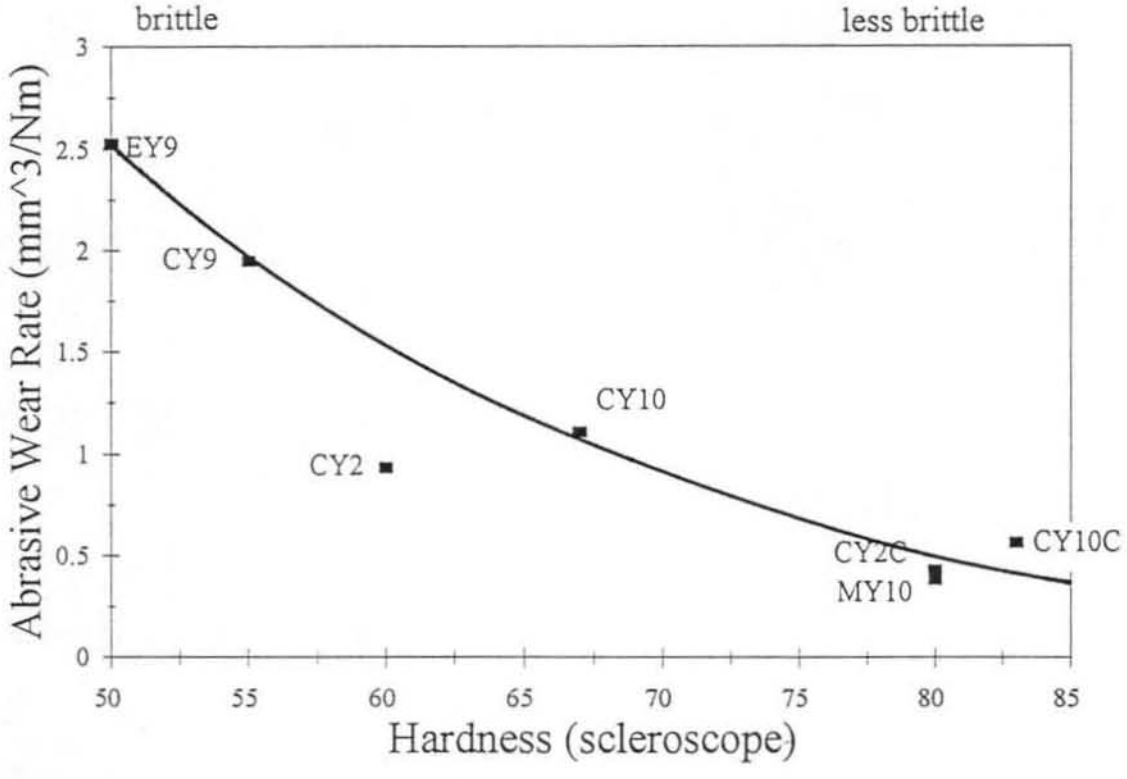

Fig. 4.1.5: Mean abrasive wear rate as a function of hardness for each grade (grit size 23 μm)

The $\log_{10}$ graph shown in fig. 4.1.6 illustrates the way in which the volume displaced per unit distance of sliding varies with scleroscope hardness. Although there is a considerable amount of scatter an inversely proportional relationship is apparent. The slope of the best straight line is however significantly larger than -1 reported by Lancaster [21] in his investigation into the wear behaviour of carbons against rough metal surfaces and is in fact equal to -3.5. He did however use Vickers hardness in his investigation and as there is no direct correlation between Vickers and Scleroscope hardness a true comparison cannot be made. The ranking of the various grades is however

similar in both studies with the softer electrographitic materials exhibiting inferior wear rates and the impregnated grades showing the best properties.

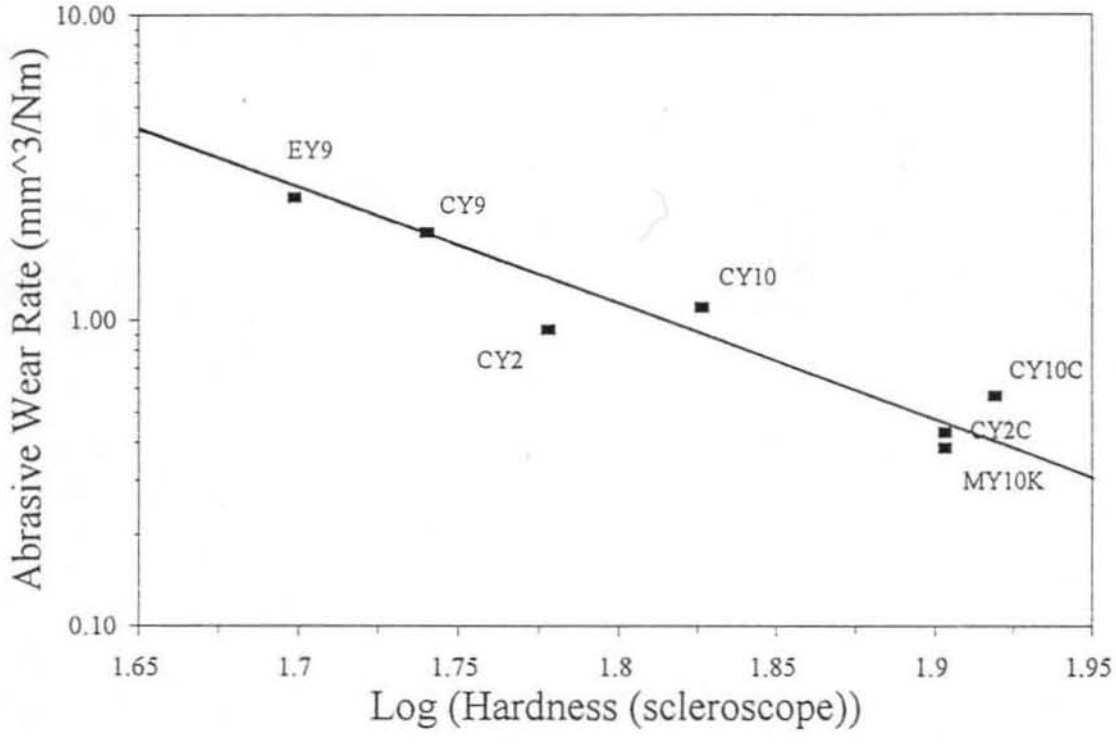

Fig. 4.1.6: Graph showing the variation of mean abrasive wear rate with hardness for each grade (grit size 23 μm)

b) The Effect of Elastic Modulus

The results shown in fig. 4.1.7 reveal an inverse correlation between the elastic modulus and the abrasive wear rate of the various carbon grades. Those materials with higher elastic moduli (CY2C, CY10C and MY10K) consistently produced lower wear rates than the electrographitic and plain carbon grades. The size of the abrasive grit used in this these tests is sufficiently large to exceed the elastic criterion for brittle fracture of all the carbon grades and the amount of elastic recovery is therefore presumed to be negligible. The ability of

the impregnated grades to deform plastically may explain their superior wear resistance.

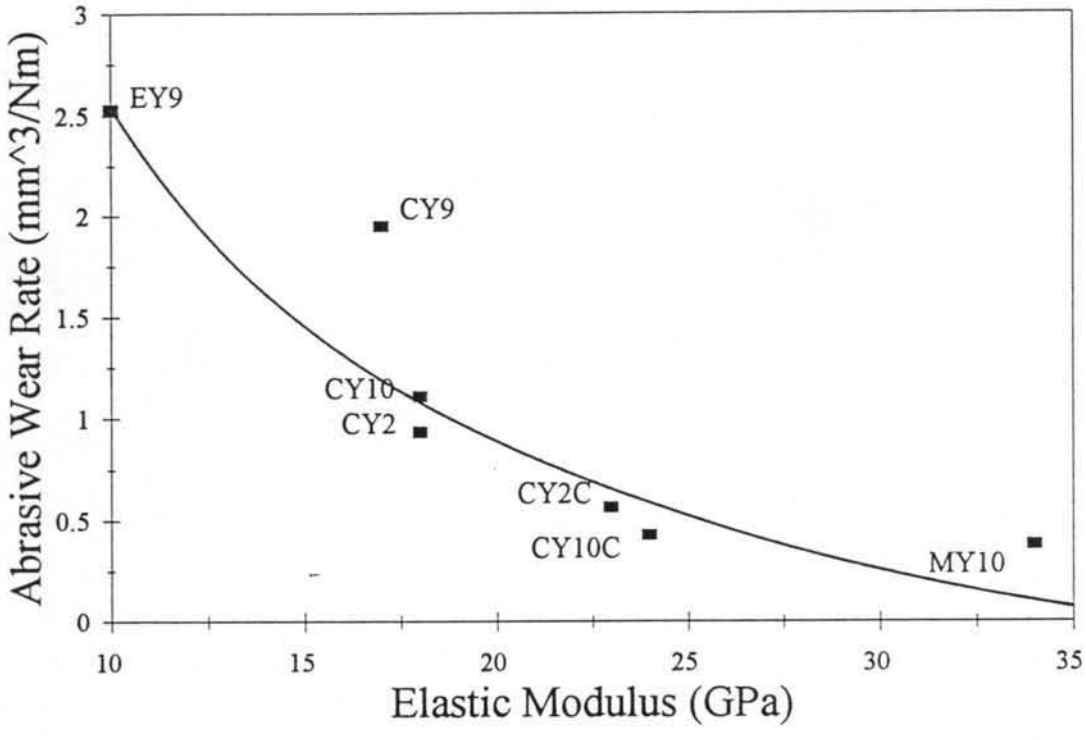

Fig. 4.1.7: The variation of abrasive wear rate of carbons on alumina with their elastic moduli (grit size 85 μm)

The Variation of Abrasive Wear Rate with Grit Size

The graph shown in fig 4.1.8 illustrates the way in which the rate of wear varies with grit size for the range of carbon-graphites sliding on alumina.

It can be seen that from a grit size of 23 μm to 85 μm, all materials displayed significant increases in abrasive wear rates, EY9 increased 14 %, CY9 by 40 % and MY10K's wear rate increased by 75 %. Against larger abrasive particles however, grit size appears to have a less pronounced effect; the wear rates of EY9 and MY10K increased by 2.5 % and 42 % respectively, whilst CY10 showed improved wear resistance and decreased by 10%. In general the volume

displaced per unit distance travelled was of a similar value against 85 μm and 266 μm abrasive particles.

It is suggested that at this level of abrasive diameter (>23 μm) the majority of the grits exceed the elastic criterion required for brittle fracture. The effects of grit size and grit density cancel each other out giving similar wear rates for all three sizes. There is evidence to support this in the paper by Porgess and Wilman [22] (fig. 2.2.), they observed very little increase in wear rate for grit sizes above 40 μm but a dramatic reduction as it falls to less than 10 μm.

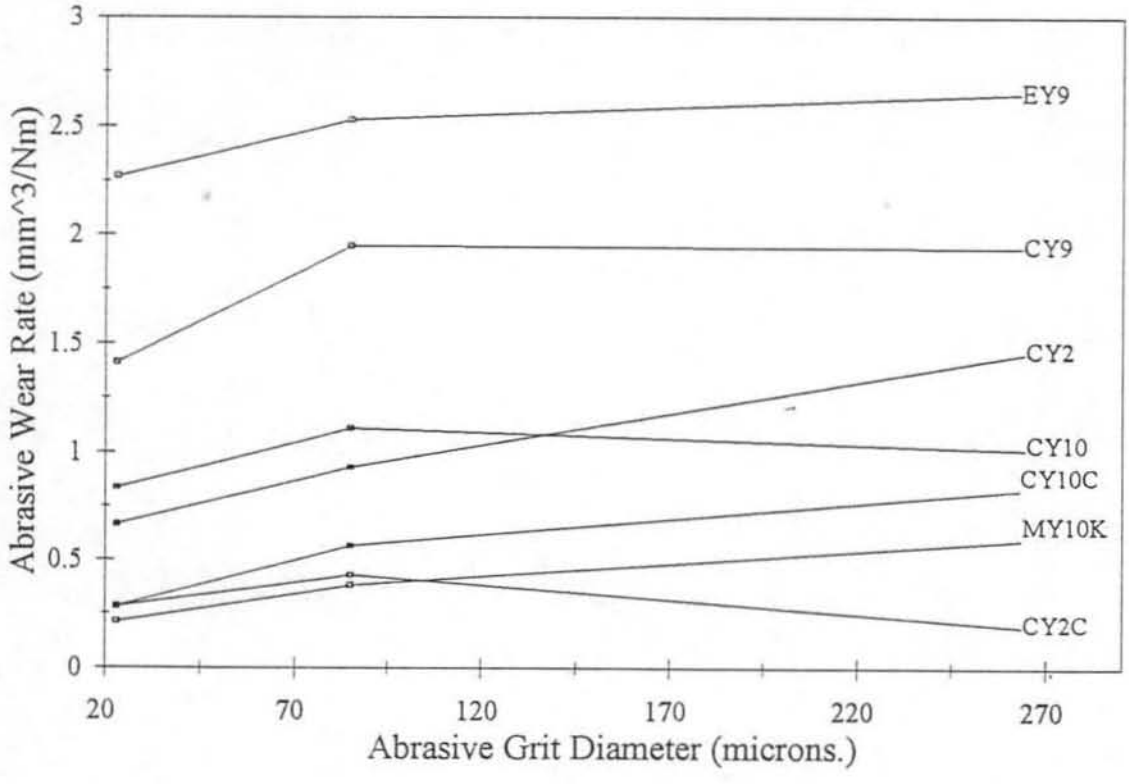

Fig. 4.1.8: Mean abrasive wear rate as function of abrasive particle diameter for each carbon grade

4.2 Dry Sliding Wear

Wear Studies on 0.3 µm Counterfaces

The variation in volume loss for a selection of carbon-graphite materials with sliding distance is shown in fig. 4.2.1. The graphs show that the wear pattern for all materials tested was similar, initially the wear rate is high but this falls with increasing sliding distance until a steady state wear regime is established, generally after several thousand metres. This pattern, shown diagramatically in fig. 4.2.2 can be fitted by the empirical equation:

$$\frac{V}{Px} = ax^b \qquad \text{equation (1)}$$

taking logs:

$$log\ (wear\ rate) = log\ a + b\ log\ x \qquad \text{equation (2)}$$

Where :-

- V = Volume lost by wear
- P = Normal load
- x = Sliding distance
- a, b = constants

Equation (1) is derived from the Archard equation which is of the form:

$$V = kPx$$

Where :-

- k is the dimensional wear coefficient [18]

The dry sliding wear studies using carbon-graphite material have shown that k is not constant but:

$$k = ax^b$$

where :- $b < 0$

so k falls with x

Equation (1) suggests that when the sliding distance x becomes very large the wear rate falls to effectively zero.

For very large sliding distances the data could be fitted more accurately using the equation:-

$$\frac{V}{Px} = ax^b + c$$

Where :- • $a >> c$ In the initial stages of sliding the first term dominates but as the sliding distance x increases the second constant wear rate term becomes more significant.

The sliding distances covered in this study however are not sufficiently high and the data can be fitted to equation (1) with a high degree of accuracy. Values for **a** and **b** are given in Table A1 (appdx.) and are shown graphically in figs. 4.2.11, 12, 13 and 14

Plotting the wear data in this manner has the advantage that the greater wear rate at the start of each run is emphasised. The reason for this behaviour is believed to be due to the process of transfer film formation in the early stages of sliding wear and a subsequent decrease in the abrasive component of the asperities of the metal counterface. During steady state wear, a transfer film completely covers the metal counterface as shown in figs. 4.2.5, 6 & 7.

It can be seen that within the normal speed and load application range, wear tended to be lower in the resin and metal impregnated grades. The electrographitic grade (EY9) showed a steady state wear rate that is an order of magnitude higher that of the antimony grade.

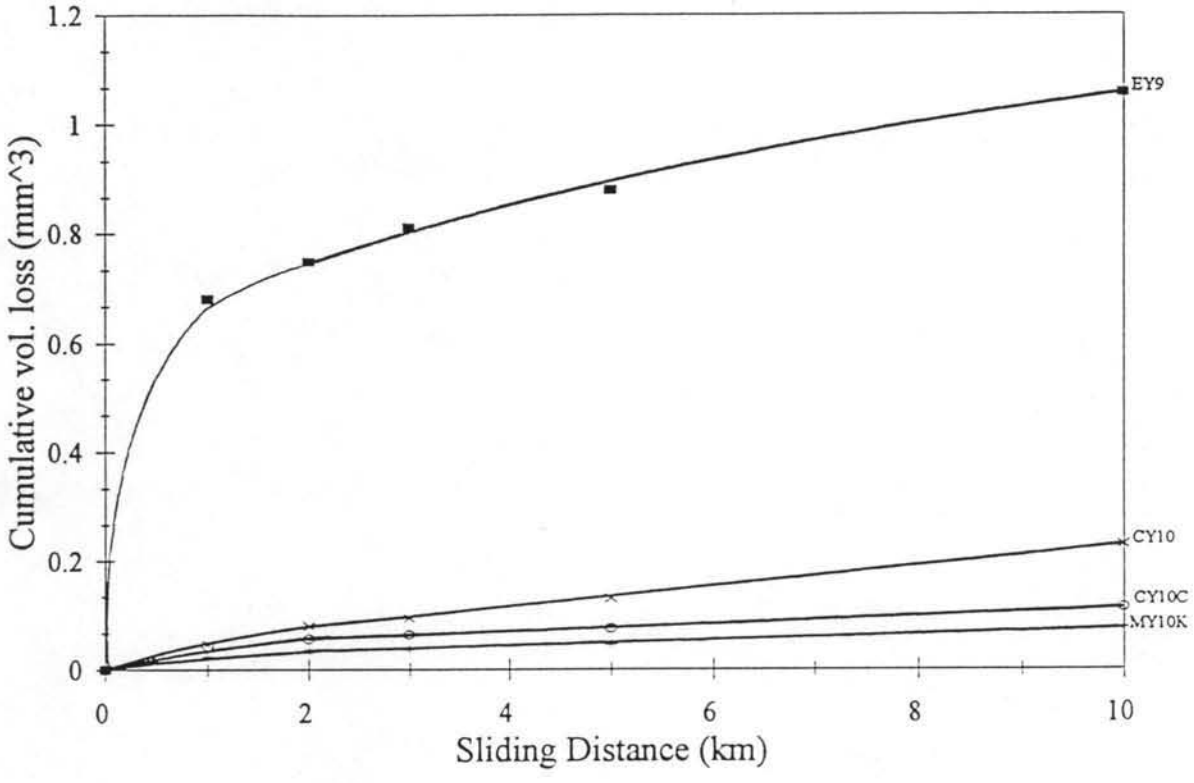

Fig. 4.2.1: Cumulative volume loss (mm^3) plotted as a function of sliding distance (km). Surface roughness (Ra):- 0.3μm

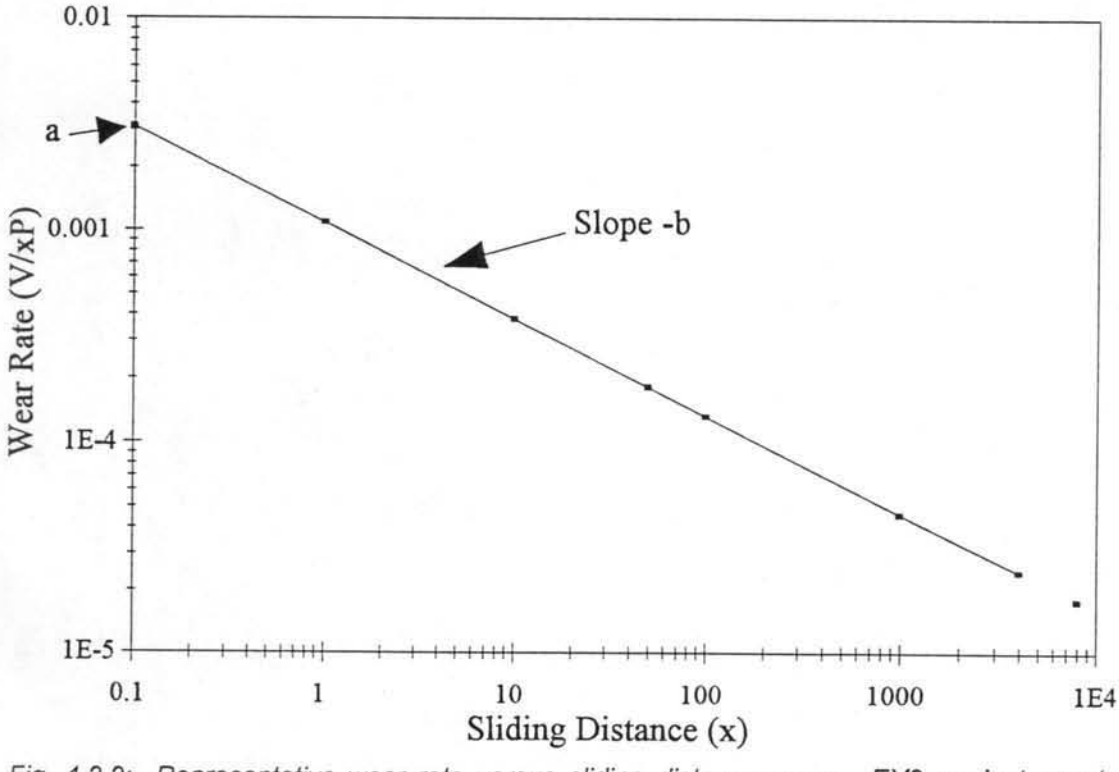

Fig. 4.2.2: Representative wear rate versus sliding distance curve. EY9 against counterface roughness (Ra):- 0.3 μm

Examination of the wear surfaces and worn counterfaces reveal a difference in behaviour between the carbons, both filled and unfilled, and the electrographites. The worn surface after 30 metres of sliding shows longitudinal grooving with little evidence of delamination. As the sliding distance increases, the surface layer grows smoother and there is evidence of crazing (fig. 4.2.3). Manufactured carbons inevitably contain hard impurities and if these are released during sliding three body abrasion may occur. This was particularly apparent in the electrographitic grade EY9 which suffered considerable chipping at the interface as shown in fig. 4.2.4 and partly explains its' inferior wear rate.

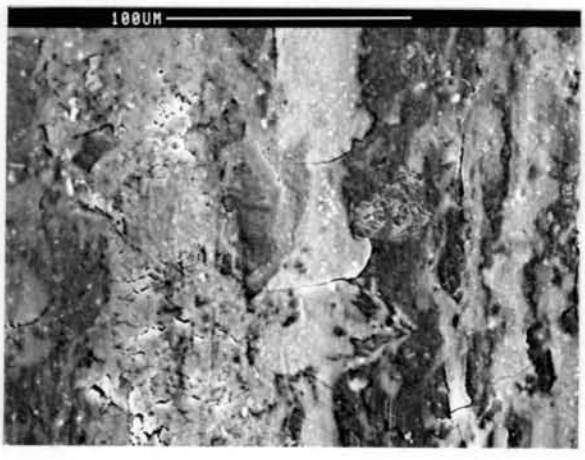

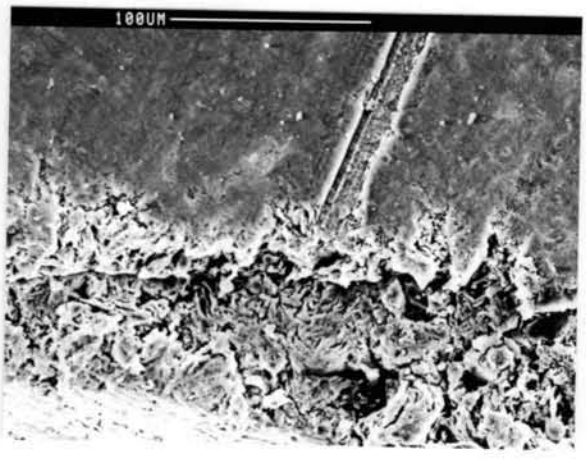

Fig. 4.2.3 (left): The wear surface of EY9 after 3000m sliding (Ra = 0.3μm). Note the smooth compacted layer and evidence of crazing

Fig. 4.2.4 (right) SEM micrograph showing chipping at the leading edge of EY9 electrographite specimen after 30 metres dry sliding wear (Ra = 0.3 μm)

Transfer Layer Formation

The stages in the development of transfer films for EY9, CY2 and CY2C are shown in figs. 4.2.5, 4.2.6, and 4.2.7. Transfer layers were found to occur most readily from plain and graphitic carbons. After 3000m sliding fully developed films were observed as seen in figures 4.2.5.c and 4.2.6.c. Conversely counterface asperities were still in evidence for the impregnated grades

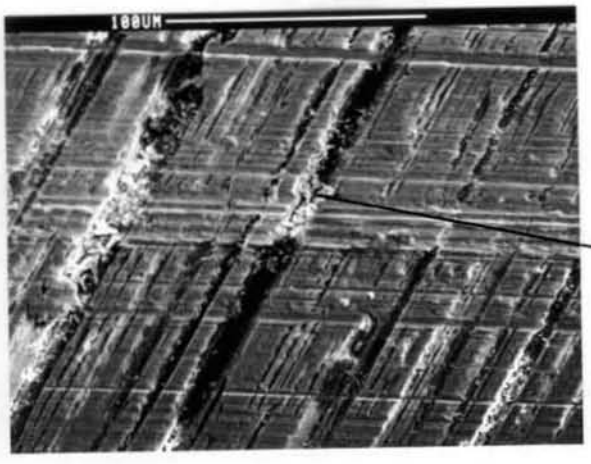

Sliding Direction

Wear debris already starting to fill troughs in counterface surface

a.) 30 m sliding: wear debris build up in the counterface irregularities

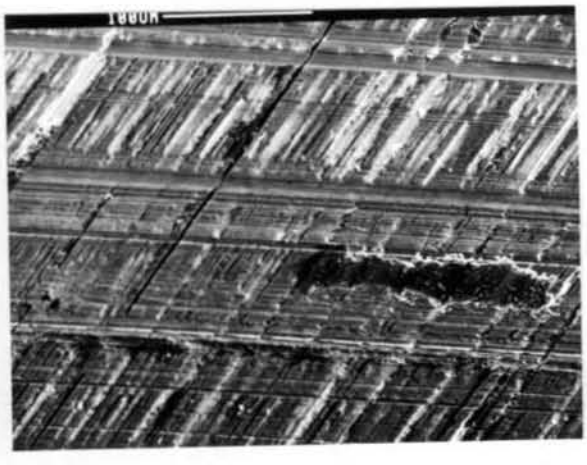

b.) 300 m sliding: development stage. Wear debris compaction on the counterface surface. A delaminated flake is apparent on transfer film surface

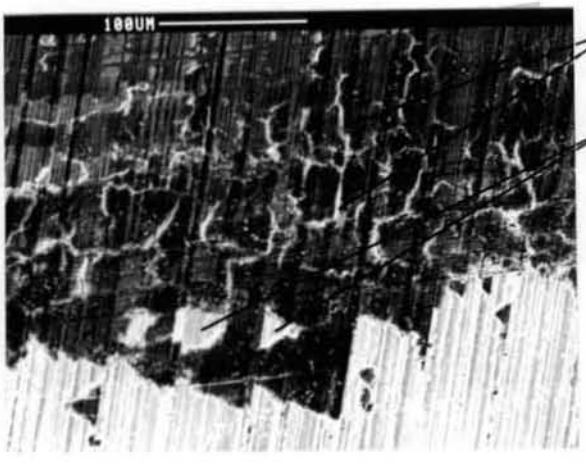

Discontinuities in transfer film display evidence of crazing

Plucked area of transfer film

c.) 3000 m sliding: detail of established transfer film. The film appears incoherent with evidence of cracks and crazing. "plucked" regions can also be observed

Fig. 4.2.5: Development of transfer film on stainless steel counterface for CY2 electrographite (Ra = 0.3μm)

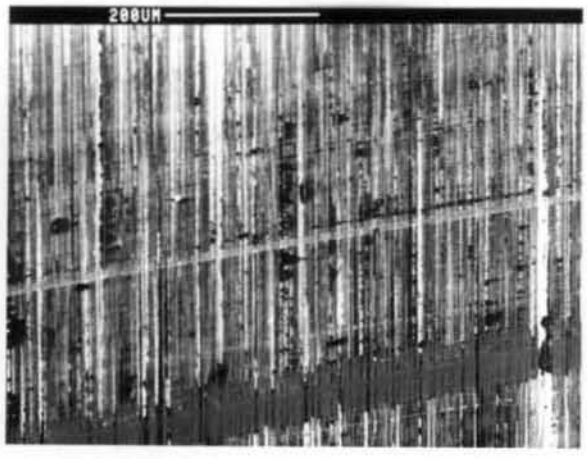

Sliding Direction

a.) 30 m sliding. Initiation phase of transfer layer formation

several carbon wear tracks have formed on the counterface surface

b.) 300 m sliding. Development of transfer layer

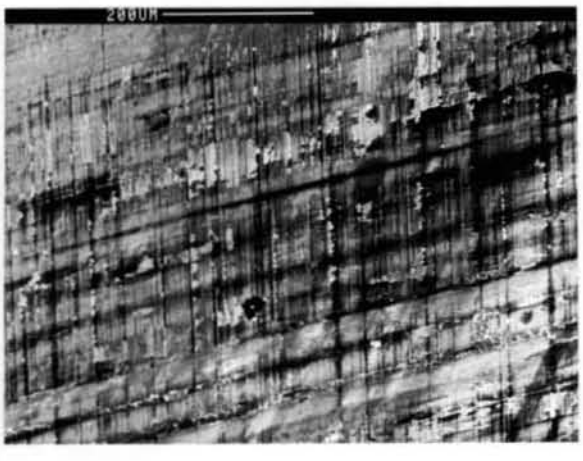

c.) 3000 m sliding. Fully established transfer layer, all asperities appear to be "buried" by the film

Fig. 4.2.6: Development of transfer film on stainless steel counterface for EY9 electrographite (Ra = 0.3 μm)

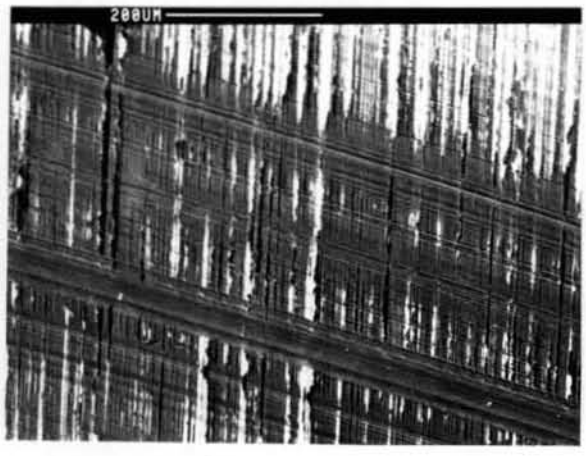

← *Sliding Direction*

a.) 30 m sliding

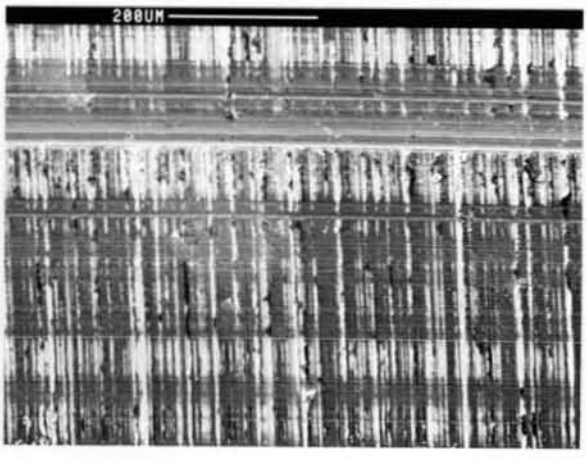

b.) 300 m sliding

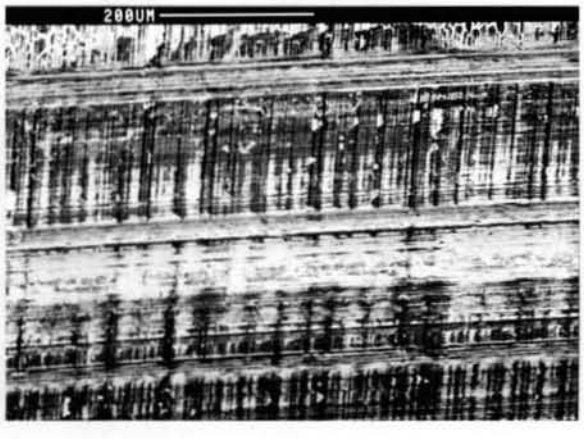

c.) 3000 m sliding. Counterface asperities not fully covered indicating that the transfer film is not yet fully established

Fig. 4.2.7: Development of transfer film on stainless steel counterface for CY2C electrographite (Ra=0.3µm)

suggesting that the film is not yet fully established (fig. 4.2.7.c). The comparatively large amount of debris the unfilled carbons produce is readily transferred to the metal counterface filling in the troughs and valleys on its surface as seen in figs. 4.2.5 a) and b). Initially the mode of wear appears to be predominantly abrasive, however rapid modification of the steel surface soon leads to the development of a steady state wear regime. After 300 metres the abrasive component of the counterface asperities is lessened and there is evidence of sheets of material adhering to the counterface (shown in fig. 4.2.5.b). After several thousand metres of sliding, wear by the delamination of sheets of material seems to be the dominant mechanism in all the carbon grades. These sheets may be swept away or entrained in the contact depending on the particular geometry involved.

Material loss was also observed from the transferred layer. In fig 4.2.5.c it can be seen that crazing of the film has occurred and that regions are apparent where sheets of material have been removed. Regions within the film continually flake off and reform and for this reason the wear rate doesn't approach zero. It is suggested that similar fatigue processes occur in the transfer layer as in the sliding specimen. Transfer layers were evident for all the grades of carbon tested; however the plain and electrographitic carbons generally established thicker films within shorter sliding distances.

The Effect of Small Changes in Counterface Roughness, Ra, on Wear Rates

In order to determine the effect of relatively small changes in counterface roughness, Ra, tests were conducted on counterfaces of controlled Ra values both rougher and smoother than the 0.3μm Ra initially selected for the wear tests. In figs. 4.2.8 to 4.2.10 the cumulative volume losses are plotted as a function of sliding distance for the various surface roughnesses.

The wear pattern against all counterfaces was similar to that observed against the 0.3μm Ra surface with the mean wear rate decreasing with sliding distance,

the filled grades showing superior wear resistance to dry sliding wear than the plain and electrographitic grades. All materials suffered moderate increased volume losses against rougher surfaces, the exception was EY9, which was greatly influenced by changes in Ra. Against the roughest surfaces, the test piece completely abraded away before a mass loss measurement could be made after 5 km.

The coefficients a and b in the equation $\frac{V}{Px} = ax^b$ were obtained by linear regression for each wear test, the values of which are shown in appendix (ii). The values of b (slope) lie in the range -0.15 to -0.67 and initial wear rates (a) vary significantly from 1.7×10^{-2} to 8.0×10^{-5} mm^3/Nm.

The variations in a give rise to widely differing wear rates at low sliding distances, but diminishes in importance at greater sliding distances. The major effect of surface roughness is therefore the slope of the wear rate distance curve ie. the value of b as indicated in table A1. and figs 4.2.11, 12, 13 & 14. The initial wear rates of all the materials tested showed an upward trend with increasing counterface roughness; conversely the slope of the graphs of the impregnated grades decreased with increasing counterface roughness. This effect was less pronounced for the plain carbons and electrographite.

Against all counterface roughnesses the initial wear rates of CY10, CY10C and MY10K were within two orders of magnitude of each other and converged to within one order of magnitude once a steady state wear regime had been established suggesting that the importance in choice of carbon grade as a bearing partner diminishes once a transfer layer has formed. The transfer film of the electrographitic grade (EY9), although thicker, appears to be less mechanically coherent and consequently a a steady state wear regime was not established against the rougher counterfaces. For this reason the wear rates against the counterfaces of surface roughness 1.5 μm and 0.8 μm did not approach those of the smoother surfaces (0.1 μm and 0.3 μm) after 8000m.

The wear rates after 500m and the steady state wear rate after 8000m were established for the carbon grades and plotted as a function of surface roughness

(figs. 4.2.15 and 4.2.16). It can be seen that the unfilled carbons were most susceptible to changes in surface topography. The steady state wear rate of EY9 increased by two orders of magnitude from the smoothest to roughest surfaces, whilst the impregnated grades were largely unaffected and within the range of experimental error. In all cases the wear rate after 500 metres was significantly higher than the steady state wear rate, sometimes by an order of magnitude. This is due to the establishment of a surface layer after greater sliding distances.

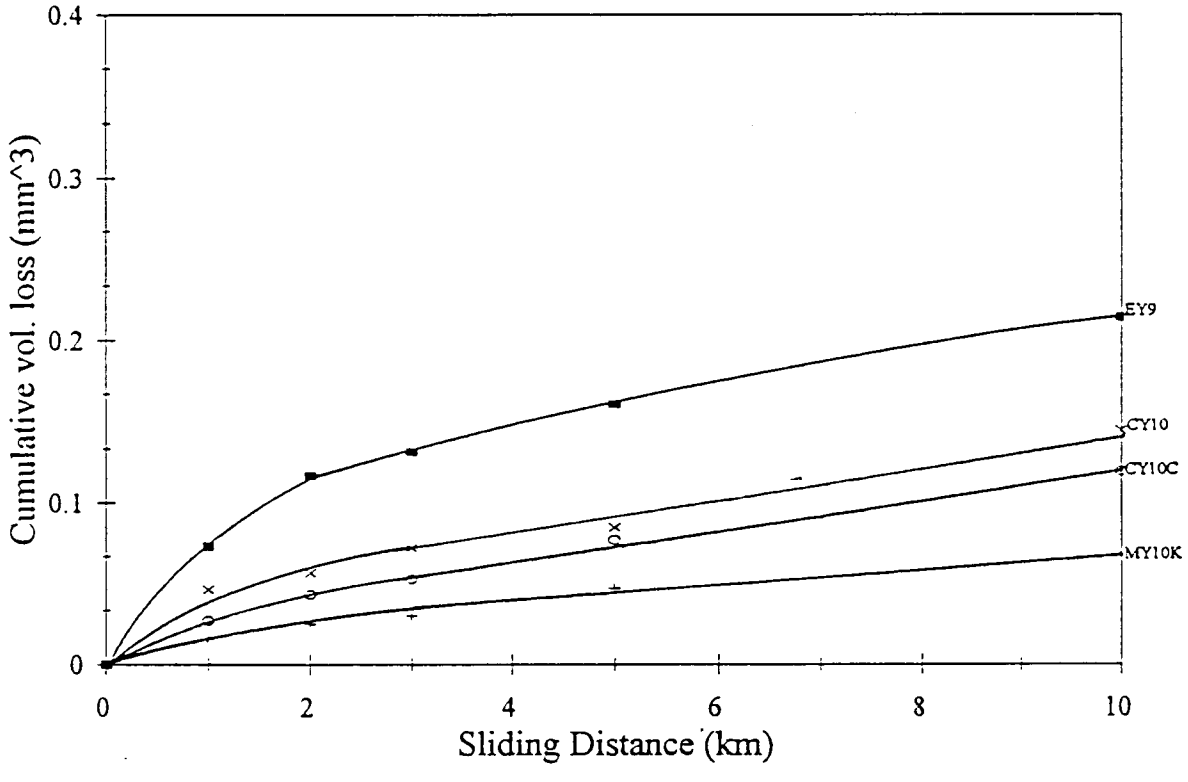

Fig. 4.2.8: Cumulative volume loss (mm^3) plotted as a function of sliding distance (km). Surface roughness (Ra):- 0.1μm

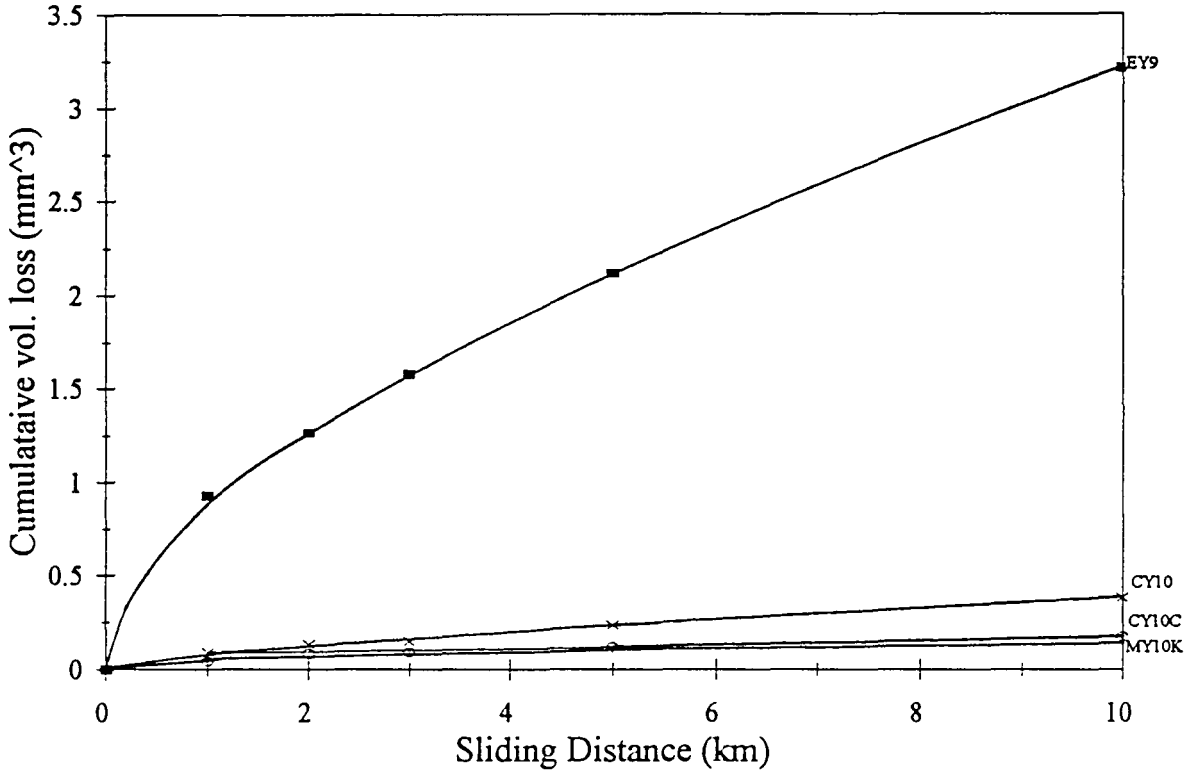

Fig. 4.2.9: Cumulative volume loss (mm^3) plotted as a function of sliding distance (km). Surface roughness (Ra):- 0.8μm

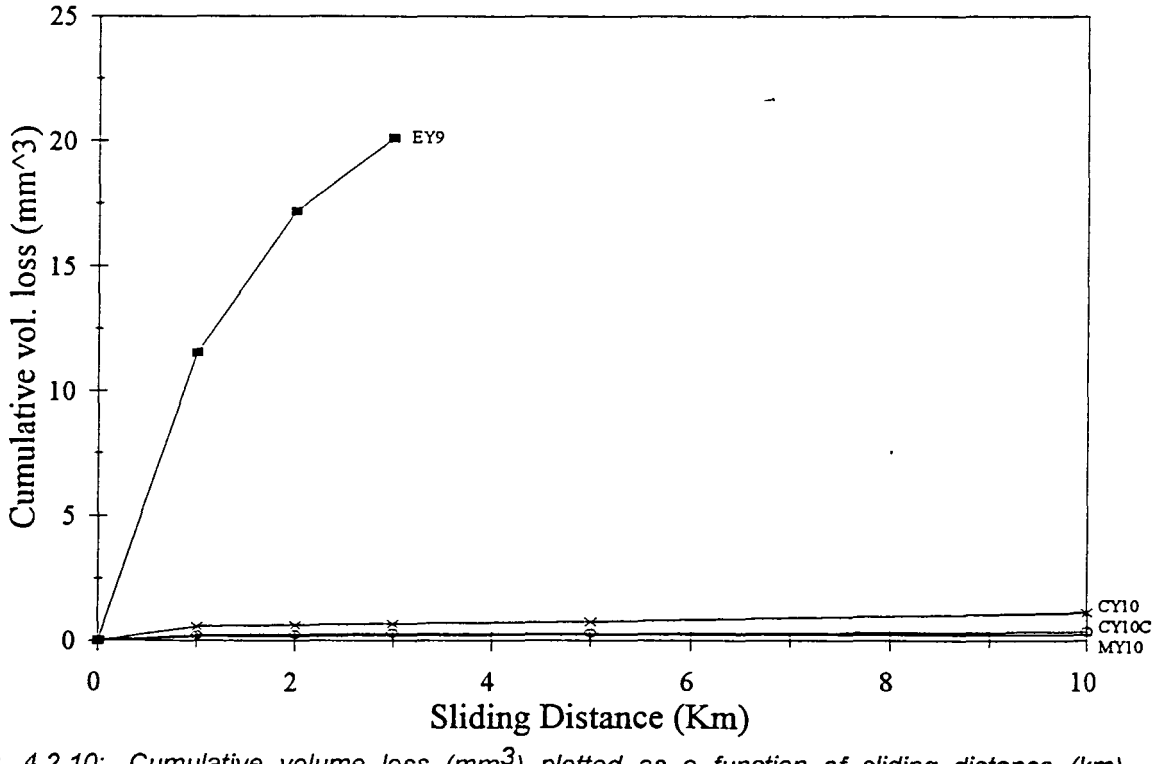

Fig. 4.2.10: Cumulative volume loss (mm^3) plotted as a function of sliding distance (km). Surface roughness (Ra):- 1.5μm

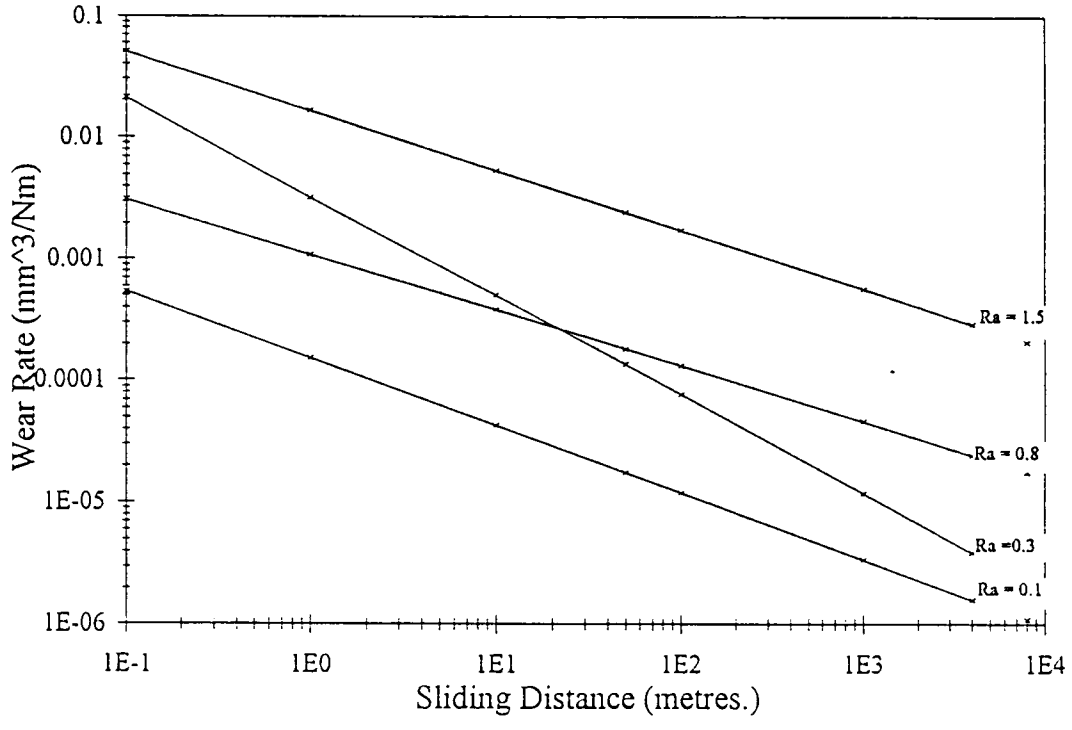

Fig. 4.2.11: Wear rate versus sliding distance curve for EY9 against counterfaces of surface roughness Ra 0.1 to 1.5

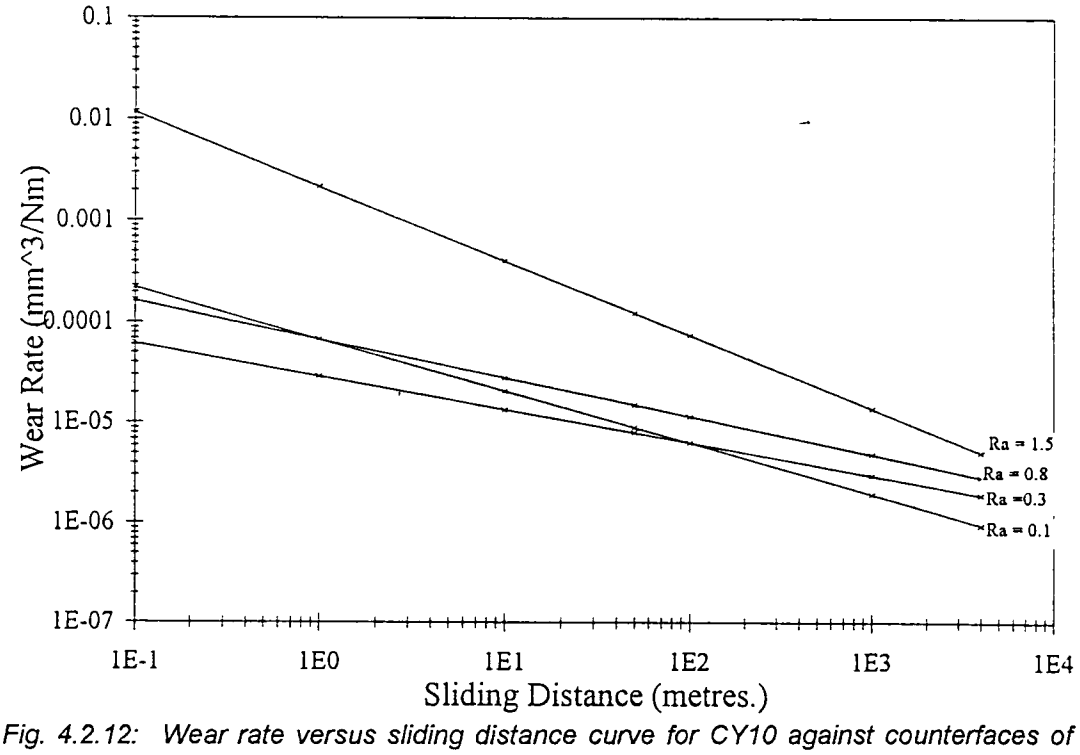

Fig. 4.2.12: Wear rate versus sliding distance curve for CY10 against counterfaces of surface roughness Ra 0.1 to 1.5

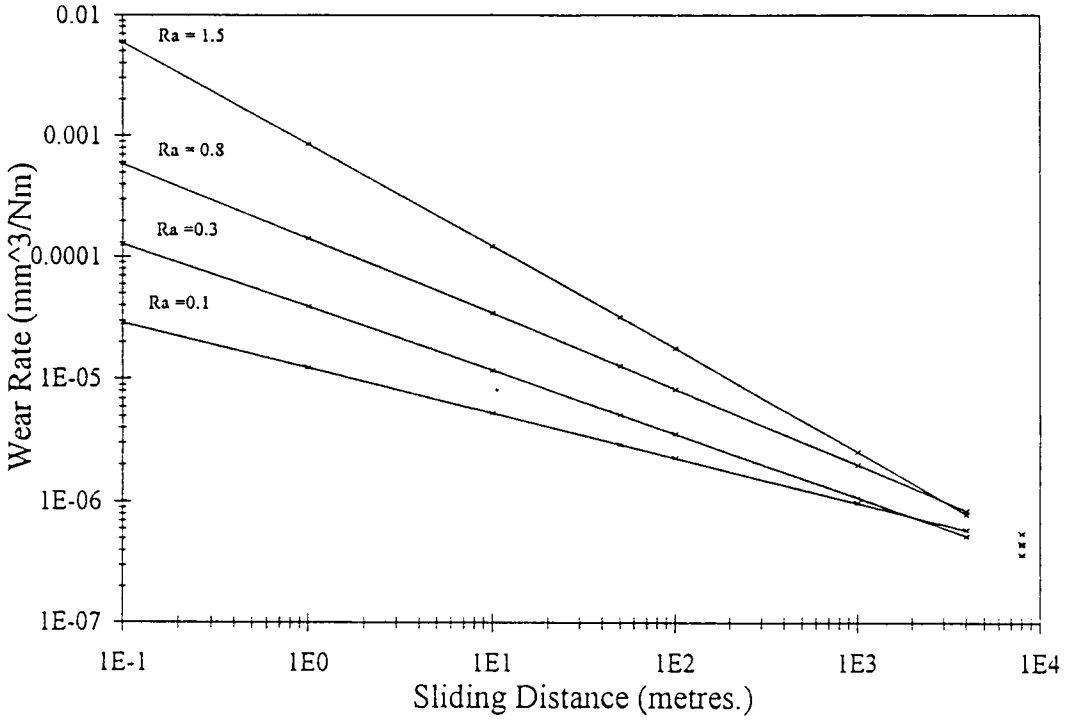

Fig. 4.2.13: Wear rate versus sliding distance curve for MY10K against counterfaces of surface roughness Ra 0.1 to 1.5

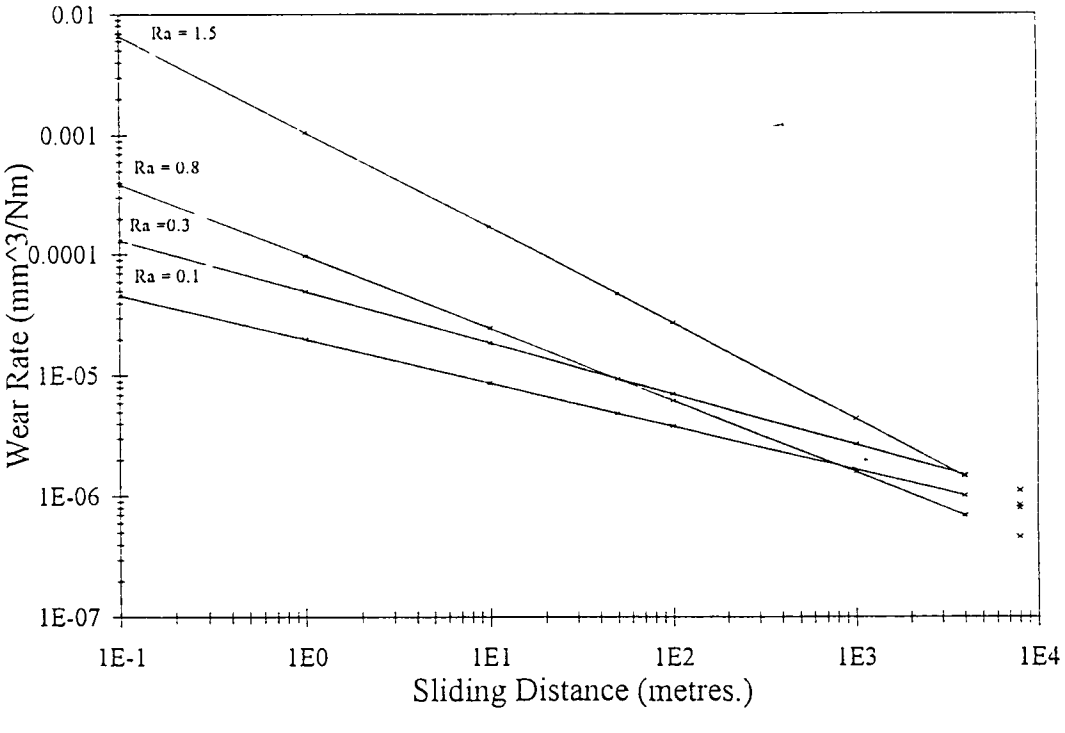

Fig. 4.2.14: Wear rate versus sliding distance curve for CY10C against counterfaces of surface roughness Ra 0.1 to 1.5

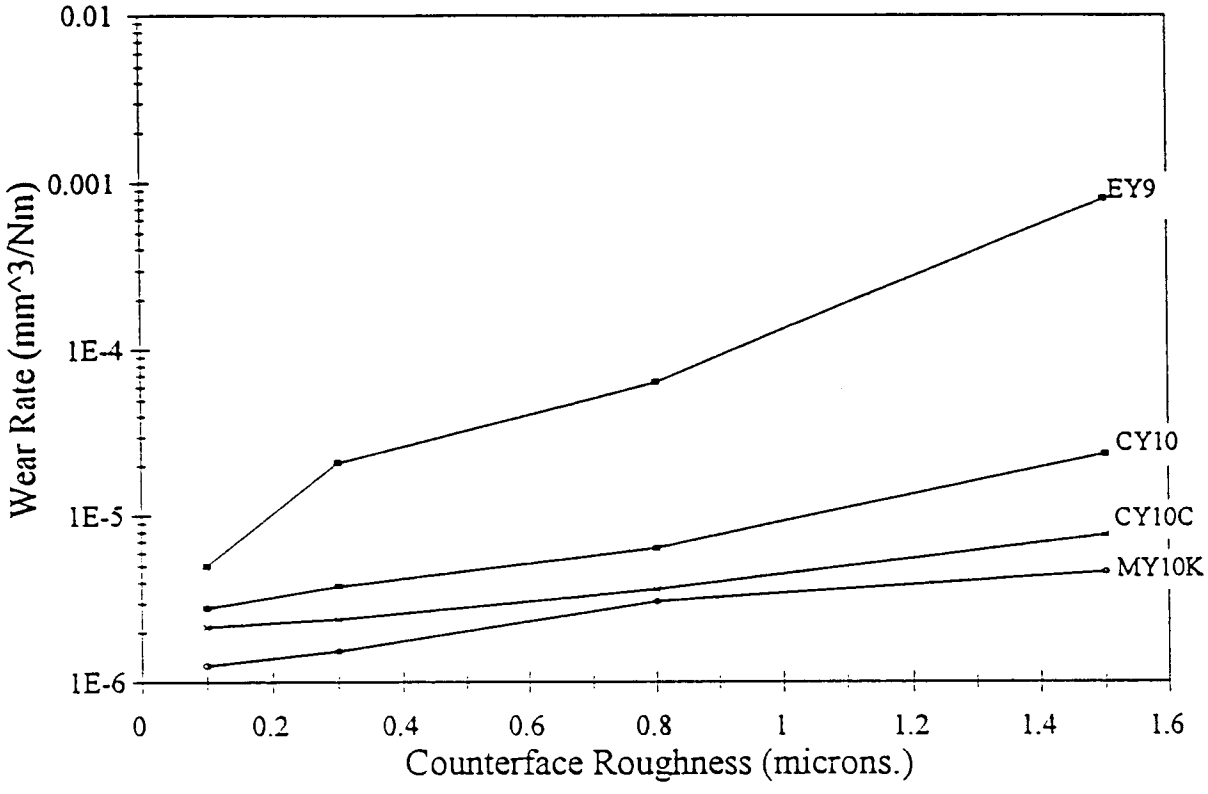

Fig. 4.2.15: Wear rate at 500m as a function of surface roughness, Ra, for various carbon grades

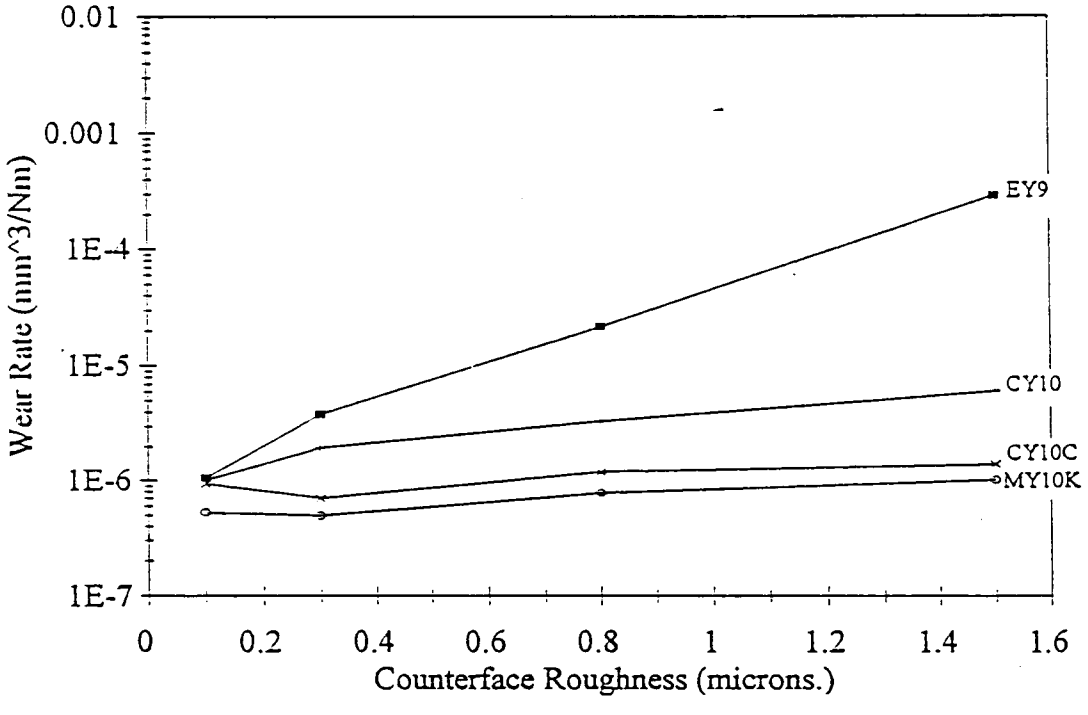

Fig. 4.2.16: "Steady state" wear rate (taken at 8000m) as a function of surface roughness for various carbon grades

The Effect of Material Hardness on Wear Rates

A general trend was observed in the relationship between steady state wear rate and specimen hardness as shown in fig 4.2.17. The harder, tougher impregnated MY10K and CY10C grades displayed superior wear resistance and were largely unaffected by changes in counterface roughness. Conversely EY9 and to a lesser extent CY10 exhibited poor wear resistance and were susceptible to small changes in surface topography.

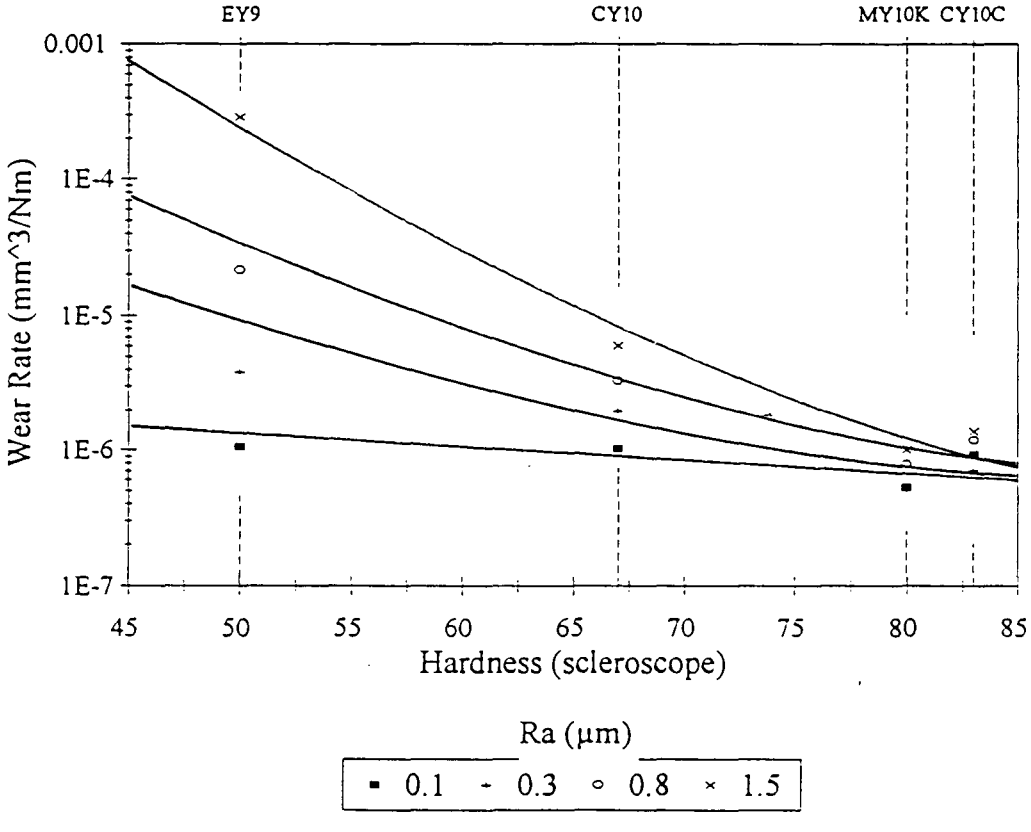

Fig. 4.2.17: The variation of steady state wear rate (8000m) with specimen hardness for the carbon grades

Friction

Steady state coefficients of friction (μ) for the materials tested are shown in Table 4.2.1 and lie in the range 0.37 to 0.43 against the smoothest counterface and 0.13 to 0.32 against a surface roughness of 1.5μm Ra.

In all tests the friction coefficient of the unfilled materials tended to be slightly lower over the initial few metres of the test reaching a steady value within 100 metres of running. Generally the coefficient of friction decreased with increasing surface roughness. This can be attributed to the fact that initially only the counterface asperities are in contact with the sliding material. As the sliding distance increases however, a transfer layer forms and there is an increase in the true contact area. All of the grades exhibited values of μ of approximately 0.4 against counterfaces of low counterface roughness (0.1 μm, 0.3 μm) suggesting that fully established transfer films have increased the true contact area. The average coefficient of friction for EY9 remains quite constant for all counterfaces, a transfer layer is readily formed on the counterface surface but is not very mechanically coherent and consequently its wear rate is high. Despite the variation in coefficients of friction for the various materials and counterface roughnesses, there is no distinct correlation between friction and mode of wear.

	Average coefficient of friction (μ)			
Grade	Ra = 0.1 μm	Ra = 0.3 μm	Ra = 0.8 μm	Ra = 1.5 μm
EY9	0.37	0.35	0.30	0.32
CY10	0.41	0.41	0.39	0.15
MY10K	0.43	0.41	0.19	0.13
CY10C	0.43	0.41	0.25	0.15

Table 4.2.1: Average values of coefficients of friction

4.3 Dry Particle Erosion

Plots of cumulative volume loss for solid particle erosion tests, conducted at an erosive impact angle of 45° to the sample surface for the range of carbon-graphite grades are shown in fig. 4.3.1. An "incubation period" is not displayed; all materials are characterised by the immediate onset of "quasi" steady state conditions.

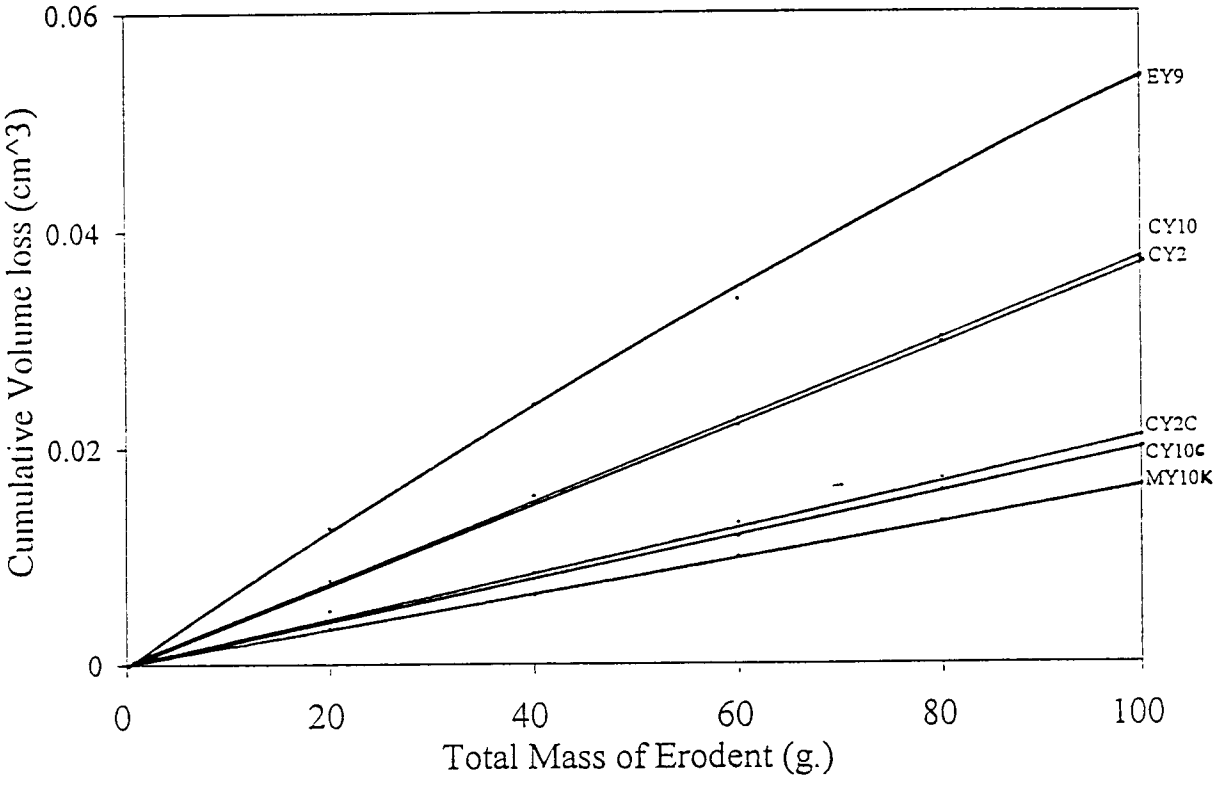

Fig. 4.3.1: Cumulative mass losses for the range of carbon-graphites, for erosion by 120 grit SiC particles at a 45° impact angle and a velocity of 40 ms^{-1}

The erosive behaviour of the different groups ie. the plain carbons (CY2, CY10, CY9), impregnated carbons (MY10K, CY10C, CY2C) and the electrographite (EY9) can be seen to be very distinct from each other, with the electrographite

exhibiting greatest volume losses. Wear rates are described by volume loss per gram of erodent (mm^{-3} g^{-1}) and were determined from the slopes of linear regions of the cumulative erosion mass loss curves of each. It can be seen that the impregnation of carbon by polymers or metals, improves a materials resistance to dry particle erosion. However, the variation between each grade within their respective groups is negligible and may be within experimental error.

Electron micrographs of the eroded surfaces of the grades EY9, MY10K and CY10C are shown in figs 4.3.2 a), b) and c) respectively. The eroded surface of the electrographitic grade EY9 features a distinct lack of ductility accompanied by extensive fracture and fragmentation of material in each impact zone. Surface spallations are evident indicating the presence of considerable lateral and subsurface cracking. In contrast, the antimony impregnated carbon eroded at 45° shown in fig. 4.3.2.b displays evidence of material cutting, a degree of plastic deformation and ductile shear of its surface. Material build up and shear lips are visible at the edges of the impact site.

The surface of the epoxy impregnated carbon CY10C shown in fig. 4.3.2.c also displays evidence of plastic deformation but is considerably less ductile and fractured in appearance when compared with the metal filled grade. The micrograph also displays evidence of an eroding particle fragment having embedded into its surface. The nature of the fragments were confirmed by electron dispersive microscopy (E.D.S.); the trace is shown in appendix (iii).

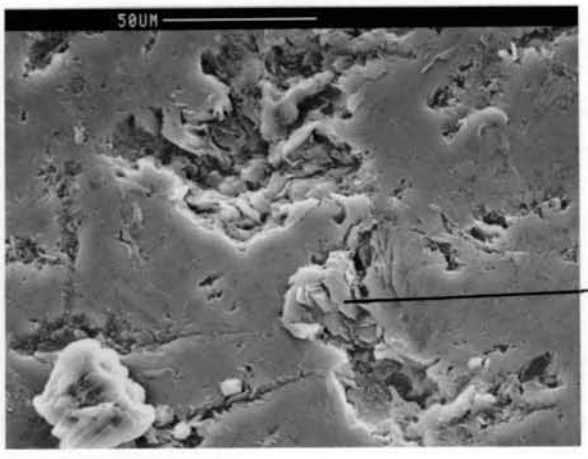

a.) Electrographitic grade EY9

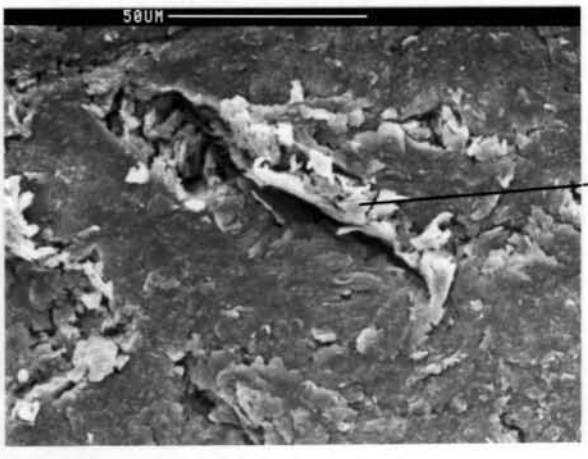

b.) Single impact site on antimony impregnated grade MY10K. Shear lips can be seen on the edges of the impact crater

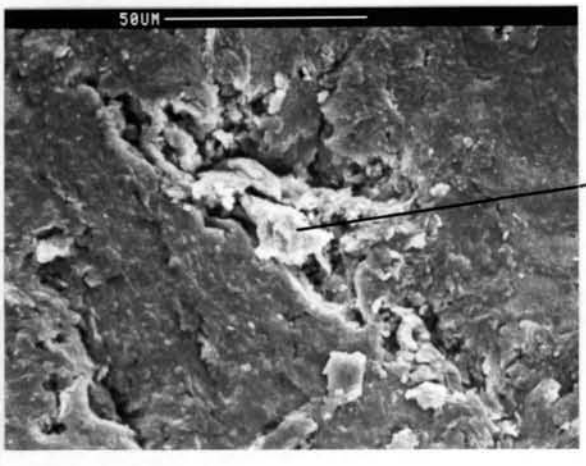

c.) Particle Embedment on wear surface of epoxy impregnated CY10C grade. (See Appendix (iii))

Fig. 4.3.2: Particle erosion single impact sites for EY9, MY10K and CY10C carbon-graphite grades. Dose <0.3 g of 120μm SiC

The Effect of Mechanical Properties on Wear Rate

The effects of target hardness on erosion rate are shown in fig. 4.3.3. Although there is a trend of increased wear rate with lower scleroscope hardness, the wear appears to be more influenced by the inherent nature of the materials ie. different materials displayed similar wear rates within their respective groupings. In general the tougher, higher hardness impregnated carbons reduce the amount of reversible deformation at the impact site and consequently the driving force for lateral crack formation will be lower.

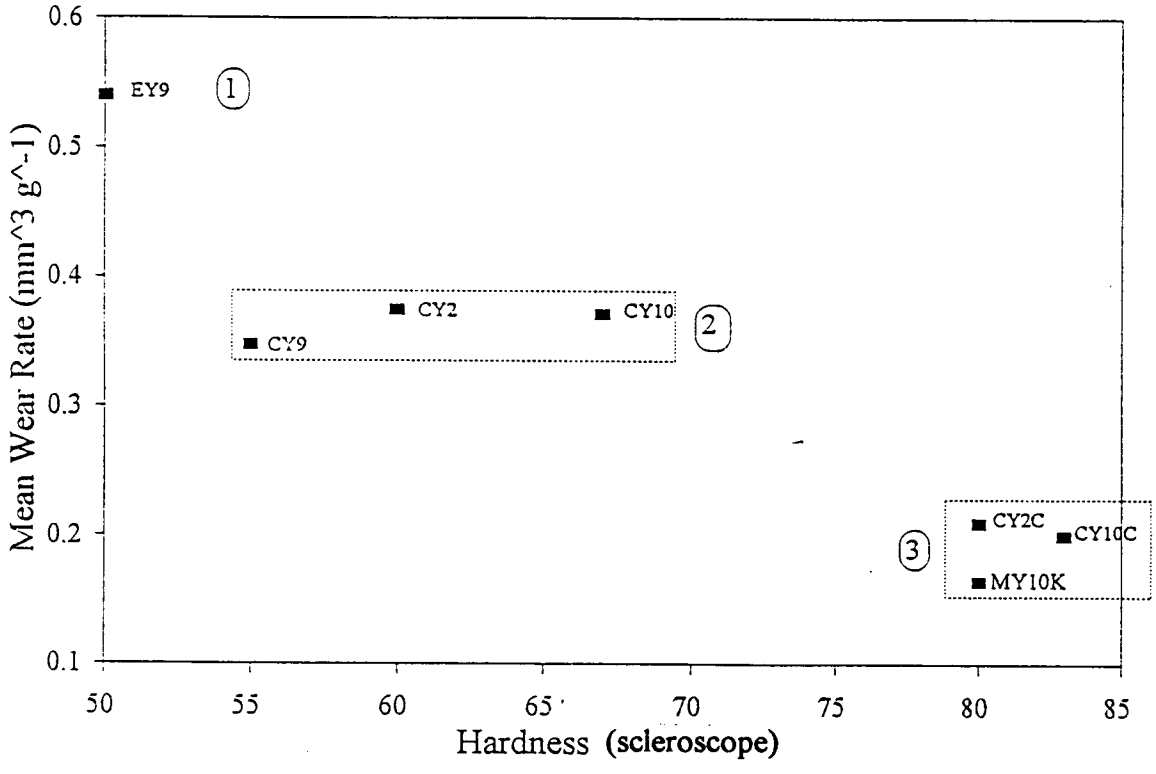

Fig. 4.3.3: Airborne particle erosion rate as a function of target hardness
① electrographite; ② plain carbons; ③ impregnated carbons

A general increase in erosion rates with increasing porosity can be seen in fig. 4.3.4. As with the hardness relationship, the wear rates of the different carbons within their respective groups are similar, the more porous electrographite showing inferior properties. The inherent pores appear to act as

sites for crack initiation and propagation; however the high porosity of several of the grades result in SiC fragments becoming embedded within them and this led to an enhanced measured performance due to a slight increase in mass.

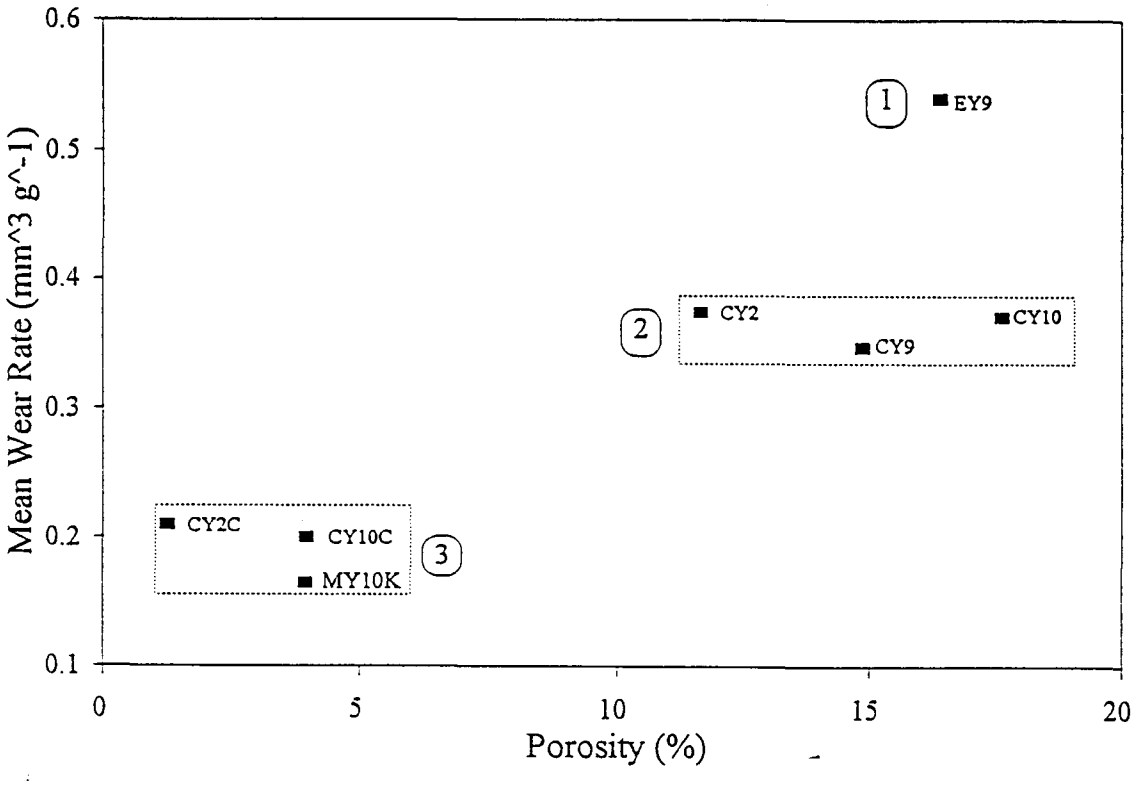

fig. 4.3.4: Airborne particle erosion rate as a function of porosity.
① electrographite; ② plain carbons; ③ impregnated carbons

4.4 Slurry Erosion

Water borne particle erosion (slurry erosion) caused severe damage to all specimens. There was no incubation period and mass loss occurred after only a few seconds. Figure 4.4.1 shows the variation of slurry erosion cumulative volume losses with time. It can be seen that the volume loss of the impregnated grades (CY10C, CY2C, MY10K) increased almost linearly with time throughout he period of measurement, with the epoxy filled materials exhibiting the best

properties. Conversely the unfilled carbon grades (CY10, CY2, CY9, EY9) show a high initial wear rate which tended to decrease with time of erosion.

The cumulative volume loss of the unfilled carbons is considerably greater than that of the impregnated grades and consequently the geometry and distance of the wear surface from the slurry jet increases dramatically (from 20 mm to 25 mm for EY9). This has the effect of limiting the intensity of the slurry on the specimen and could explain the non linearity of the plain carbons' and electrographite's wear rate. Scanning electron microscopy indicates that no particle embedment occurred during the slurry erosion tests so the variation in wear rate cannot be attributed to mass gains from attached erodent particles.

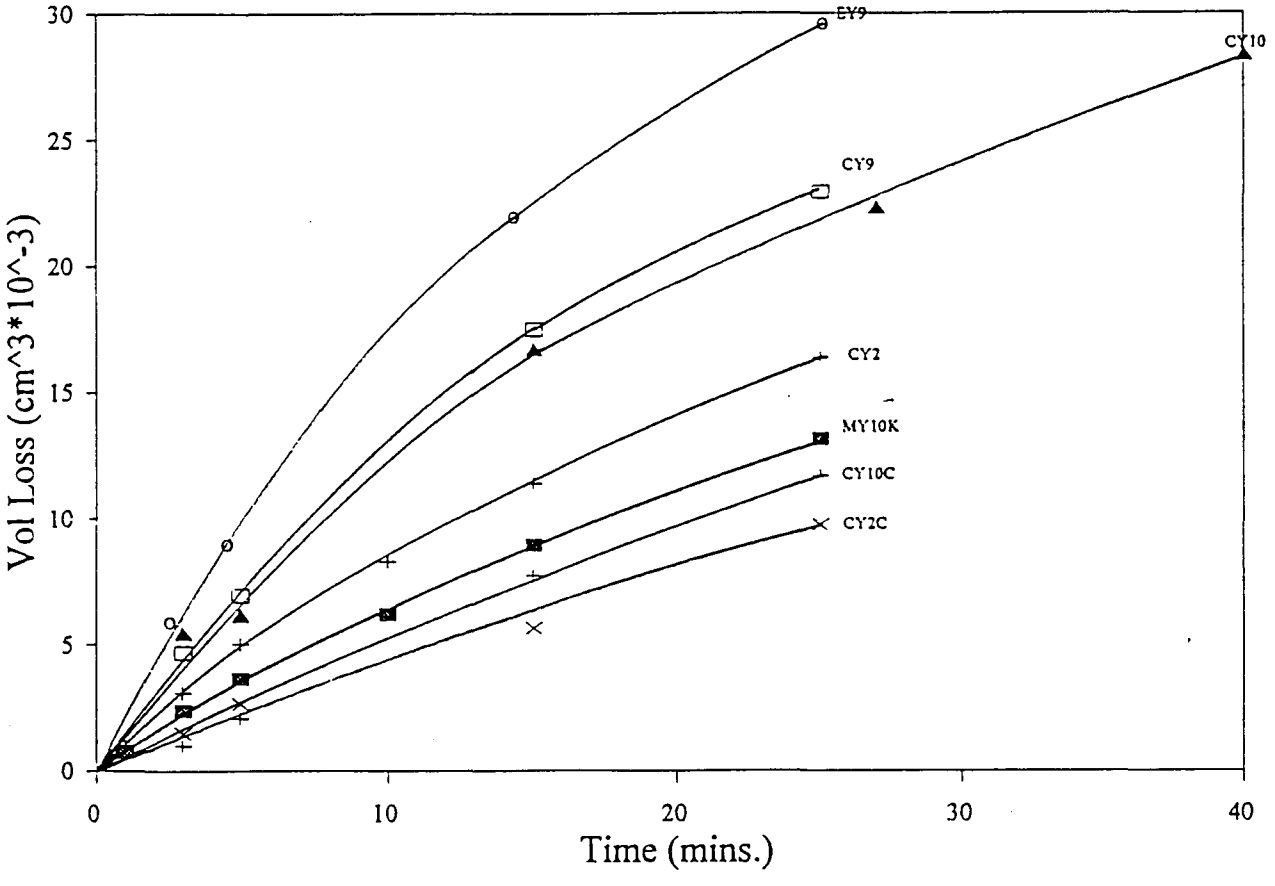

Fig. 4.4.1: Cumulative volume loss as a function of time for slurry erosion

Impact sites on the wear surface of the electrographitic grade EY9, the epoxy filled carbon CY10C and the antimony impregnated carbon MY10K are shown in

figs. 4.4.2 a), b) and c) respectively. EY9 and the CY10C grade show little evidence of plastic flow; the preponderance of cracks and surface spallations adjacent to the impact site are more characteristic of a brittle type fracture. Conversely MY10K exhibits signs of both plastic deformation and brittle fracture. In addition to the network of lateral cracks visible on its eroded surface, material build up in the form of "shear lips" is apparent around the impact crater, a feature characteristic of plastic deformation.

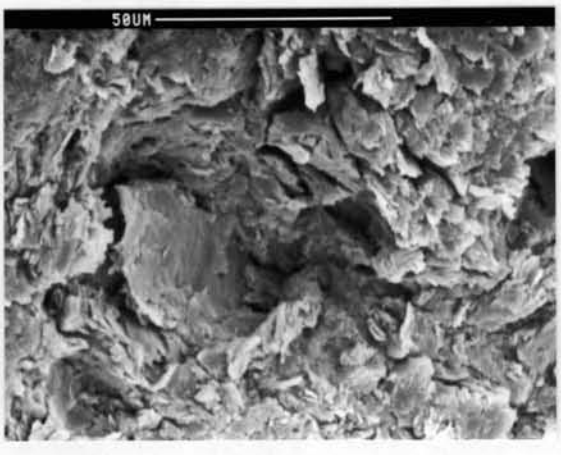

a.)

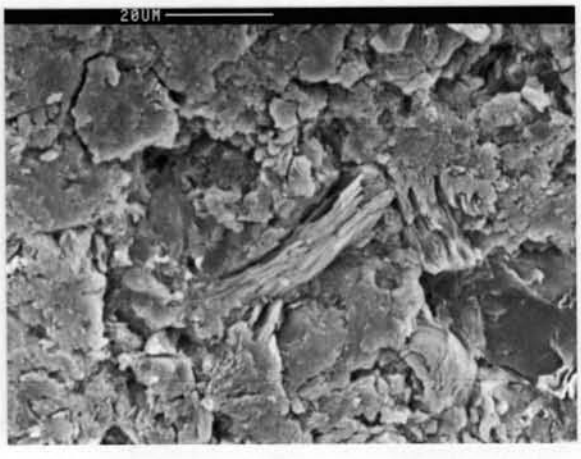

b.)

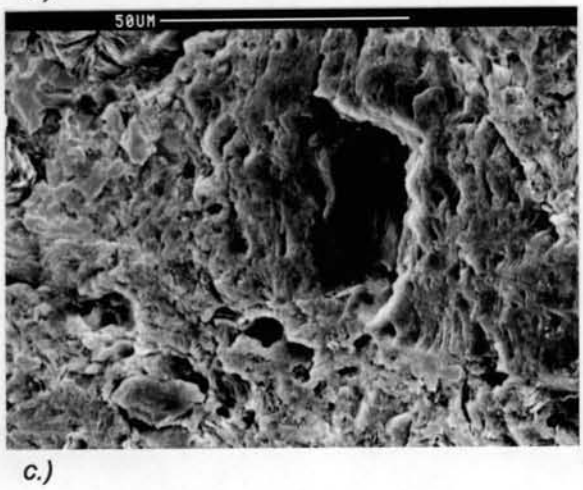

c.)

Fig. 4.4.2 *a.)Electrographite EY9*

b.)Epoxy impregnated carbon CY10C. Little evidence of plastic flow is apparent. Note the preponderance of cracks

c.)Antimony impregnated carbon MY10K

4.5 Cavitation Erosion

The plots of cumulative volume losses for carious carbon-graphite materials as a function of cavitation erosion time are shown in fig. 4.5.1. The cavitating fluid caused severe damage to all specimens, the extent of which brought about the collapse of several of the samples after only thirty minutes.

The unfilled carbon grades all exhibited high initial wear rates which tended to decrease as the total time of cavitation increased, conversely the impregnated carbon grades show a relatively constant wear rate, with CY10C exhibiting the best properties.

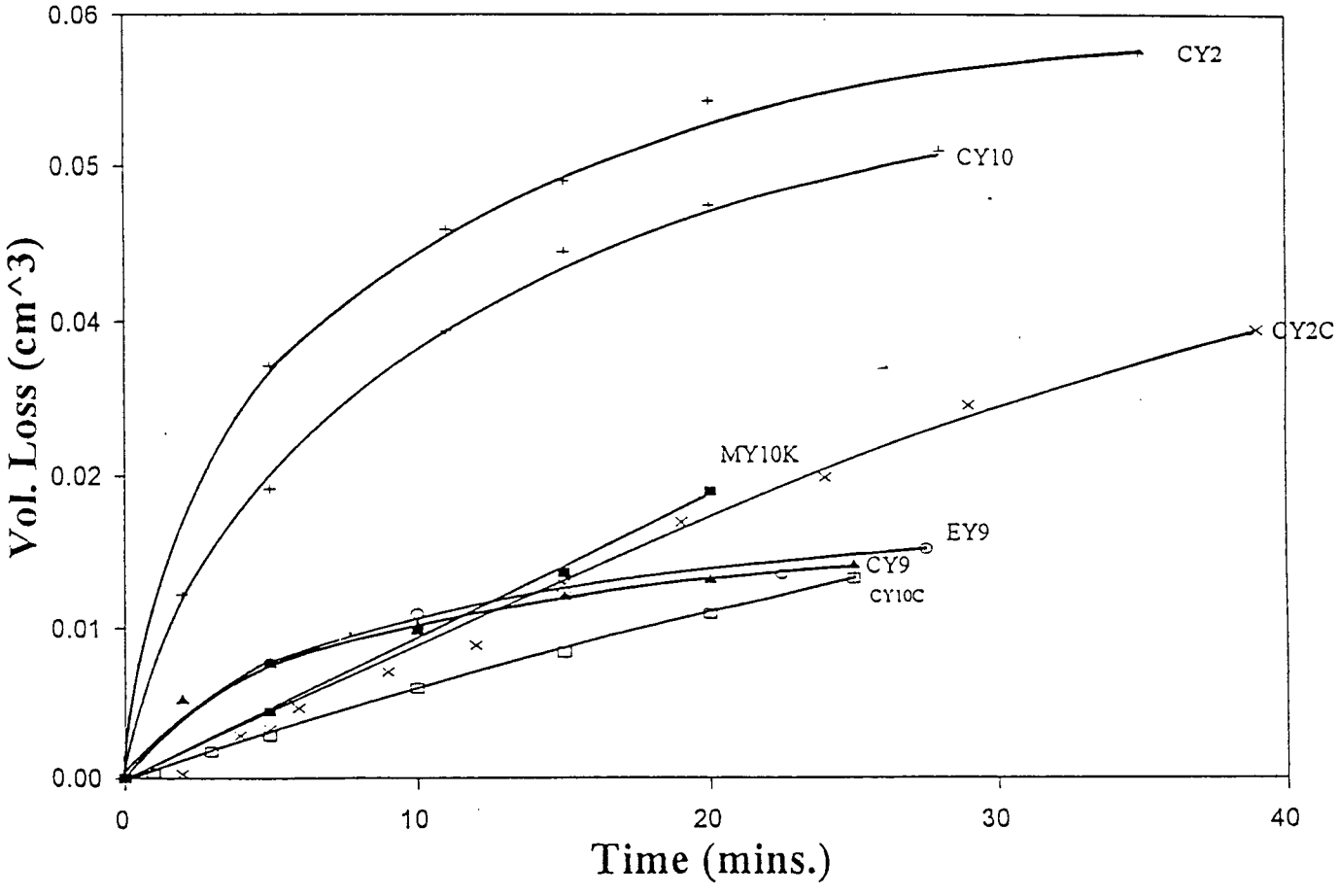

Fig. 4.5.1: Cumulative volume loss as a function of cavitation erosion time for each carbon-graphite grade.

Inspection of the worn surfaces of specimens subjected to cavitation for thirty minutes reveals the presence of deep pores and channels (fig. 4.5.2). In all the materials investigated, extensive cracking and chipping occurs on the surface adjacent to the pores. The pores appear to act as initiation sites for cavitation attack; the impregnation of the carbons with fillers effectively lowers the initial wear rate by creating fewer large areas of attack for the cavitating fluid.

The pits and channels formed in the wear surfaces of the plain carbons and electrographite are very deep compared with those exhibited by the impregnated grades. The pits formed in the CY9 grade, shown in fig. 4.5.3 were found by taper section to be approximately four times deeper than those in MY10K (± 0.5 mm).

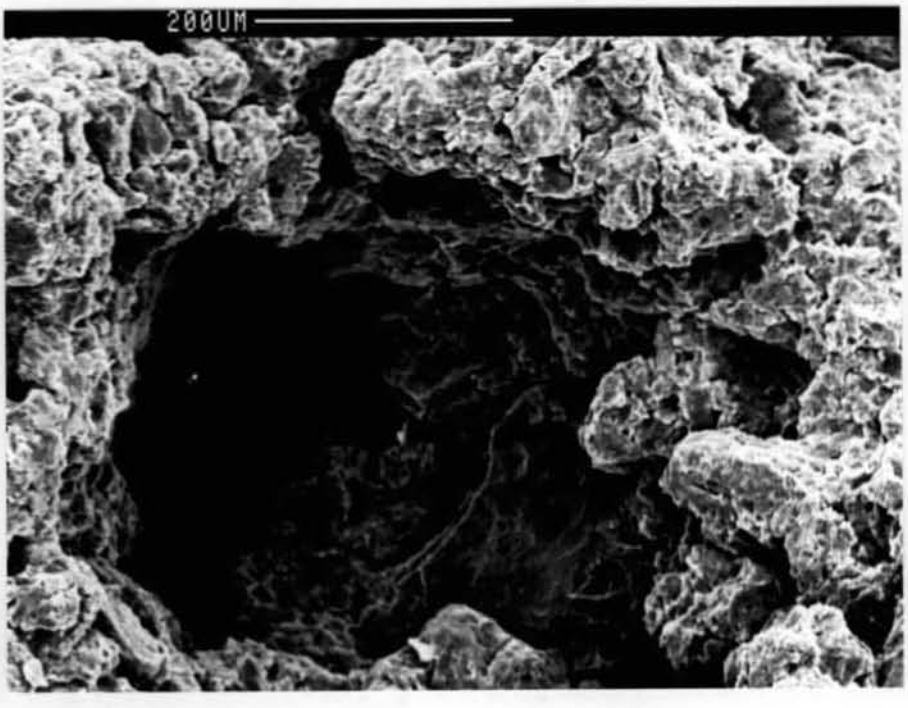

Fig. 4.5.2: Deep pit in CY2 specimen after 35 minutes cavitation erosion

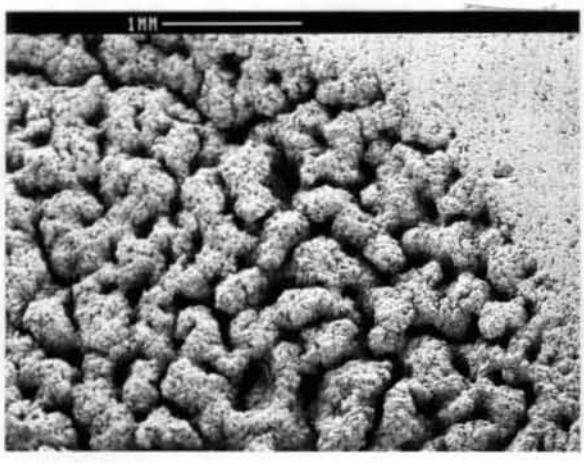

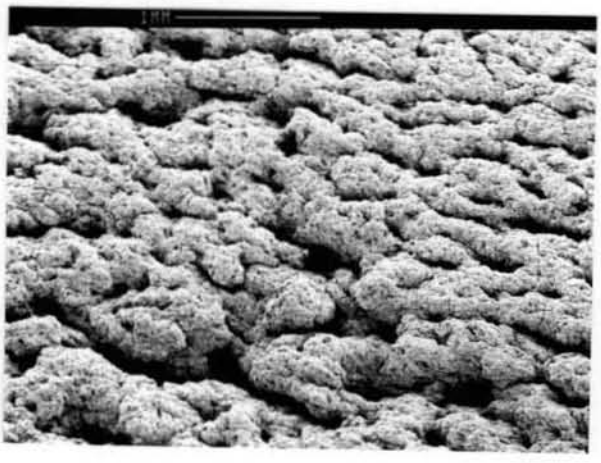

Fig. 4.5.3 (left): Scanning electron micrograph showing the deeply pitted wear surface of unfilled CY9 after 15 minutes vibratory cavitation erosion. (electron beam to specimen angle :- 20°)

Fig. 4.5.4 (right) The relatively even wear surface of antimony impregnated MY10K grade after 15 mins cavitation erosion. (electron beam to specimen angle :- 20°)

The Effect of Surface Finish

Fine surface polishing of a plain carbon (CY10) was performed in an attempt to create fewer sites for cavitation attack. The wear rate curve, shown in fig. 4.5.5, was however unaffected and there is no evidence of an incubation period as has been observed for other materials [49, 53, 54]. The immediate onset of erosive losses is undoubtedly due to the materials inherent porosity. This implies that cavitation erosion is controlled by microstructure and not surface condition.

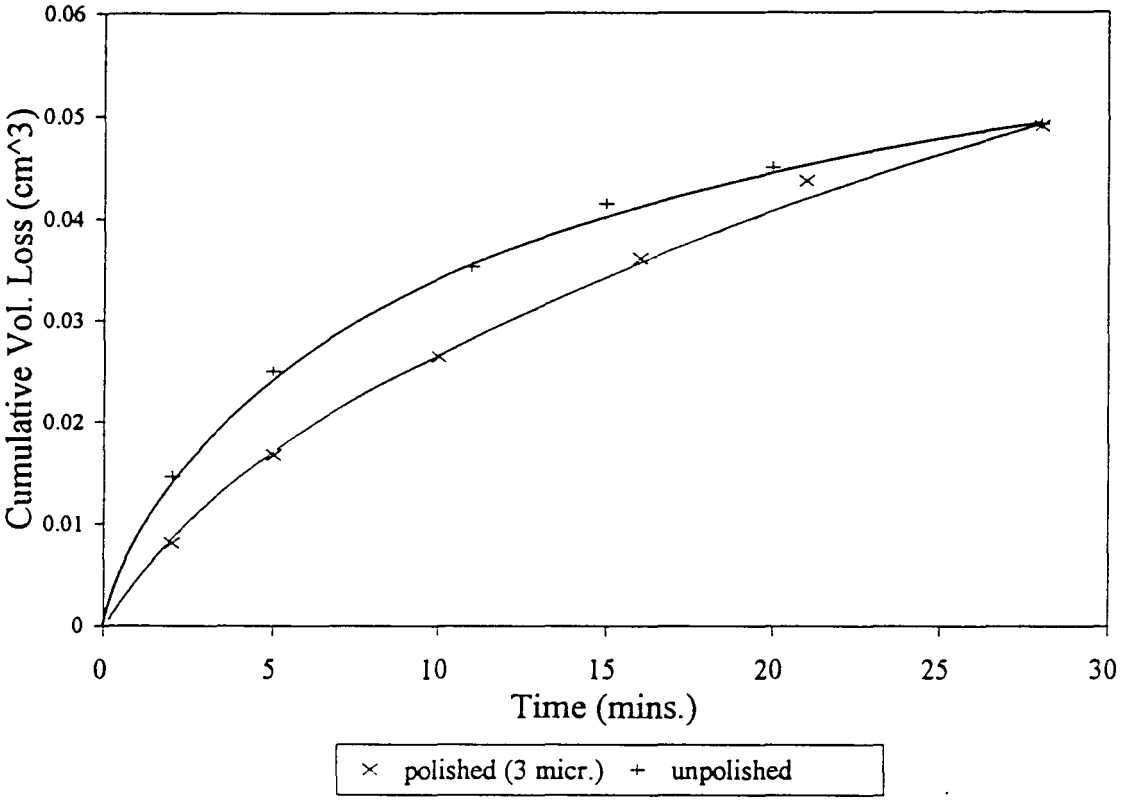

Fig. 4.5.5: Cumulative volume loss as a function of cavitation erosion time for both polished and unpolished CY10 specimens.

CHAPTER 5

DISCUSSION

5.1 Abrasive Wear

The abrasive wear environment involves a situation where a hard body indents, impinges or slides against another softer surface. Because of this, the elastic moduli, hardness and the magnitude of the stress and strain are important factors which determine the depth of abrasive indentation and the mode by which the material responds and loses material.

The plain carbon and electrographitic grades generally display higher wear rates than the impregnated carbons. Wear modes are typical of those found in brittle materials, as shown by the absence of pile up along the edges of the grooves produced during sliding against various grades of alumina abrasive. Conversely, the antimony impregnated grade and to a lesser extent the resin impregnated grades exhibit evidence of ploughing and appreciable pile up along the trough edges, indicating more apparent deformation.

The elastic modulus of the unfilled carbons is low and consequently the minimum grit size at which the elastic limit is exceeded is greater for a plain carbon than for a metal or resin filled grade. The elastic moduli of the plain carbons is sufficiently low for part of the load to be supported elastically against smooth surfaces; however the proportion depends markedly on the topography of the opposing surface. The level of roughness at which these materials were tested exceeds the elastic criterion of all the carbon grades and consequently when these carbons slide over a hard, rough irregularity, the high localised stresses lead to the brittle fracture, chipping and relatively high wear rates observed. The fact that the antimony grade can undergo plastic deformation may partly explain the superior wear rate shown in fig. 4.1.7. ie. it is less brittle than the unfilled grades despite having a higher hardness.

A material's resistance to indentation appears to be an important consideration determining wear resistance under abrasive conditions. This is illustrated in fig. 4.1.5 which shows the abrasive wear rate of each filled and unfilled carbon as a function of their respective bulk hardness values. An approximate inversely proportional relationship exists, the softer plain carbons and electrographite showing inferior wear resistance than the impregnated carbons. This relationship is supported by research performed by Lancaster [21] into the abrasive wear of graphite and by Moore and King [27] who investigated the inverse relationship of various brittle materials. Despite this trend some grades which have similar hardnesses exhibit different wear resistances when worn against the same abrasive grit sizes (eg. CY2C and MY10K against 85 μm alumina). It is therefore apparent that bulk hardness is not the only determining factor of abrasion resistance. It should be noted that the scleroscope cannot be regarded as a true measure of the permanent deformation of the carbon graphites; it is however a readily measurable quantity that differs significantly in the various grades and was therefore considered of interest to examine its effect on the abrasive wear rate.

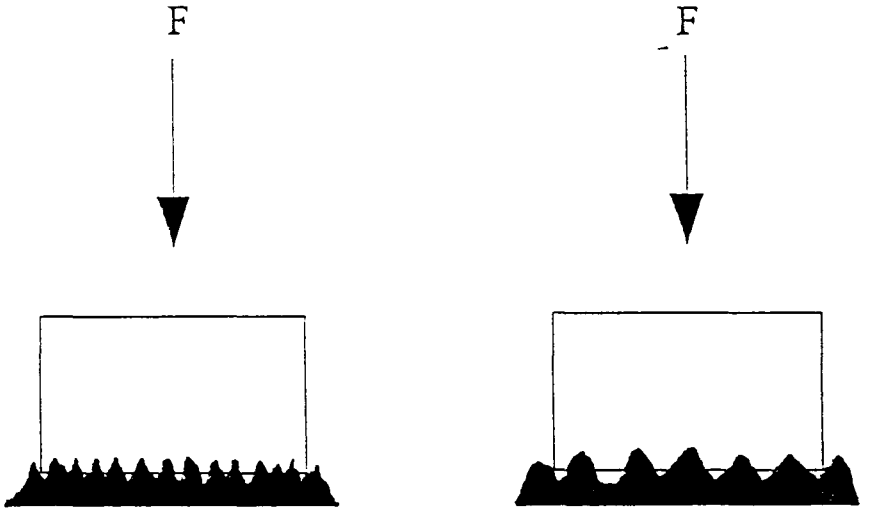

a.) b.)

Fig. 5.1.1: Schematic diagram showing load distribution for abrasive grit diameters a) 85 μm and b) 266 μm. In a) there is less load per particle but more particles per unit area than b) and consequently the two effects counteract each other yielding similar wear rates. At very small grit sizes the reduced load per particle and depth of indent result in lower wear rates.

The effect of varying the abrasive grit diameter shown in fig. 4.1.8 appears to have little effect on the abrasive wear rate of the different carbon grades. At this level of surface roughness it is assumed that all grit sizes exceed the elastic criterion of the carbon materials. Consequently, although individual grits generate more wear, there are fewer of them per unit area. The effects of grit size and grit density cancel each other out giving similar wear rates for all three abrasive diameters.

In normal sliding applications carbon-graphites are usually mated with a smooth bearing partner or counterface. However, initially rough components and products of wear and corrosion can necessitate a degree of abrasion resistance when selecting a suitable carbon material. The abrasive wear rates of the carbons tested in this study have been found to be large when compared to various other materials. Soft metals vary from 0.06 mm^3/Nm for copper to 0.2 mm^3/Nm for tin [1], whilst Böhm, Betz and Ball reported abrasive wear rates ranging from 0.14 mm^3/Nm to 0.5 mm^3/Nm for different polymeric materials [26]. The carbons tested in this study display comparatively poor resistances, from 0.2 mm^3/Nm for the antimony impregnated grade (MY10K) to 2.7 mm^3/Nm for the electrographitic grade (EY9).

It can be concluded from this study into the abrasive wear of carbon-graphites that maximum wear primarily occurs in the unfilled carbon grades and is as a consequence of irreversible deformation in the form of extreme microcracking.

5.2 Dry Sliding Wear

A common feature of the interaction between stainless steel and carbon-graphite, as they come into sliding contact, is the rapid formation of a transfer layer of carbon on the steel surface . The present study attempts to give further understanding of the manner in which the layer affects the wear and also suggest how the build up of the layer occurs.

A high initial wear rate is frequently observed when two loaded surfaces move over one another. With metals this can often be attributed to microcutting of the softer surface by the opposing asperities on the harder counterface [32]. Carbons, in particular unfilled grades, show no appreciable ability to deform plastically and so this mechanism is unlikely. The initial abrasive process produces loose carbon wear particles which are retained within the interface until attachment or escape. On the surfaces investigated the attached particles filled the topographical troughs and valleys of the stainless steel counterface and as wear continued, started to reduce the effectiveness of the abrasive asperities by physically burying them . The debris produced rapidly becomes compacted and an increasing fraction of the load becomes supported and the number of contact points becomes sufficiently large to support the wear surface elastically. As the transfer film develops the abrasive component of the counterface asperities decreases as a greater proportion of the load is carried elastically. The high initial wear rate observed can also be attributed to the asperities on the initial unworn carbon surface. Despite pre-conditioning the various carbon grades with 1200 grit, the wear surface is relatively rough and as a result prominent asperities are overstressed and fracture during the initial stages of sliding.

The initial rate of formation of these compacted areas is very large and is related to the efficiency with which wear debris is trapped in the contact zone. However, a considerable sliding distance may be required before an equilibrium wear rate is established (> 1000m). The unfilled electrographitic and plain carbon grades consistently displayed initial wear rates an order of magnitude greater than the impregnated materials and subsequently transfer layers were found to occur most readily from these materials. However against the roughest counterfaces EY9 could not effectively modify the steel topography and as a result abrasive wear continued until the specimen had insufficient material to continue the test. Three body abrasion was also seen to be evident in the initial stages of sliding when hard carbon debris or non-metallic oxide constituent impurities were released from the leading interface, resulting in abrasive troughs appearing on the carbon wear surface.

The eventual equilibrium low wear rate phase seems likely to be a result of a fatigue process in which load supporting transfer layers are worn and replenished. The continuous polishing effect of the counterface transfer film leads to crazing on the carbon surface. As each lamella breaks away it exposes carbon beneath it in a comparatively unchanged form. This small area rapidly becomes modified, the local wear rate is high, until sufficient debris has been produced to form a coherent surface layer again. This layer is subsequently removed once more depending on the magnitude of fatigue and the adhesive forces. Similar processes are apparent in the transfer film, layers are continuously being removed and replenished during the polishing process as the adhesive force between them and the counterface is relatively low.

The steady state wear rates observed for each carbon grade in these tests did not vary considerably with counterface roughness (Ra). It appears that at this degree of roughness (0.1μm-1.5μm) once a coherent transfer layer has been well established and the abrasive component is reduced, the carbon slides primarily on the transfer film and wear is independent of the initial surface finish. The exception is the electrographite EY9 whose steady state wear rate increased by two orders of magnitude from 1.1×10^{-6} mm^3/Nm against a counterface of 0.1μm to 2.1×10^{-4} mm^3/Nm against the roughest counterface of 1.5μm. It is suggested that despite readily producing wear debris in the initial stages of sliding, the counterface asperities, troughs and valleys have not been efficiently buried and an equilibrium phase has not been reached where fatigue is the dominant mechanism, but rather abrasion is mainly responsible for the wear even after long sliding distances.

The coefficients of friction for all the carbons and electrographites tested showed little variation with sliding distance. However, an increase in friction was noted for all the materials in the initial stages of sliding, this variation can be attributed to an increase in the contact area which occurs when the debris builds up into a flat glazed surface film. The total (adhesion force) frictional force can be represented by the equation:

$$F = As$$

Where A is the real area of contact and s is the shear strength per unit area of the regions over which the adhesive forces operate. Thus, as asperities in the carbon surface are removed and the hollows and depressions in the counterface are filled, the real contact area increases resulting in a larger frictional force. A similar argument can be used to explain the decrease in friction coefficient against rougher counterfaces. No correlation between changes in the friction coefficient and changes in the wear mechanisms is apparent. Cyclic build up and reduction in friction force has been observed with these materials in other geometries and when sliding against themselves [34]. This was not observed in this study, presumably because the loaded surfaces do not conform sufficiently closely.

The tendency for lower wear rates with increased scleroscope hardness is the reverse of expectations for other types of bearing material and previous studies into the wear behaviour of carbons [28]. Resistance to indentation is an important factor in the initial stages of the sliding process when wear is predominantly abrasive (as described in ch 5.1); the effect on the steady state wear phase is unclear because insufficient number of materials have been tested to establish an accurate form of the relationship.

The numerical value of the wear rates observed in this study once steady state conditions are achieved, are similar to those reported in the literature for comparable materials in a variety of geometries. Booser and Wilcock [28], tested a wide variety of commercially available carbons and electrographites. Their lowest limit on the measured coefficient of friction was 0.12 and the most wear resistant grade exhibited a wear rate of about 8×10^{-7} mm^3/Nm. In comparison the antimony impregnated carbon (MY10K) tested in this study yielded optimum wear behaviour with a wear rate of 4×10^{-7} mm^{-3}/Nm and a friction coefficient of 0.13. The specific wear rates compare favourably to those reputed for various polymeric materials, Böhm, Betz & Ball [26] found rates that varied

from 7 x 10^{-9} mm^3/Nm for ultra high molecular weight polyethylene (UHMWPE) to 1 x 10^{-4} mm^3/Nm for polyether-ether-ketone (PEEK).

It can be concluded that within the normal load and application range at which these materials were tested, both wear and friction tended to be lower in both resin and antimony filled grades. Impregnants can also greatly improve strength of carbons by minimising chipping, cracking and subsequently the three body abrasion observed for EY9.

5.3 Air borne Particle Erosion

The wear rates of the different groups of carbon-graphite materials (plain carbons, impregnated carbons, electrographites) were distinct and found to be very dependent on the mechanical properties and the mode of deformation of the target materials.

Material loss during solid particle erosion of the plain carbon and electrographitic grade was typical of brittle erosion. Scanning electron micrographs of single impacts on the target surface revealed a preponderance of cracks adjacent to the impact site and the presence of surface spallations indicating that a negligible amount of plastic deformation had occurred. Material removal occurred through the interaction of the lateral cracks with each other and the surface of the target causing the loss of chips of material. The mechanisms of erosive damage that are likely to occur during the solid particle erosion of plain carbons and electrographites are shown in fig. 5.3.1

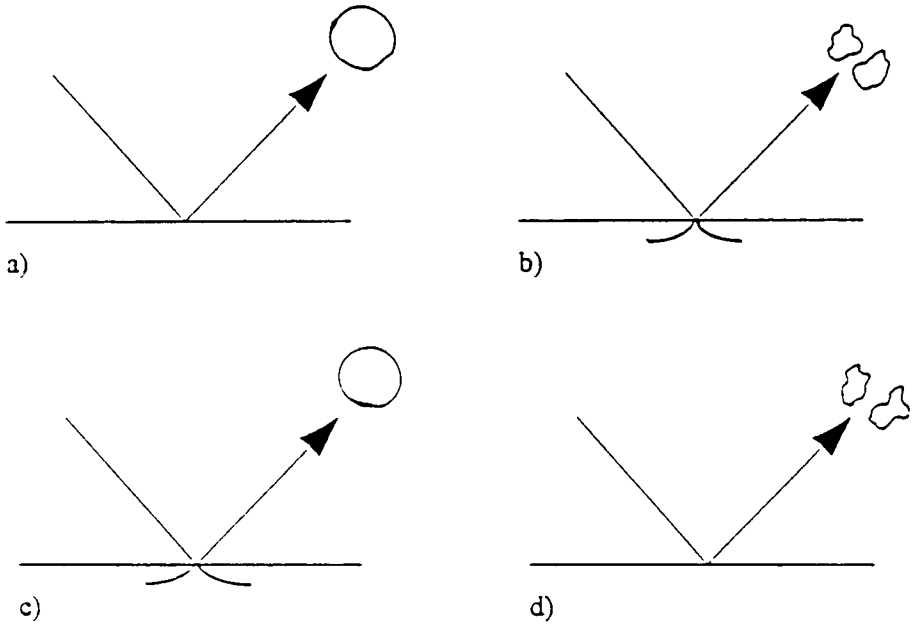

Fig. 5.3.1: The responses of unfilled carbon materials to solid particle impact (after Wellman[39])

a) Carbon - elastic; particle - elastic

b) Carbon - brittle; particle - brittle

c) Carbon -brittle; particle - elastic

d) Carbon - elastic; particle - brittle

In contrast to the plain carbons, the impregnated grades (particularly MY10K) displayed additional features characteristic of plastic deformation. Scanning electron microscopy revealed the presence of shear lips and material build up at the edge of the impact crater The lower wear rate exhibited by these materials is partly brought about by this deformation process; more energy is associated with plastic deformation and less to crack propagation which can ultimately lead to chipping and material removal as illustrated in fig. 5.3.2.

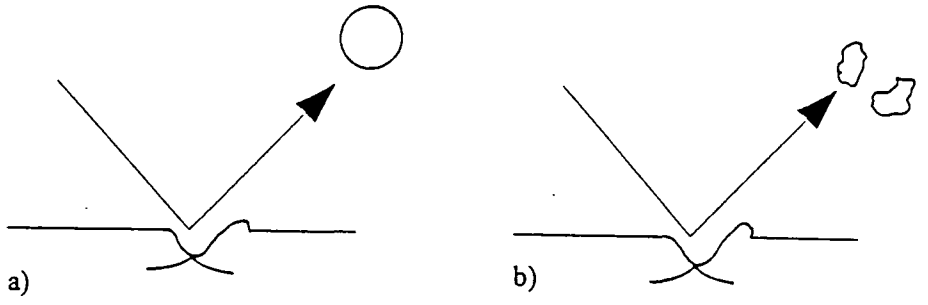

Fig. 5.3.2: Additional erosive mechanisms displayed by impregnated materials (MY10K, CY10C, CY2C)

a) Carbon - brittle/plastic; particle - elastic

b) Carbon - brittle/plastic; particle - brittle

The Effect of Microstructure on Air borne Particle Erosion

The role of microstructure on the solid particle steady state erosion rate appears to be an important consideration when selecting suitable materials for use in erosive environments. Microstructure greatly affects fracture resistance which in turn is an important factor in the erosion resistance of carbon graphites.

Under the test conditions employed, erosive wear rates of the impregnated grades were approximately 50% of the plain carbons and 30% of the electrographite EY9. The variation can be partly ascribed to microstructural constraint. Lateral cracks in the plain carbon materials cannot traverse to their full extent due to plastic blunting within the non-graphitic binder. Similarly crack propagation in impregnated grades is further inhibited by the epoxy or antimony filler. By controlling the spread of lateral cracks erosion is significantly reduced.

The effect porosity has on the particle erosion rate of materials is less clear. Wiederhorn et al [44] suggested that porosity can inhibit crack propagation by blunting crack tips. However, from the tests performed in this study it can be

seen that there is a general increase in erosion rates with increasing porosity. It is probable that the pores are in fact acting as stress raisers by concentrating and intensifying the subsurface stresses, thus enhancing the initiation of lateral cracks. It was also noted that the pores acted as sites for particle embedment, although mass losses were sufficiently large to nullify the mass of any additional attached particles.

The Effect of Hardness on Particle Erosion

The harder impregnated grades displayed superior wear resistance to the unfilled carbons. This inverse relationship between the target hardness and erosion rates is supported by previous research into the solid particle erosion of other brittle materials [38, 39]. The target hardness determines the amount of deformation and hence the size and extent of the stress field. This results in the driving force for lateral crack propagation being reduced, the softer but more brittle unfilled carbon grades are more likely to suffer lateral cracking to relieve the strain imposed by the erodent particles. It has been suggested that for softer erodents and oblique angles of attack damage accumulation is necessary to build up the required stress to produce lateral cracks [59, 60]. The SiC erodent used in these tests is much harder than the target material implying that crack initiation is inevitable and that crack propagation is the rate controlling factor. Silicon carbide is a very brittle material and no plastic deformation of the erodent particles was observed although brittle fracture did occur and fragments became embedded in the target surface. Electron dispersive spectroscopy of the fragments yielded high proportions of silicon confirming its identity.

The numerical value of the wear rates (0.17 to 0.55 $mm^3\ g^{-1}$) established in these tests do not compare favourably with results from similar investigations into various materials. Wellman [39], studying particle erosion of brittle materials quoted wear rates of 0.14 mm^3g^{-1} for glass and 0.017 mm^3g^{-1} for 10% WC-Co. Böhm, Betz and Ball [26] measured the airborne particle erosion wear rates for various polymers, for a particle velocity of 60 ms^{-1} wear rates varied from 0.004 mm^3g^{-1} for polyurethane to 0.2 mm^3g^{-1} exhibited by a polyamide. The wear

rates exhibited by glass and polyamide are comparable to those displayed by the epoxy impregnated grades.

At this level of erodent hardness, target material lateral crack initiation is inevitable. The primary factors affecting the airborne particle erosion rate appear to be the mode of deformation and the ability of the microstructure to inhibit lateral crack propagation.

5.4 Slurry Erosion

The wear models described in chapter 5.3 for airborne particle erosion equally apply to erosion due to particles in a liquid carrier. However differences in test parameters such as velocity, size, shape, erodent hardness and impingement angle make direct comparisons between wear rates of the two tests invalid.

Superior wear resistance was again displayed by the impregnated grades and is best considered in relation to their microstructure and erosive mechanisms:

The addition of epoxy and antimony fillers in carbons improves wear resistance by inhibiting the spread of lateral cracks initiated from particle impact, the presence of a non-graphitic binder in the plain carbons also provides a barrier to crack propagation and consequently erosion rates of the plain carbons are superior to that of the electrographite. The lower porosity found in the impregnated grades is also beneficial to wear resistance, the dense material has more integrity and inhibits crack initiation and propagation

Scanning electron microscopy of the wear surfaces of the impregnated grades revealed a high concentration of cracks in the CY10 epoxy filled grades, whilst the MY10K metal filled grade displayed additional evidence of plastic deformation. It is suggested that the inferior wear rate exhibited by MY10K with respect to the epoxy filled carbons is as a result of repeated impact wear brought about by the large impingement angle (90°). The shear lips present at the edge of the damage zone are vulnerable to subsequent impacts from the erodent.

An important factor in the removal of material by abrasive slurries is the effect of the carrier fluid. Scanning electron micrographs of the eroded surfaces revealed that particle embedment did not occur to a detectable extent as it did with the airborne particle erosion. Several factors account for this: the erodent silica particles are relatively large (500μm) compared with the mean pore radius and are travelling at a lower velocity (6.5 ms^{-1}). In addition, erodent particles are efficiently removed from the surface by the carrier fluid. The improvement of the unfilled carbons wear rate with time of erosion is therefore not a result of particle embedment but is rather a consequence of a reduced erosive component of the slurry jet due to changes in geometry of the wear surface.

5.5 Cavitation Erosion

The carbon-graphite specimens displayed very different cavitation erosion characteristics to other materials previously investigated with the same apparatus. Wilson [53], testing the wear resistance of aluminium matrix composites found that after an initial period of low erosion rate, known as the incubation period, wear increased linearly. He quotes wear cumulative mass losses of 3 mg after 30 minutes. Hankey [49] found that appreciable volume losses for WC-Co were only obtained after 5 hours vibratory cavitation erosion and varied from 1.0 to 1.5 mg. The comparative wear behaviour exhibited by the various carbon grades is poor; cumulative mass losses vary from, 100 mg (CY2) to 35 mg (CY10C) after 30 minutes cavitation erosion.

Heathcock et al [54] observed that materials with a greater elastic resilience displayed better resistances to cavitation erosion. The addition of high modulus impregnants to the plain carbons results in an overall increase in their ability to absorb and dissipate impact energy in an elastic manner. Thus, an increase in erosion resistance with greater volume fractions of fillers would be expected. However, the cumulative erosion volume losses of the carbon-graphites in some cases contradicts these considerations because the stresses imposed by the cavitating fluid are always large enough to propagate damage in flaws.

Ranking of the various grades based on the erosive volume losses of the various grades bears little resemblance to results obtained for other wear tests, the more highly graphitic specimens exhibiting greater volume losses than the plain carbons and impregnated grades. However a more accurate indication of the relative cavitation behaviour of the grades can be obtained by looking at wear rate variations for each material over the course of the test. The unfilled carbons all showed a high initial wear rate which tended to decrease with increasing cavitation time, whilst the filled carbons showed a relatively constant wear rate. This is explained in terms of **a.)** microstructure and **b.)** specimen geometry with respect to the ultrasonic source.

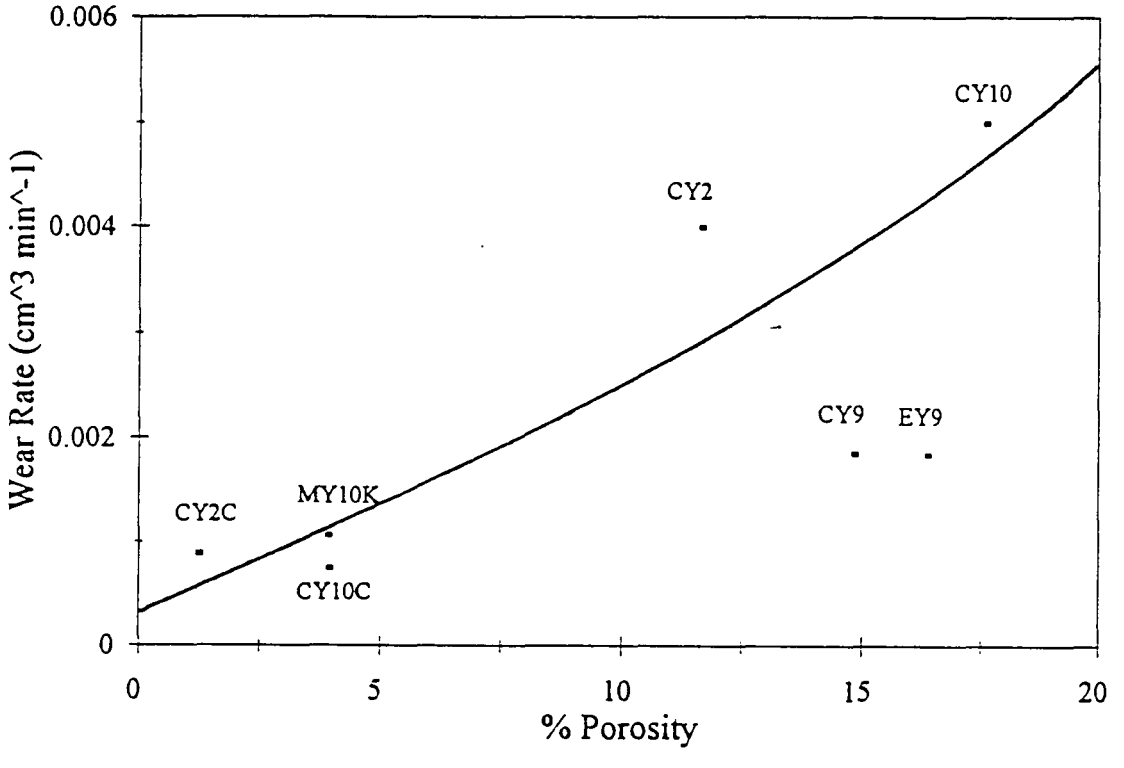

Fig. 5.5.1: Erosive wear rate after 5 minutes cavitation erosion plotted as a function of porosity for each carbon-graphite material

a.) Inspection of specimens subjected to cavitation for thirty minutes reveals a presence of deep pits and channels amongst the pores and inclusions in the unfilled grades. Conversely the impregnated grades tended to form a relatively flat, even wear surface. It appears that the pores act as initiation sites for cavitation attack. By impregnating the carbons with fillers the initial wear rate is effectively reduced by creating fewer large areas of attack for the cavitating fluid. The five minute erosion rate shown in fig. 5.5.1 displays a diffuse trend of increased wear resistance for the lower porosity materials. The impregnated carbons (MY10K, CY10C, CY2C) have fewer sites for cavitation attack and additionally the non carbonaceous fillers prevent the spread of lateral cracks, conversely the higher porosity plain carbons show a greater volume of pores which are susceptible to attack.

Fine surface polishing of a plain carbon was performed in an attempt to create fewer sites for cavitation attack and effect an "incubation period". The resulting wear characteristics, shown in fig. 4.5.5, are similar to the unpolished grade. A high initial wear rate is still observed, which is undoubtedly due to the materials high inherent porosity (17%). This implies that cavitation erosion is controlled by microstructure and not surface condition.

b.) Results obtained from mercury porosimetry show that the impregnated grades have a lower median pores size, more regular distribution and a higher specific surface area than the unfilled materials. As a consequence, there are more small areas of attack for the cavitating fluid and a more even wear surface is eroded than for the plain carbons and electrographite. Heathcock [61], using the same test rig configuration showed that maximum cavitation erosion occurred when the drill tip was 0.35 mm from the wear surface. Despite resetting the ultrasonic horn to 0.35 mm after each weighing the deep pits formed in the unfilled grades, effectively reduce the amount of material at the critical distance for cavitation and consequently the wear rate decreases with time for the unfilled grades (refer to fig. 5.5.2).

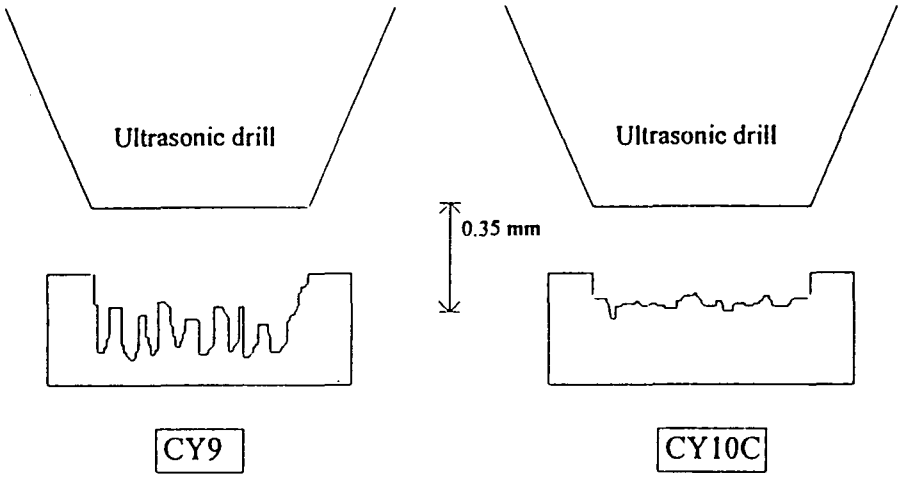

Fig. 5.5.2: Schematic diagram showing cross section of the cavitation rig. The more deeply pitted wear surface of the CY9 grade presents less material than CY10C to the region where optimum cavitation occurs

5.6 Relative Wear Performance of the Materials

This investigation has demonstrated that the different groups of carbon material (plain, impregnated and electrographitic carbons) exhibit different performances depending on the type of tribological situation as shown in fig. 5.6.1. This has important consequences for components manufactured from these materials which are subjected to different types of wear during normal or adverse operating conditions.

Some important points of interest arise from this work for designers intending to use carbon-graphite in sliding applications, particularly where the opposing surface may be initially rough or become roughened with time. The use of a single constant specific wear rate for carbons in any situation is invalid; the specific wear rate will vary with distance and with debris removal efficiency. The wear behaviour of carbon-graphite is strongly influenced by its' ability to build up a transfer film on the opposing counterface. Against very rough abrasive

surfaces none of these materials can achieve this and consequently the wear rate is correspondingly high. The harder, tougher epoxy and metal filled grades are more suitable candidates for such situations though various metallic and polymeric materials could prove more suitable. Against smooth counterfaces all of the grades tested were able to produce a transfer film and the wear rates were correspondingly low and consequently could be considered for components in sliding applications.

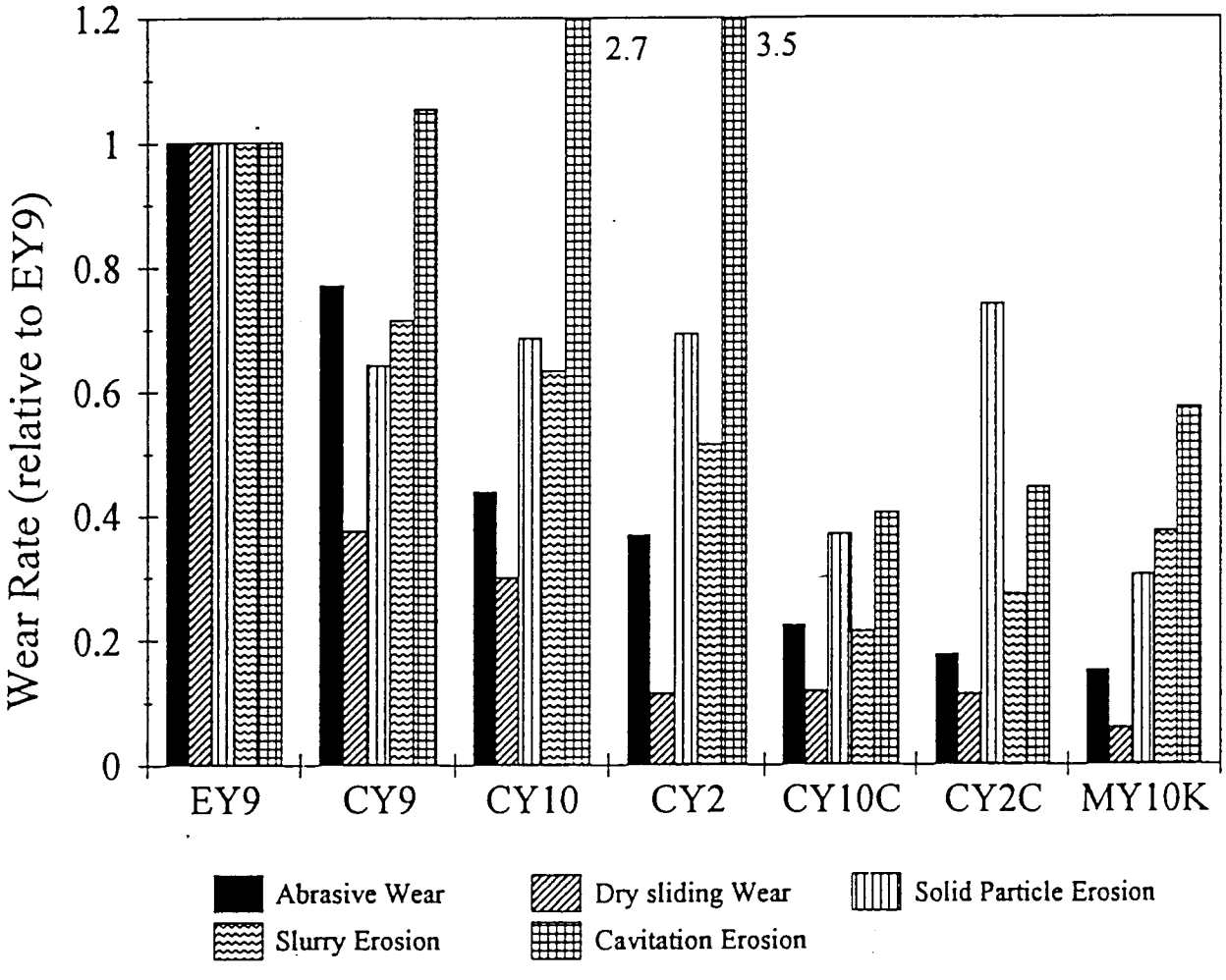

Fig. 5.6.1: Wear rates relative to EY9 for all tests

- *Abrasive wear (grit size 85μm)*
- *Dry sliding wear (steady state wear, 8000m, 0.8μm Ra)*
- *Solid particle erosion (mean wear rate over course of test)*
- *Slurry erosion (wear rate after 5 mins)*
- *Cavitation erosion (wear rate after 5 mins)*

In general the harder and tougher grades of carbon display superior wear resistance although the long term effect these may have on the opposing counterface is unknown.

The resin and antimony impregnated grades also consistently displayed superior erosive wear rates (shown in fig. 5.6.1). It is therefore considered a more suitable material use in hostile environments. Possible applications include seals for process pumps, where the components must be able to withstand abrasive slurries and products of erosion and corrosion. Although alternative materials may be more resistant to the erosive processes studied, the self lubricating properties, high temperature capability and unreactivity of carbons make them potential materials.

Despite exhibiting superior erosion and wear rates in all tests, it is not a forgone conclusion that metal impregnated grades are optimum materials for all applications. The antimony filled grade is strong compared with plain carbons and can deform before failure in tension or flexure; these properties make it suitable as a bearing which must carry heavy loads and may be required to deform. However, metal impregnated carbons are likely to reduce counterface life and are much more costly than the equivalent resin filled grades and are therefore likely to be used when service conditions are severe and necessitate the employment of a material which is resistant to different types of erosion.

The Epoxy filled grades showed only slightly inferior wear rates to MY10K in all the wear tests and consequently could be considered as a suitable material for most of carbon's application, except where a system requires a deformable bearing. An advantage CY10C and CY2C have over MY10K is that relatively complex close tolerance parts can be cheaply formed by compression molding.

The low modulus exhibited by the plain carbons make them suitable for sliding and fluid sealing applications. Their low elastic modulus helps provide conformity to a parallel surface to minimise the seal gap over the entire contact

region. However if the mating metal surface finish is coarser than ≈ 1μm (Ra), the carbon will suffer abrasive wear and this will lead to high wear rates.

The high electrical conductivity of the electrographites lends them to applications as brush materials in rotating electrical machinery and their high thermal conductivity make them suitable for applications where the rubbing interface must remain cool. Although the more highly graphitic unfilled carbons' wear properties were found to be inferior to all other grades tested, these could be improved by impregnating them with either a metal or a resin filler. This would however, effect its conductivity and may not be desirable in certain of carbon-graphites applications where counterface life and the materials' electrical properties are of prime importance.

CHAPTER 6

CONCLUSIONS

1.) In all tests, hardness, elastic modulus and porosity were found to influence the wear rates of the carbon graphite grades. Maximum wear loss was consistently observed for the softer, more porous unfilled carbons (designated CY2, CY10, CY9, EY9).

2.) All of the carbons showed poor wear rates when abraded against rough surfaces (0.2 mm^3/Nm for MY10K to 2.7 mm^3/Nm for EY9). The highly localised stresses lead to chipping, brittle fracture and a high wear rate. The more highly graphitic specimens have a lower elastic moduli and their lack of plasticity means that brittle fracture is more likely to occur at any stress depending upon the size of flaw or defect. Metals, however, can undergo plastic flow and this partly explains the superior wear rate exhibited by the tougher, less porous antimony impregnated grade MY10K. For large abrasive particle diameters (>85 μm), the effect of grit size and grit density neutralise one another yielding small variations in wear rate.

3.) Abrasion is the dominant process in the initial stages of sliding against stainless steel until a transferred layer of crushed and compacted debris forms on the counterface asperities. After several thousand metres an equilibrium regime is established in which the load supporting layers are worn and replenished. Small variations in counterface roughness affect the wear rate of all the materials in the initial stages of sliding. Once a coherent transfer layer is fully established, wear is independent of the original surface finish.

4.) Films transferred from more graphitic carbons are formed rapidly. They are thicker but appear to be less mechanically coherent than those of the filled grades.

5.) Sliding wear rate and friction tend to be lower in both epoxy and antimony impregnated grades. Additionally impregnants can improve the strength of the carbons by minimising chipping, cracking and subsequent three body abrasion processes.

6.) Impregnation can improve a carbon's resistance to both air borne and waterborne particle erosion by inhibiting lateral crack propagation. It can also reduce wear caused by cavitation erosion by decreasing the porosity and reducing the areas for cavitation attack.

APPENDIX (i)

Particle velocity was measured using the Ruff and Ives rotating discs method [58]. Two parallel discs, illustrated in fig. A1, are placed in the path of an air/particle stream such that some of the particles pass through the slit in the front disc (**A**) and strike the back disc (**B**) leaving a mark. The discs are then rotated at a constant rate, the particles passing through the slit in the front disc strike the back disc at a point away from the first mark. The distance between the two marks can then be measured and related to the particle velocity via the following equation:

$$v = \frac{2rwL\pi}{S}$$

Where: r = radius from disc centre
w = disc rotational velocity
L = disc separation
S = linear separation of the two marks

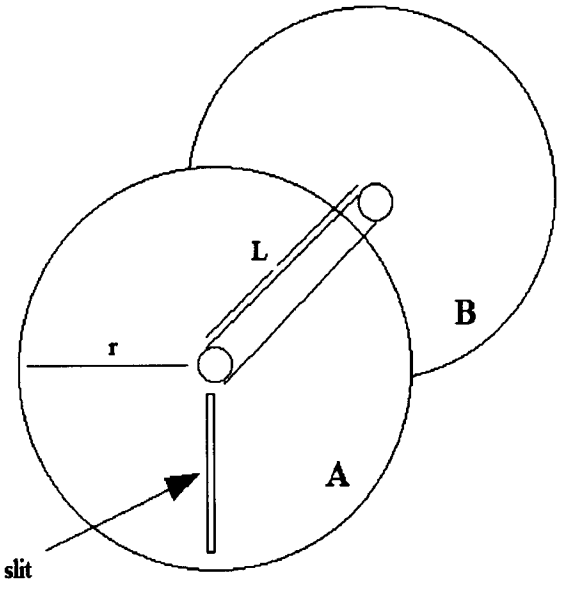

Fig. A1: Schematic diagram of the two parallel discs

APPENDIX (ii)

	(i)		Wear rate mm^3/Nm		(ii)
Grade	a	b	500 metres	8000 metres	average μ
EY9	3.4×10^{-4}	- 0.45	5.0×10^{-6}	1.1×10^{-6}	0.37
CY10	1.4×10^{-4}	- 0.49	2.8×10^{-6}	6.7×10^{-6}	0.41
MY10K	1.9×10^{-5}	- 0.63	1.3×10^{-6}	4.6×10^{-7}	0.43
CY10C	3.1×10^{-5}	- 0.64	2.1×10^{-6}	7.9×10^{-7}	0.43
Ra = 0.1μm					
EY9	1.7×10^{-2}	- 0.19	2.1×10^{-5}	2.2×10^{-6}	0.35
CY10	4.3×10^{-5}	- 0.67	3.8×10^{-5}	1.5×10^{-6}	0.41
MY10K	8.0×10^{-5}	- 0.48	1.5×10^{-6}	3.7×10^{-7}	0.41
CY10C	2.4×10^{-4}	- 0.40	2.4×10^{-6}	4.6×10^{-7}	0.41
Ra = 0.3μm					
EY9	2.0×10^{-3}	- 0.54	6.3×10^{-5}	1.8×10^{-5}	0.30
CY10	1.1×10^{-4}	- 0.62	6.4×10^{-6}	2.2×10^{-6}	0.39
MY10K	3.7×10^{-4}	- 0.38	3.1×10^{-6}	5.5×10^{-7}	0.19
CY10C	8.5×10^{-5}	- 0.58	1.1×10^{-6}	3.6×10^{-4}	0.25
Ra = 0.8μm					
EY9	3.2×10^{-2}	- 0.52	7.9×10^{-4}	2.1×10^{-4}	0.32
CY10	8.0×10^{-3}	- 0.27	2.3×10^{-5}	3.1×10^{-6}	0.15
MY10K	5.4×10^{-3}	- 0.16	4.6×10^{-6}	4.4×10^{-7}	0.13
CY10C	5.1×10^{-3}	- 0.21	7.6×10^{-6}	8.5×10^{-7}	0.15
Ra = 1.5μm					

Table A1: Wear rates carbon grades on each counterface in dry sliding wear experiments

(i) Empirical coefficients in wear equation $\frac{V}{Px} = \alpha x^b$, mm^3/Nm

(ii) Average values of coefficient of friction μ

APPENDIX (iii)

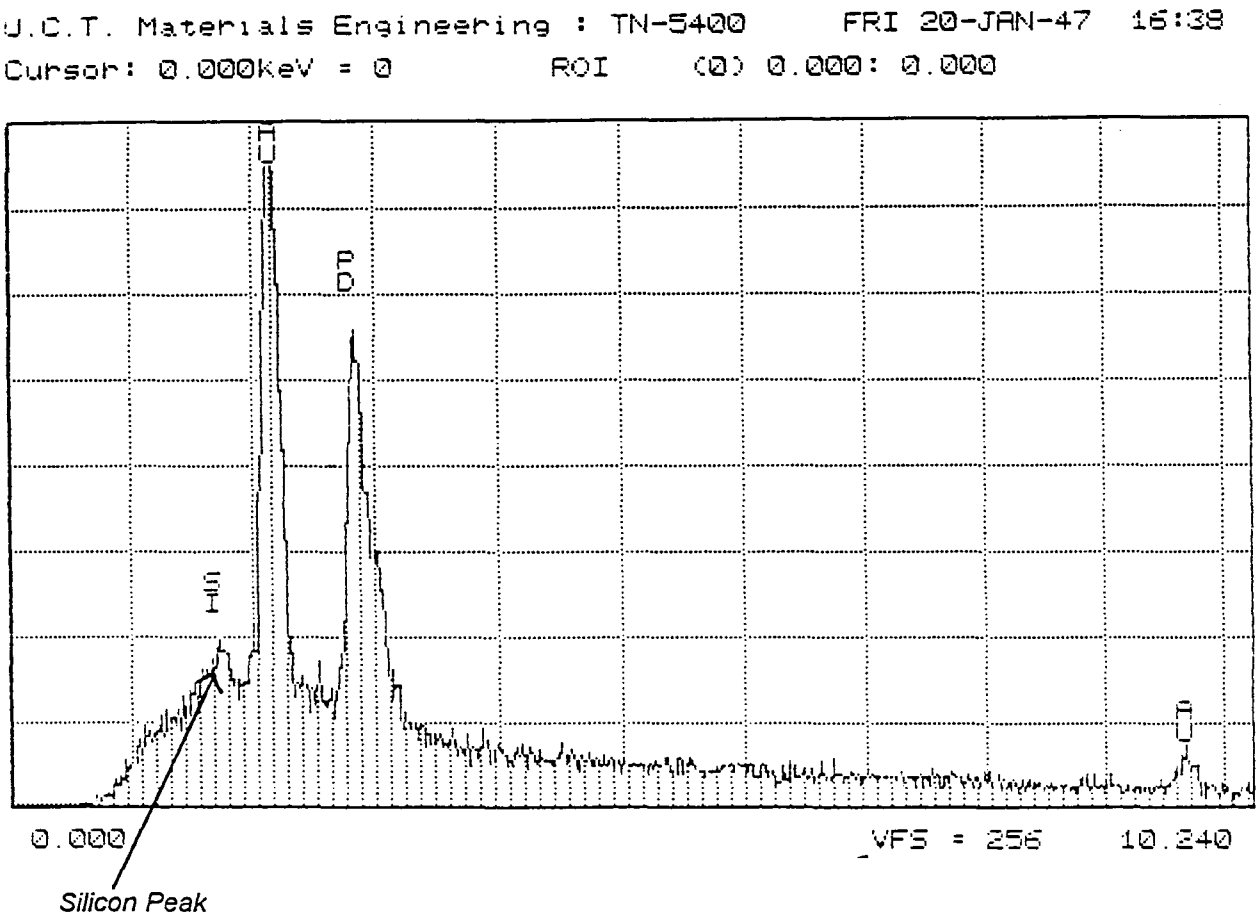

Fig. A2:- Electron dispersive microscopy scan of the foreign particle embedded on the wear surface of epoxy impregnated CY10C grade (fig. 4.3.2.c). The silicon peak, not present in scans of uneroded surfaces suggests that the embedded particle is SiC. The Au and Pd peaks are present because of the gold-palladium coating process used to improve conductivity in the microscope.

REFERENCES

1.) Lancaster, J. K., Treatise on Materials Science and Technology, Academic Press, (1979), 13, 141

2.) Bokros, J. C., Price, R. J. and Tully, G. R., "The anisotropy of extruded Graphite Tubes", Journal of Nuclear Materials, (1965), 1, 33-42

3.) Warburton, C., "Surface roughness of graphite and its effect on friction factor", Proc. Instn. Mech. Engrs., (1974), vol. 188, 457-460

4.) Boey, S. Y. and Bacon, D. J., "Bend strength of graphite under pressure", Carbon, (1986), 24, 571-574

5.) Loch, L. D. and Austin, A. E., "fine pore structure :- crystallite size relationships in carbons", Proc. Conf. on Carbon, Columbus, Ohio, (1955), 65-73

6.) Losty, H. H. W. and Orchard, J. S., "The strength of graphite", Proc. Conf. on Carbon, (1962), vol. 1, 519-532

7.) Taylor, R. E., Kline, D. E. and Walker, P. L., "The dynamic Mechanical Behaviour of graphites", Carbon, (1968), 6, 333-347

8.) Morelli, G. W. and Rusinko, F., "Graphite and carbon", Chemical Engineering, (1963), dec.23, 69-76

9.) Virgil'ev, Yu. S., Kurolenkin, E. I., Makarchenko, V. G. and Pekal'n, T. K., "Relationship between the strength properties of graphite and the temperature of its processing", Strength of Materials, (1973), 11, 1336-1340

10.) Williams, J. A., "The dry running of carbon graphite materials against 316 stainless steel", Report CUED/C-Mech/TR23, Massachusetts Institute of Technology, (1982)

11.) Surkov, S. A., Trofimova, E. G. and Shipkov, N. N., "Influence of the characteristics of raw materials on the properties of graphites", Solid Fuel Chemistry, (1985), v.19, 3, 133-135

12.) Gillis, P. P., "Calculating the elastic constants of graphite", Carbon, (1984), 22, 387-391

13.) Polisar, E. L., "Connection of the strength of graphitized materials with their porosity", Khimya Tverdogo Topoliva, (1976), 10, 130-176

14.) Hutcheon, J. M. and Price, M. S. T., "The dependence of the properties of graphite on porosity", Proc. Conf. on Carbon, (1960), 645-656

15.) Wakely, K. W., "Engineering in carbon", Engineering, (1985), Tech. File No. 134

16.) Glaeser, William A., Materials for Tribology, Elsevier, (1992)

17.) Mrozowski, S., "Mechanical strength, thermal expansion and structure of cokes and carbons", (1954), 31-45

18.) Hutchings, I. M., Tribology: Friction and Wear of Engineering Materials, Edward Arnold, (1992)

19.) Freti, S. and Simm, W., "Abrasive wear of multiphase materials", Wear, (1989), 129, 105-121

20.) Khrushschov, M. M., Wear, (1974), 28, 69-88

21.) Lancaster, J. K., "The wear of carbon and graphitic materials sliding against rough metal surfaces", Inst. Mech. Engrs.; Lubrication and Wear Convention, Bournemouth, (1963), Paper 16, 190

22.) Porgess, P. V. K. and Wilman, H., "Surface re-orientation, friction and wear in the uni-directional abrasion of graphite", Proc. Physical Society, (1960), 76, 513-525

23.) Gordelier, S. C. and Skinner, J., "Graphite wear against rough surfaces-the effects of sliding distance and interface gas flow", Proc. Instn. Mech. Engrs., Conference on Wear of Nonmetallic Materials, (1976), Leeds, 202-209

24.) Larsen-Badse, J., "Influence of grit diameter and specimen size on wear during sliding abrasion", Wear, (1963), 12, 35-53

25.) Khrushschov, M. M., "Resistance of metals to wear as related to hardness", Instn. Mech. Engrs, Proc. Conf. Lubrication and Wear, (1957), 655

26.) Böhm, H., Betz, S. and Ball, A., "The wear resistance of polymers", Tribology International, (1990), 399-406

27.) Moore, M. A. and King, F. S., "Abrasive wear of brittle solids", Wear, (1979), 60, 123-40

28.) Booser, E. R. and Wilcock, D. F., "Assessment of carbon graphite wear properties", Proc. Instn. Mech. Engrs., Conference on Wear of Nonmetallic Materials, (1976), 196-201

29.) Midgely, J. W. and Teer, D. G., "An investigation of the mechanism of the friction and wear of carbon", Trans. A.S.M.E., (1962), Paper No. 62-lub-15

30.) Lancaster, J. K., "Anisotropy in the mechanical properties of lamellar solids and its effect on wear and transfer", Wear, (1966), 9 169-188

31.) Rigney, D. A., Chen, "Adhesion theories of transfer and wear during sliding of metals", Wear, (1990), 136, 223-235

32.) Rigney, D. A., Chen, L. H. and Naylor, M. G. S., "Wear processes in sliding systems", Wear, (1984), 100, 195-219

33.) Clark, W. T. and Lancaster, J. K., "Breakdown and surface fatigue of carbons during repeated sliding", Wear, (1963), 6, 467

34.) Longley, R. I., Midgley, J. W., Strang, A. and Teer, D. G., "Mechanism of the frictional behaviour of high, low and non-graphitic carbon", Instn. Mech. Engrs., Lubrication and Wear Convention, (1963), 193

35.) Lancaster, J. K., "Instabilities in the frictional behaviour of carbons and graphites", Wear, (1975), 34, 275-290

36.) Hollander, A. E. and Lancaster, J. K., Wear, (1973), 6, 155

37.) Wilson, S. and Ball, A., "Performance of metal matrix composites in various tribological conditions", Advances in Composite Technology, ed.-K. Friedrich, Elsevier Science Publishers, (1993), 311-366

38.) Vaughan, R. A. and Ball, A., "The effect of hardness and toughness on the erosion of ceramic and ultrahard materials", Wear of Materials Proc., ASME, Vol. 1, (1991), 71

39.) Wellman, R. G. and Allen, C., "Solid particle erosion of ceramics", MSc Thesis, University of Cape Town, 1993

40.) Finnie, I., " Erosion of surfaces by solid particles", Wear, (1960), 3, 787-103

41.) Tilly, G. P., "Two stage mechanism of ductile erosion", Wear,(1973), 23, 87-96

42.) Lawn, B. R. and Swain, M. V., "Microfracture beneath point indentations in brittle solids", Journal of Materials Science, (1975), 10, 113-122

43.) Tilly, G. P., Treatise on Materials Science and Technology, Academic Press, (1979), 13, 287-319

44.) Wiederhorn, S. M. and Hockey, B. J., "Effect of material parameters on the erosion resistance of brittle materials", Journal of Material Science and Technology, (1983), 766-780

45.) Zu, J. B., Burstein, G. M. and Hutchings, I. M., "A comparative study of the slurry erosion and free-fall particle erosion of aluminium", Wear, (1991), 149, 73-84

46.) Bester, J. A. and Ball, A., "The performance of aluminium alloys and particulate reinforced aluminium metal matrix composites in erosive-corrosive slurry environments", Wear, (1993), 162-164, 57-63

47.) Zu, J. B., Burstein, G. T. and Hutchings, I. M., "A comparative study of the slurry erosion and free-fall particle erosion of aluminium", (1991), 149, 73-84

48.) Zu, J. B., "Bridging slurry erosion and airborne solid particle erosion", Dept. of Materials Science and Metallurgy, University of Cambridge

49.) Hankey, S. E., "Cavitation Erosion Of WC-Co", MSc Thesis, University of Cape Town, S.A., (1987)

50.) Preece, C. M., Treatise on Materials Science and Technology (Erosion), Academic Press, (1979), vol. 16,

51.) Vyas, B. and Preece, C. M., Journal of Appl. Phys., (1976), 47, 5133-5138

52.) Hutchings, I. M. and Wang, A., Proc. Conf. on New Materials and Their Applications, Inst. Phys. Conf. Series, Warwick, (1991), 112-120

53.) Wilson, S. and Ball, A., in P. K. Rohatgi, Yust, C. S., Blau, P. J. (eds.), Proc. Conf. Tribology of Composite Materials, Oak Ridge TN, (1990), ASM Int., 103-112

54.) Heathcock, C. J., Protheroe, B. and Ball, A., "The influence of external variables and microstructure on the cavitation erosion of materials", Proc. 5th Int. Conf. on Erosion by Liquid and solid Impact, Cambridge, England, (1979), 63-

55.) Lancaster, J. K., "Material specific wear mechanisms: relevance to wear modelling", Wear, (1990), 141, 159-183

56.) Whittemore, O. J., "Mercury Porosimetry of Ceramics", Powder Technology, (1981), 29, 167-175

57.) "Scleroscope hardness testing of fine-grained carbon and graphite materials", Annual Book of ASTM Standards, (1991), vol. 15.01, 284-285

58.) Ruff, A. W and Ives, L. K., "Measurement of solid particle velocity in erosive wear", Wear, (1975), 35, 195-199

59.) Murugesh, L. and Scattergood, R. O., "Effect of erodent properties on the erosion of alumina", Journal of Matl. Sci., (1991), 26, 5454-5466

60.) Srinivasan, S. and Scattergood, R. O., "Effect of erodent hardness on erosion of brittle material", Wear, (1988), 128, 139-152

61.) Heathcock, C. J., "Cavitation erosion of materials", Ph.D. thesis, University of Cape Town, (1980)

62.) Paxton, R. Robert, "Manufactured Carbon: a Self Lubricating Material for Mechanical Devices", CRC Press, (1979)

63.) Savage, R. H., Graphite Lubrication, J. Appl. Physics, 19, 1, (1948)

64.) Marcus, K., "Micromechanisms of polymer sliding wear",Ph. D Thesis, University of Cape Town, (1992)